Plasma polymerised organic thin films-A study on the structural, electrical and nonlinear optical properties for possible applications

Thesis submitted to

Cochin University of Science and Technology

In the partial fulfillment of the requirements for the award of the degree of

DOCTOR OF PHILOSOPHY

by

Sajeev U.S

Department of Physics
Cochin University of Science and Technology
Cochin-682022, India

August 2006

Illustration of the cover page

Front cover

AFM image of rf plasma polymerised aniline thin film in its iodine doped form

&

Polyaniline network

Back cover

Tea tree plant *(Melaleuca Alternifolia*)

to my parents...

Dr. M.R. ANANTHARAMAN
Reader

Department of Physics
Cochin University of Science and Technology
Cochin Kerala, India 682 022

CERTIFICATE

Certified that the work presented in this thesis entitled ***"Plasma Polymerised Organic Thin Films-A Study on the Structural, Electrical and Nonlinear Optical Properties for Possible Applications"*** is based on the bonafide research work done by Mr.Sajeev.U.S under my Guidance in the Department of Physics, Cochin University of Science and Technology, Cochin-682022, India, and has not been included in any other thesis submitted previously for the award of any degree.

Cochin-22
23-08-2006

Dr.M.R.Anantharaman
(Supervising Guide)

DECLARATION

I here by declare that the work presented in this thesis entitled ***"Plasma Polymerised Organic Thin Films-A Study on the Structural, Electrical and Nonlinear Optical Properties for Possible Applications"*** is based on the original research work done by me under the guidance of Dr.M.R.Anantharaman, in the Department of Physics, Cochin University of Science and Technology, Cochin - 682022, India, and has never been included in any other thesis submitted previously for the award of any degree.

Sajeev U.S

Cochin-22
21-08-2006

Preface

Polymers and polymer based materials find enormous applications in the realm of electronics and optoelectronics. They are employed as both active and passive components in making various devices. Enormous research activities are going on in this area for the last three decades or so, and many useful contributions are made quite accidentally. Conducting polymers is such a discovery, and eversince the discovery of conducting polyacetylene, a new branch of science itself has emerged in the form of synthetic metals. Conducting polymers are useful materials for many applications like polymer displays, high density data storage, polymer FETs, polymer LEDs, photo voltaic devices and electrochemical cells. With the emergence of molecular electronics and its potential in finding useful applications, organic thin films are receiving an unusual attention by scientists and engineers alike. This is evident from the vast literature pertaining to this field appearing in various journals. Recently, computer aided design of organic molecules have added further impetus to the ongoing research activities in this area.

Polymers, especially, conducting polymers can be prepared both in the bulk and in the thinfilm form. However, many applications necessitate that they are grown in the thin film form either as free standing or on appropriate substrates. As far as their bulk counterparts are concerned, they can be prepared by various polymerisation techniques such as chemical routes and electrochemical means. A survey of the literature reveals that polymers like polyaniline, polypyrrole, polythiophene, have been investigated with a view to studying their structural electrical and optical properties. Among the various alternate techniques employed for the preparation of polymer thin films, the method of plasma polymerisation needs special attention in this context.

The technique of plasma polymerisation is an inexpensive method and often requires very less infra structure. This method includes the employment of ac, rf, dc, microwave and pulsed sources. They produce pinhole free

homogeneous films on appropriate substrates under controlled conditions. In conventional plasma polymerisation set up, the monomer is fed into an evacuated chamber and an ac/rf/dc/μ w/pulsed discharge is created which enables the monomer species to dissociate, leading to the formation of polymer thin films. However, it has been found that the structure and hence the properties exhibited by plasma polymerized thin films are quite different from that of their counterparts produced by other thin film preparation techniques such as electrochemical deposition or spin coating. The properties of these thin films can be tuned only if the interrelationship between the structure and other properties are understood from a fundamental point of view. So very often, a through evaluation of the various properties is a pre-requisite for tailoring the properties of the thin films for applications. It has been found that conjugation is a necessary condition for enhancing the conductivity of polymer thin films. RF technique of plasma polymerisation is an excellent tool to induce conjugation and this modifies the electrical properties too. Both oxidative and reductive doping can be employed to modify the electrical properties of the polymer thin films for various applications. This is where organic thin films based on polymers scored over inorganic thin films, where in large area devices can be fabricated with organic semiconductors which is difficult to achieve by inorganic materials. For such applications, a variety of polymers have been synthesized such as polyaniline, polythiophene, polypyrrole etc. There are newer polymers added to this family every now and then.

There are many virgin areas where plasma polymers are yet to make a foray namely low-k dielectrics or as potential nonlinear optical materials such as optical limiters. There are also many materials which are not been prepared by the method of plasma polymerisation. Some of the materials which are not been dealt with are phenyl hydrazine and tea tree oil. The advantage of employing organic extracts like tea tree oil monomers as precursors for making plasma polymers is that there can be value addition to the already existing uses and

possibility exists in converting them to electronic grade materials, especially semiconductors and optically active materials for photonic applications.

One of the major motivations of this study is to synthesize plasma polymer thin films based on aniline, phenyl hydrazine, pyrrole, tea tree oil and eucalyptus oil by employing both rf and ac plasma polymerisation techniques. This will be carried out with the objective of growing thin films on various substrates such as glass, quartz and indium tin oxide (ITO) coated glass. There are various properties namely structural, electrical, dielectric permittivity, nonlinear optical properties which are to be evaluated to establish the relationship with the structure and the other properties. Special emphasis will be laid in evaluating the optical parameters like refractive index (n), extinction coefficient (k), the real and imaginary components of dielectric constant and the optical transition energies of the polymer thin films from the spectroscopic ellipsometric studies. Apart from evaluating these physical constants, it is also possible to predict whether a material exhibit nonlinear optical properties by ellipsometric investigations. So further studies using open aperture z-scan technique in order to evaluate the nonlinear optical properties of a few selected samples which are potential nonlinear optical materials is another objective of the present study. It will be another endeavour to offer an appropriate explanation for the nonlinear optical properties displayed by these films.

Doping of plasma polymers is found to modify both the electrical conductivity and optical properties. Iodine is found to modify the properties of the polymer thin films. However *insitu* iodine doping is tricky and the film often looses its stability because of the escape of iodine. An appropriate *insitu* technique of doping will be developed to dope iodine in to the plasma polymerized thin films. Doping of polymer thin films with iodine results in improved and modified optical and electrical properties. However it requires tools like FTIR and UV-Vis-NIR spectroscopy to elucidate the structural and optical modifications imparted to the polymer films. This will be attempted here to establish the role of iodine in the modification of the properties exhibited by

the films. The main objectives of the present study can be summerised and are listed below.

Objectives of the present work

- Preparation of optical quality organic thin films by rf/ac plasma polymerisation techniques.
- Modification of the optical and electrical properties by *insitu* doping of iodine
- Evaluation of structural properties of these films by FTIR analysis
- Morphological studies using scanning electron microscopy
- Determination of the optical band gap of thin films and calculation of the defect levels from UV-Vis-NIR studies.
- Elucidation of the mechanism of conduction in these films for the fabrication of devices.
- Evaluation of permittivity and loss factor at various frequencies.
- Determination of the optical and thin film parameters using Spectroscopic Ellipsometric studies.
- Determination of the nonlinear optical properties of the films by z-scan technique
- Study the effect of ultrafine coating on magnetic/ non magnetic nano particles on the electrical and structural properties.

This proposed thesis is entitled **"Plasma Polymerised Organic Thin Films: A study on the Structural, Electrical, and Nonlinear Optical Properties for Possible Applications"** and consists of ten chapters

Chapter I contains a brief history and application potential of conducting polymers including plasma polymerisation and plasma polymerised thin films. The importance of the modification of the properties by doping is also described in this chapter. The motivation for the present study is brought out in this chapter.

Preface

The theoretical aspects of the mechanism of conduction, the basic theory of the ellipsometric technique for thin film analysis and nonlinear optical properties of the polymers are discussed in ***Chapter II***

The experimental techniques used in the various stages of this study are briefly described in ***Chapter III***. It deals with the preparation of the thin films by rf/ac plasma polymerisation, *insitu* doping with iodine, structural, optical and morphological studies, and the electrical characterisation. Also the techniques of spectroscopic ellipsometric and nonlinear optical characterization are described in detail.

The structural and optical characterisation of various plasma polymerized thin films is described in this ***Chapter IV***. FTIR studies gives a picture of the structural difference occurring during the process of plasma polymerisation and the optical band gap and the defect level calculation from the UV-Vis-NIR studies is described.

Chapter V gives a detailed analysis on the current voltage characterisation of plasma polymerized thin films. The various conduction models for different polymers and electrode configurations and the low temperature effects on the charge transport mechanism in plasma polymers are discussed.

The permittivity measurements carried out on various plasma polymers are described in ***Chapter VI.*** The low-k characteristics exhibited by different plasma polymers are described in this chapter.

Chapter VII deals with the spectroscopic ellipsometric characterisation of plasma polymerized poly aniline thin films in the pristine and doped form. The evaluation of the optical constants, dielectric constants and band gap are discussed in this chapter.

The nonlinear optical properties of plasma polymerized thin films are evaluated by z-scan technique. The nonlinear optical properties of plasma polymerized thin films in the pure and doped form is described in ***Chapter VIII***

The effect of a thin polymer coating on inorganic nanocomposites by plasma polymerisation and modification of the permittivity and ac conductivity and the electrical properties of the composites are described in ***Chapter IX***.

Chapter X is the concluding chapter where in the inference drawn out of the study are detailed. The scope of further work and the lacunae observed in this study are brought out.

Chapter 1
Introduction

Polymers and polymer based materials are increasingly finding innumerable applications in day today life of human beings. Polymers are high molecular weight long chain components consisting of low molecular weight identical repeating units connected by covalent bonds[1]. The low molecular weight components are called monomer units and these atomic or molecular groups repeat themselves to form the polymer. Most of the physical properties exhibited by the polymers are determined by the chemical structure and the nature of the repeating units. Polymers have become an integral part of human life so much so that it is very difficult to find an appliance in daily use without the presence of a polymer. They form part of many devices and find application in the form of passive as well as active components. They find extensive applications in many devices such as capacitors, protection and anticorrosion coatings etc[2,3].

In the initial days many scientists and engineers thought that polymers are electrical insulators and their applications are limited by this property. However, the chance discovery of polyacetylene in 1977[4,5] transformed this concept and this discovery gave birth to a new class of materials called synthetic metals or what are known as conducting polymers. They are highly anisotropic and quasi one dimensional in structure. Their properties can be tailored to suit various applications. They differ considerably from that of conventional inorganic semiconductors. The chain like structure of organic semiconductors need strong coupling of electronic states to conformational excitations, peculiar to a one dimensional system.

The cost effectiveness of these materials combined with the less infra structure facilities needed for the large scale manufacturing or production of these materials has lead to the rapid growth of a separate branch of science itself and is popularly known as organic semiconductors. Their light weight, flexibility, transparency and ease of tuning has lead to the realization of various polymer devices such as light emitting diodes (LED), waveguides, solar cells, displays

etc[6]. These devices are important not only because they are efficient and can perform well but also they can be patterned by inexpensive techniques such as spin casting, photo lithography and inkjet printing[7,8].

Conducting polymers offer the possibilities of combining the desirable processing and structural properties of polymers together with the electronic functionality of a metal or a semiconductor. Over the past few years a number of these materials have been developed for use as conductors and semiconductors for various applications which include lithium polymer batteries, polymer super capacitors and polymer electrochromic devices[9]. The electrical and optical properties of the conjugated polymers have received considerable attention in the context of potentiality and low cost, leads to the replacement of conventional metals and inorganic semiconductors. Charge transport of these organic materials has been characterized in both the doped-metallic and semi conducting states. The metal-insulator transition of the polymers has been reported[10]. Organic materials with sensitive optical and electric response present a very promising alternative to the conventional inorganic opto-electronic materials. The added advantages of these materials are the flexibility of processing and the control over the properties by doping[11].

Chemists, chemical engineers and physicists are playing their roles in understanding the underlying physics of these materials at the macromolecular level. Most often such studies in polymer science sans boundaries and are interdisciplinary in nature. It is in this context that physicists have an important role to play, especially in identifying the critical parameters and factors responsible for the improved properties of these materials and pave the way for the tailoring of the properties[12].

Conducting polymers can be prepared in the bulk form as well as in the thin film form. The preparation of bulk materials employs methods like chemical and electrochemical[13]. Thin films of semiconductor conjugated polymers received considerable attention, since they can be used for a variety of photonic devices[14]. Polymers with conjugated π-electrons have the potential for electronic devices. Polymeric thin films are being investigated for their use in the telecommunication devices, optical wave guides, El Devices, photo refractive

materials, low k dielectric materials, display devices, nanostructured materials, in non linear optical devices, light emitting devices and in semiconductor devices[15].Various techniques such as spin coating, solution casting, electro chemical deposition and plasma polymerization exist for the preparation of the thin films. Among them plasma polymerization plays a significant role due to its cost effectiveness and simplicity[16].

The process of plasma polymerization and various techniques of plasma polymerization are described here very briefly since it is the focal theme of this thesis. The process of plasma polymerization and the subsequent deposition of thin films on various substrates are based on three key features of plasma like i. production of light, ii. production of chemically active species, iii. deposition of sufficient energy on to the surface by ion bombardment to drive chemical reaction with out excessive heating or damage to the processed material or substrate[17,18,19].

The method of plasma polymerisation can be suitably modified to provide provisions for controlling the parameters like monomer feed, plasma power and plasma frequency. The properties of the thin films are dependent on the above parameters[20,21]. The plasma polymerisation technique involves dc, ac, rf, pulsed and magnetron assisted plasmas. The methods are suitably modified according to the monomer, the application of the thin film, substrate, carrier gas, input power, monomer flow rate and the other kinetic and mechanical aspects of plasma polymerisation[22,23] in accordance with the application of the thin films.

1.1 Electrical properties of conducting polymer thin films

Ever since the discovery of conducting polymers, theoreticians have tried to explain the fundamental mechanism of conduction in polymers especially in organic thin films. In a polymer, the σ and the π -bonded systems lead to the conduction in a π conjugated polymer, the bond between adjacent carbon atoms alternate between single and double bonds[24]. The π -electrons are not tightly bound and they become delocalized along the polymer chain. In 1950 Rudolf Peierls[25] found that it is energetically favorable for such a chain to distort spontaneously, creating a gap between the filled valance and the unfilled conduction band and converting a chain from a conductor to a semi conductor.

The ac mobility $\mu(\omega)$ provides information of the charge transport process occurring in a time scale of order ω^{-1}. It yields a practical insight into the conduction mechanisms involved in a disordered system. By applying a basic hopping formalism[26] to the measured $\mu(\omega)$ in a polymer thin film, it is possible to estimate the local barriers and to follow the evolution of the hopping time and distances in the macroscopic high mobility regions as a function of energy.

When a π-conjugated polymer is doped with an acceptor atom such as iodine each iodine atom grabs an electron from a π-bond, creating a hole in the π- conjugated chain. The negatively charged iodine ion remains associated with the polymer but is not as mobile as the hole. The hole together with the local distortion produced in the carbon chain is called polaron and the bonded pairs of polarons are called bi-polarons[27]. The SSH, SSU, etc are the models describing the charge transport in polymer chains. Even though there exist many models, the details of how polymers carry current are still not fully understood. The enhancement of the carrier mobility and hence the conductivity is a major challenge in the polymer device fabrication, since the chain length is limited in polymers. Another fascinating property of conducting polymers is its electro luminescence (EL) property invented by RH Friend and his coworkers who fabricated the first organic LED in 1990[28].

Modern organic LEDs demand current densities $\geq$ 3 mA cm^{-2} for injecting EL with characteristic efficiencies of 0.5 to 3cd/A. Generally mobility in organic luminescent materials is low, typically 10^{-5} to 10^{-8} $cm^2/V.s$. Such strong injection into low mobility materials inevitably leads to charge accumulation in organic films. The built up charge partially screens out the applied electric field leading to its redistribution and the resulting behaviour of J(V) or I(V) is that of space charge limited current (SCLC)[29]. In the absence of trap levels or with single shallow traps the I(V) characteristics would be quadratic in V. The local increase in the quasi Fermi level due to strong injection of carriers may lead to charge immobilization in the deep states of the disorder induced distribution of HOMO or LUMO levels. The resulting Trap Charge Limited Current (TCLC) model predicts a generally high exponent power law $I \propto V^{\alpha}$ with $7 \leq \alpha \leq 9$. The study trap levels in various electrically active

organic films yielded the data required to explain the dc I-V curve in most common types of organic LEDs[29]

1.2 Space charge dynamics in photorefractive polymers

Photorefractive (PR) effect in polymers involve a change in refractive index in an electro-optical material resulting from the redistribution of charge carriers created under the influence of the light beams. The response of a polymer to the electromagnetic wave will depend on the dynamics on charge generation, mobility, trap density, acceptor density and their associated rates[30]. The chromophores present in the polymer are the key parameters which determine the optical absorption as well as the optically induced states of the polymer. The optical absorption in polymers and the related properties such as mobility, charge generation efficiency, trapping, de-trapping and recombination rates are influenced by the degrees of disorder, trap depths, ionization potentials of the constituents of the polymers and the presence of ionic impurities etc[31].

1.3 Doping of organic semiconductors

Like in the case of inorganic semiconductors doping has been found to be a useful means inorder to modify the electrical and optical properties of these materials. Dopants like HCl, halogens etc has been found to improve the electrical properties of polymers like polyaniline, polypyrrole, polythiophene[32] etc. For example, CSA doped polyaniline has been found to be exhibiting a near metallic conductivity[10].

It is well known that incorporation of iodine in the polymer chain by appropriate techniques modifies the electrical properties of polymers like polyaniline, polypyrrole etc[33]. Normally iodine is susceptible to vaporisation and *insitu* doping of iodine into the polymer is necessary to achieve the stability. In plasma polymerisation *insitu* doping of iodine is achievable because iodine vapors can be let into the polymerisation chamber along with the precursor monomers[34]. When iodine is doped into a π -conjugated polymer, iodine acts as an acceptor and these iodine atoms are capable of grabbing an electron from a π -bond creating a hole in the conjugated chain of the polymer. The relatively charged iodine remains associated with the polymer but its mobility is limited as

compared to the hole. These holes together with the local distortion in the polymer chain are called polarons and pairs of polarons are called bipolarons[35].

The effect of doping in a polymeric system is widely studied and many models are invoked to explain the doping effect in various polymeric materials. Even though the doped polymers are utilized in many potential applications in various fields the exact phenomena behind the doping of polymers is not clearly understood. Doping of plasma polymers with dopants like iodine is described in the literature[34]. It is expected that with the addition of a polar, electron accepting or an electron withdrawing group to the polymeric system, the energy disorder or charged trap states in the system will increase. The charge induced disorders changes the binding energy of the polymers and by this way the transport properties can be modified[33].

1.4 Motivation for the present study

A survey of literature on various plasma polymerisation techniques reveals that though various methods of plasma polymerisation exist, rf and ac techniques can easily be adopted in any laboratory and can be home made. So emphasis is given to employ ac and rf polymerisation techniques for the growth of polymer thin films. Further more the employment of the rf plasma polymerisation technique results in conjugation, which is an essential criterion in improving the optical and electrical properties of plasma, polymerised thin films.

Most of the devices based on polymers necessitate that they be fabricated as thin films. This enables quick integration into existing systems immaterial of the nature of the devices and the substrate materials of the device namely inorganic or organic. For the preparation of good quality, pinhole free and homogeneous films, rf and ac plasma polymerisation can be employed. This is one of the motivations for using rf and ac plasma polymerisation method for the preparation of organic thin films. The film thickness can be controlled by varying the plasma parameters *viz.* current density, pressure and monomer flow rate. Another advantage of utilizing plasma polymerisation is that the precursors can be in the form of monomer liquids and the input to the plasma chamber can be controlled by needle valves and the flow rate can be regulated and monitored by flow meters.

The technique of plasma polymerisation will come handy for growing thin films of polymers based on natural products. It has also been found that there exists no systematic study on the growth of polymer thin films based on phenyl hydrazine. The monomer phenyl hydrazine has the structure of aniline, with an additional amine group. The presence of amine groups in the monomer and the possibility of making similar structure resembling polyaniline exist in such a molecule. The properties of plasma polymerised phenyl hydrazine does not exist in literature and in this respect this is an unexplored material where optical and electrical properties are of interest from both an application point of view and fundamental perspective.

So the methods of ac and rf plasma polymerisation will be used to prepare thin films based on phenyl hydrazine. The evaluation of their structural, electrical and optical properties will lead to structural property correlation and assumes importance from a fundamental point of view. Hence preparation and characterization of plasma polymerised thin films based on phenyl hydrazine is an objective of the present study.

Reports in the literature on adding value to the natural extracts like tea tree oil and eucalyptus oil are scanty. The extract derived from the tea tree plants commonly found in parts of Australia and New Zealand is investigated in the form of plasma polymerised thin films. At present tea tree oil is used for medicinal purposes such as fungicidal and antimicrobial activities.

Both tea tree oil and eucalyptus oil consists of a multitude of components[36,37]. The complexity of this molecular structure gives scope for identifying the components responsible for the pronounced optical and electrical properties of these materials that will be displayed upon plasma polymerisation. Such studies using ac/rf plasma polymerisation techniques provide a rare opportunity of preparing plasma polymer thin films based on tea tree oil. A systematic evaluation of their properties and the structural properties correlation can lead to the development of materials based on plasma polymerised tea tree oil for possible use as electrical grade materials. For this a systematic study on the growth of thin film based on tea tree oil by plasma polymerisation technique is necessary. Hence the growth of polymer thin films based on tea tree oil is yet

another motivation of the present study. Identification of active groups and their role in deciding the optical and electrical properties will lead to the immobilization of such groups from such natural products. This adds value to these materials.

Reports on polyaniline and polyaniline based materials are in plenty in literature[38,39]. But no where in the literature there is emphasis on determining optical constants of these films by spectroscopic ellipsometric technique. A comparison of optical properties of ac and rf plasma polymerised thin films will be another objective of the present study.

The optical and electrical properties of the polymer can be modified by doping. Iodine is such a dopant and it has been found that *insitu* doping of iodine into plasma polymer films greatly modify their properties. An indigenous set up has been fabricated in the laboratory for this purpose. *Insitu* doping of plasma polymerised thin films with iodine for studying the effect of iodine on the optical and electrical property is yet another objective of the present study.

Plasma polymerised polyaniline and polypyrrole exhibit low k characteristics. These films with good thermal stability can be integrated as low k dielectrics. The development of low k materials based on monomers like phenyl hydrazine appears to be a good proposition. Thus evaluation of dielectric constant at various frequencies is another part of this study.

The evaluation of non linear optical (NLO) properties of these films is yet another property which is of relevance from a photonic application point of view. These properties are evaluated by employing z-scan technique. The evaluation of conductivity of these films gives a correlation between the structure and properties with special emphasis on the electrical conduction mechanism.

1.5 Materials chosen for the study

Aniline, phenyl hydrazine and natural extracts like tea tree oil and eucalyptus oil are some of the materials which will be utilized as precursors for the growth of polymer thin films. Both ac and rf plasma polymerisation techniques will be employed to produce thin films. Iodine will be incorporated *insitu* in order to modify the optical and electrical properties of these films.

Superparamagnetic ion oxide nanoparticles (SPION) will be used as inorganic target materials for passivation and studies related to the surface modification of properties. So having described the motivation and materials chosen for the investigations it is imperative that the objectives are laid down.

1.6 Objectives of the present study

- Preparation of optical quality organic thin films by rf/ac Plasma polymerization techniques.
- Modification of the optical and electrical properties by *insitu* doping of Iodine
- Evaluation of structural properties of these films by FTIR analysis
- Morphological studies using scanning electron microscopy
- Determination of the optical band gap of thin films and calculation of the defect levels from UV-Vis-NIR studies.
- Elucidation of the mechanism of conduction in these films for the fabrication of the devices.
- Evaluation of permittivity and loss factor at various frequencies.
- Determination of the optical and thin film parameters using Spectroscopic Ellipsometric studies.
- Determination of the nonlinear optical properties of the films by z-Scan technique
- Study the effect of polymer thin film coating on certain inorganic oxide nanoparticles and their electrical and structural properties.

Chapter 1

References

[1] Richard H.Boyd, Paul J.Philips, *The Science of Polymer Molecules*, Cambridge University Press, New York, (2002)

[2] Frisch C.Frisch *Advances in Interpenetrating Polymer Networks*, CRC Press, 1991

[3] Paul C.Heimanz, *Polymer Chemistry, the Basic Concepts*. Marcel Dekker, New York, 1984.

[4] Terje A Skotheiem(Ed), *Hand Book of Conducting Polymers*,

[5] Alan G. Mac Diarmid, *Current Applied Physics*, **I**, (2001), 269.

[6] H.Burrouhes, D.D.C Bradley, A.R.Brown, R.N.Marks, K.Mackay, R.H.Friend , P.L.Burn, A.B.Holems, *Nature*, **347**, (1990), 539

[7] N.Teesler, G.J Danton, R.H Friend, *Nature*, **382**,(1996),695

[8] V.Bulovic, G.Gu, P.E.Burrows, S.R.Forrest, M.E.Thompson, *Nature*, **380**,(1996),29

[9] Qibing Pei, Guido Zuccarello,Markus Ahiskos,Olle Inganas, *Polymer*, **35**, (1994),1347

[10] Kwanghee Lee, Reghu Menon, C.O.Yoon, and A.J.Heeger, *Phys.Rev.B*, **52**, (1995),4779

[11] Blaise Lobo,M.R.Ranganadth,T.S.G.Ravi Chandran, G.Venugopal Rao, V.Ravindrachary and S.Gopal, *Phys.Rev.B.* **59**,(1999),13693

[12] Yong Cao, Paul Smith, Alan J.Heeger, *Synthetic Metals*, **48,** (1992), 91

[13] Terje A. Skotheim,(Ed), *Hand Book of Conducting Polymers,* Marcel Dekker, New York, (1986)

[14] Donald L.Wise, Gary E. Wnek, Derbra J.Trantolo, Thomas M.Cooper, Joseph D. Gresser, *Photonic Polymer Systems*, Marcel Dekker, New York, 1998.

[15] Maria Losurdo ,Giovanni Bruno and Eugine A.Irene , *J.Appl.Phys.* **94**,(2003),4923

[16] H.Yasuda , *Plasma Polymerization*, Academic Press(1985), NY

[17] Erika E.Johnston, Buddy D.Ratner, *Journal of Electron Spectroscopy and Related Phenomena*, **81**,(1996),303

[18] Donglu Shi, S.X.Wang, Wim J, Van Ooji, L.M.Wang, Jiangang Zhao and Zhou Yu, *Appl.Phys.Lett*, **78**, (2001), 1243

[19] Runguang Sun, Junbio Peng, Takayashi Kobayashi, Yuguang Ma, Haifeng Zhang, Shiong Liu, *Jpn.J.Appl.Phys* , **35**,(1996),1506

[20] Donglu Shi , Peng He, *Rev.Adv. Mater. Sci.*, **7**, (2004), 97

[21] L.G.Paterno, S.Manolache,F.Denes, *Synthetic Metals*,**130**, (2002),85

[22] M C Kim,S M Cho, S B Lee, Y.Kim, J H Boo. *Thin Solid Films*, **447**,(2004),592

[23] Ivan D Avramov, Shigeru Kurosowa, Michal Rapp,Piotr Ekaterina I Radeva,*IEEE Transations in Microwave Theory and Techniques*, **49**,(2001), 827

[24] A.K Mukhergee and Reghu Menon, *Pramana*, **58**,(2002),233

[25] Gerald C. L. Wong, Wim H. de Jeu, Henry Shao,Keng S. Liang & Rudolf Zentel, *Nature*, **389**,(1997),576

[26] H C F Martenes, O.Hiltand Bron, P W M Blom, J N Huiberts, *Phys.Rev.Lett*, **87**,(2001),86601

[27] Chih-Ming Lai, Hsin-Fei Meng, *Phys.Rev.**B***, **54**,(1996),16365

[28] RH Friend, R.W, Gymer, A.B.Holmes, J.H.Burroughes, R.N.Marks, C.Taliani, D.D.C. Bradley, D.A.Dos Santos, J.L.Bredas, M.Logdlund, and W.R.Salaneck, and N C Greenham, *Nature*, **397,** (1999),121.

[29] Shinar, J. and V. Savvate'ev*, Organic Light Emitting Devices*, (Springer Verlag) ,(2003),New York

[30] Oksana Ostroverkhosova and Kenneth D.Singer , *J.Appl.Phys.* **92**,(2002),1727

[31] E.Mecher, C.Brauchle, H.H.Hohold, J.C.Hummelen, and A.Meerholz, *Phys.Chem.Chem,Phys*, **1**, (1999), 1749

[32] Geofeng Li, Mira Josowicz, Jiri Janata, Klaus Mullen, *J.Phys.Chem.**B,*** **105**, (2001), 2191

[33] B.Xu, Jaewu Choi, A.N.Caruso,and P.N.Dowben,*Appl.Phys.Lett.* **80**,(2002),4342

[34] C.Joseph Mathai, S.Saravanan, M.R.Anantharaman, S.Venkatachalam, and S.Jayalekshmi, *J.Phys.D: Appl.Phys*, **35**,(2002),2206

[35] Chich-Ming Lai, Hsin-Fei Meng, *Phys.Rev.**B,*** **54**,(1996),16365

[36] D.Sakthi Kumar, Kenji Nakamura, Satoko Nishiyama, Hiromichi Noguchi,Shigeru Ishii, Kunihiro Kashiwagi, Yasuhiko Yoshida, *J.Appl.Polymer Sci,* **90**,(2003), 1102.

[37] Hammer A.A, Carson C.F and Riley T.V, 2004, *Journal of Antimicrobial Chemo Therapy*, **53**,(2004),1081.

[38] Liliana Hechavarria, Hailin Hu, Marina E.Rincon, Thin Solid Films, 441,(2003),56

[39] Sajan D.George, S.Saravanan, M.R.Anantharaman, S.Venkatachalam, P.Radhakrishnan, V.P.N.Nampoori, and C.P.G.Vallabhan, Phys.Rev.**B,69**,(2004),1.

Chapter 2
Theoretical Aspects

An insight into the theory of various process of plasma polymerisation will form an essential component of any investigation on plasma polymerised thin films. Different analytical techniques are employed at various stages to characterize the samples[1]. A brief outline of the theory of these experimental techniques is considered a prerequisite for the proper understanding of the methods and also for an accurate interpretation of the results. This chapter deals with these aspects in detail. This chapter also addresses the dynamics of nanocomposite formation in dusty plasma. This is seen from the modification of the surface of nanoparticle point of view.

2.1 Plasma polymerisation

Plasma polymerisation is a versatile and an important technique for the deposition of uniform, pinhole free and flawless thin films of organic and inorganic materials on various substrates which include, glass and metal surfaces, quartz, fabrics, nanocomposites and nano fibers[2].

2.1.1 Deposition of plasma polymer thin film on a substrate

In the plasma deposition process, a gaseous or a volatile compound is introduced into a reaction chamber. This compound is fragmented or ionized in glow discharge plasma, and assemble on a surface. The variables that can be readily controlled during this ionization-deposition process are power density, precursor flow rate and the ratio of precursor gas vapour to an inert carrier gas, pressure, reaction time, reactor geometry, plasma frequency, power and temperature of the reactor[3]. The ionized species formed acquires energies typically of 0-2 eV, while electrons and metastables can achieve energies up to 20 eV. The processes that simultaneously occur during the plasma reaction are ionization, neutralization, recombination, polymerisation, etching, implantation, mixing and deposition. Under appropriate conditions an over layer will be formed on a solid substrate introduced into the reactor. The over layer will be formed where deposition is kinetically dominant over etching, ion implantation

and atomic mixing[1]. If the molecule introduced into the gas phase is an organic compound, deposition and polymerisation is possible.

Typically plasma polymerisation reaction occurs at a pressure of 10^{-2} to 10 torr. The gas phase reaction involving polymerisation process can be explained by a modified kinetic theory of the gas. The process of plasma polymerisation involves the fragmentation of the monomer into reactive species and recombination of the fragments on a substrate which is placed inside the plasma chamber. The following kinetic and mechanistic parameters are to be considered when the polymerisation of a monomer is carried out.

The kinetic and mechanistic aspects of the polymer thin films involve some parameters and are described by Yasuda[4]. These parameters are 1. Rate of ionization 2. Reactivity of the carbo-cations used for the polymerisation, 3. Chemical nature of the monomers and dependence of initiation rate of the reaction. The ionization of a molecule with the collision of an electron is an essential process for creating plasma of a monomer with or without the presence of a carrier gas. The relative ease with which the dissociation of a molecule should depend on the activation energy associated with each reaction. The concentration of free radicals in plasma is usually five or six orders of magnitude higher than that of ions. Eventhough the ionization is a necessary step in creating and sustaining the plasma but is not the primary step in initiating the plasma polymerisation since the scission of bonds occur with a far greater frequency than the formation of ions.

Under ordinary conditions the quantity of impurities plays a major role in the plasma polymerisation process because as soon as the polymerisation process is initiated, a large number of byproduct gases are formed, and there are many species that can react with the cations including free electrons in plasma. Due to this the carbo-cations formed during the first step of ionization will play a significant role in the formation of plasma polymer.

The conventional polymerisation mechanism is highly dependent on the structure of the monomer. A particular monomer can only be polymerised by a limited polymerisation mechanisms dictated by the structure and the reaction conditions of the monomer. But in plasma polymerisation most of the

hydrocarbons can be polymerised without structural constraints. In conventional methods, according to the chemical structure the rate constant of propagation k_p varies considerably for various monomers. But in plasma polymerisation this k_p parameter is almost of the same order for most of the hydrocarbons which means that the plasma polymerisation is non specific for a particular monomer.

The empirical deposition rate of a plasma polymer depends on the energy input or discharge power of the reactor. There are two types of plasma polymerisation. First one is the flow rate controlled case and second is the discharge power controlled case. In the first type the polymer deposition rate is independent of the initiation rate and in the second case the polymer deposition rate is proportional to the initiation rate. Dissociation of excited molecules, dissociation of ions, neutralization of ion radicals and the molecular reaction ions are the basic processes in the plasma polymerisation.

2.1.2 Operational parameters of plasma polymerisation

The operational parameters affecting the plasma polymerisation mechanism can be divided into two major categories as (i) characteristic parameters of the reactor and (ii) parameters that require adjustments for each run during polymerisation. The later includes pressure in a steady state system. This parameter is dependent on the monomer pressure and the efficiency of the pumping system. The flow rate of the monomer is related to the system pressure by $F \infty p^b$, where b is a constant with a value 1<b<2. During discharge process after the monomer flow reaches a stable value, the system pressure plays an important role. The pressure of the plasma under glow discharge does not depend on the pressure of the plasma before the glow discharge is initiated. The other parameters are monomer flow rate, power input of plasma polymerisation, volume and intensity of plasma and plasma energy density.

2.1.3 Deposition kinetics of the formation of plasma polymer on a nanoparticle

Surface modification of nanoparticles is important in tailoring them for interfacial engineering application *viz* optics, ceramics catalysis and drug delivery[5,6]. Energetic electrons deeply fragment the molecular species in the plasma creating reactants are atomic in nature. The nanoparticles embedded in

the plasma are referred as dusty plasma. It refers to a stable suspension of small particles in the nanometer to low micron size range in the discharge. Particles immersed in the plasma draw both electronic and ionic currents in the surroundings. Because of the greater mobility of the electrons than ions the equilibrium charge on the particle is negative which can be thousands of elementary particles for a one micron particle. Such particles will experience electrostatic force, gravity, ion and neutral drags each with different scaling of the particle size. In the regions of the plasma, the net force on the particle vanishes; particles are collectively trapped like a cloud, generally oscillating about their equilibrium positions. Under discharge conditions when the inter particle Columbic potential far exceeds the thermal energy and the particles self orient into a highly regular array termed a plasma crystal. The different film deposition parameters like film growth rate, particle size distribution, uniformity of deposition depends mainly on the particle size of the core particle on which the plasma polymerisation is to be carried out[7].

2.2 Optical absorption polymer thin films

Generally the light absorption of a medium can be categorised into the following processes based on the conversation of the energy[8].

A- Absorbance of the material

R-Reflectance

T-Transmittance

S- Scattered part of the energy

The relative magnitudes of these quantities can be calculated from the complex refractive index of the material. $N = n + i\kappa$, where n is the real and k is the imaginary parts of the refractive index. With $\omega = 2\pi f$ and wave vector $k = 2\pi / \lambda$ inside the medium the wave will have a different phase and amplitude

$$E(z,t) = E_0 \exp(-iknz) \exp(k\kappa z) \exp(i\omega t) \qquad 2.1$$

Then the intensity $\boldsymbol{I}$ of the light wave is equal to $\left|E^2\right|$, thus

$$I = \left|E_0\right|^2 \exp(-2k\kappa z), \qquad 2.2$$

which decays exponentially with z for z>0.

In semiconductors strong absorption of light occurs when the incident photons having energies larger than the fundamental energy gap. Polymer materials are generally transparent to visible light. Strong absorptions occur in the infrared region if the incident photons have energies corresponding C-C bond or C=O bond. Depending on the nature of the material, the absorbed photon energy may be converted to different forms namely radiative transition like florescence or non radiative transition like heat etc.

When both absorption and scattering effects are considered together, they constitute the attenuation of light through a medium. The transmittance is related to the scattering coefficient by $T = \exp\left[-(\alpha + \sigma)z\right]$ and can be expressed as $(\alpha + \sigma) = \frac{4\pi\kappa}{\lambda}$, where σ is the conductivity and α is the absorbance.

In polymers, the absorption loss is classified as extrinsic or intrinsic. Intrinsic absorption loss in the UV region is associated with the electronic excitations of chromophores repeating units of polymer. Example for such UV absorbing chromophores include carbonyl, nitro or ethylenic double bonds. These electronic excitations are typically in the energy range 4-6 eV(200-310 nm) which corresponds to optical transitions of $n \to \sigma^*, n \to \pi^*$ and $\pi \to \pi^*$, where n represents a non bonding orbital.

The band gap E_g, in polymers are generally described as the transition between a LUMO (Lowest of the Unoccupied Molecular Orbit) and HOMO (Highest of the Occupied Molecular Orbit). Eventhough in polymers the $n \to \sigma^*, n \to \pi^*$ and $\pi \to \pi^*$, transitions are allowed most of the electroluminescent and optical properties are determined by the delocalized π electron system in a typical conjugated polymer, which are different from the conventional materials with σ bands. The differences between the two systems are,

i) The electronic band gap E_g, is relatively small and is in the range 1-3.5 eV with corresponding low energy electronic excitations in semiconducting behaviour.

ii) The polymer molecules can rather easily be oxidized or reduced, usually through charge transfer with atomic or molecular dopant species, to produce conducting polymers.

iii) Net charge carrier mobilities in the conducting state are large leading to high electrical conductivities.

The charge-carrying species are not free electrons or holes, but self localized quasi particles which can be delocalized through the material.

It is found that the colour of most of the plasma polymers is yellow and the yellowness of the polymer under white light indicates that, it absorbs light in the blue and violet region.

2.3 Urbach tail analysis and the calculation of defect level of plasma polymerised thin films

Band gaps in polymer thin films are evaluated by recording the absorption spectra. A very brief outline of the theory involved in the determination of bandgap is provided here. According to the Tauc relation the absorption coefficient can be calculated from the equation[9]

$$\alpha = \sum_i \alpha_i = \sum_i \frac{A_i (h\nu - E_{gi})^{m_i}}{h\nu} \qquad 2.3$$

where 'A' is a constant related to the density of states, the value of Eg_i and m_i corresponds to the energy and the nature of the particular energy transition with absorption coefficient α_i. This equation will reduce to the form

$$\alpha h\nu = B(h\nu - E_{opt})^{m} \qquad 2.4$$

For the allowed direct, allowed indirect, forbidden indirect and forbidden direct transitions the value of $m = 1/2$, 2, 3/2 and 3.respectively. From equation 2.4 it can be written as[10]

$$\frac{d(\ln(\alpha h\nu))}{d(h\nu)} = m(h\nu - E) \qquad 2.5$$

For a particular value of m and E, the graph will show a discontinuity at $h\nu = E$, where an optical transition might have occurred corresponds to a particular band gap $E = E_{g_i}$.

In 1953 Urbach proposed an empirical rule for the optical absorption coefficient $\alpha(\omega)$ associated with the electronic transition from the valance to conduction band tail in the disordered solids[11]. This rule states that

$$\alpha(E) \propto \exp[(\hbar\omega - \hbar\omega_0)/E_0] \qquad 2.6$$

where $\hbar\omega$ is the photon energy and E_0 and $\hbar\omega_0$ are fitting parameters. E_0 is proportional to kT in Urbach's original work. Subsequent experimental analysis of Urbach tail in a variety of disordered semiconductors and glasses exhibiting this Urbach exponential spectral behaviour strongly suggested that the Urbach absorption edge is nearly a universal property of the disordered solids and that the underlying physics is both simple and general and can be applied to polymeric materials also.

In contrast, theoretical efforts by various researchers focused on a variety of fundamentally different physical origins of the Urbach edge, suggested that the underling physics changes completely for tail states near the band edge where the kinetic energy of localisation plays a dominant role in determination of the scale of the most probable potential fluctuations. The other models for the explanation of the Urbach tail are the density of states of the electron band tail at the absorption edge. The universally observed Urbach tail and the dependence of different parameters are not able to determine from these models since the applications of these are specific. The disorder giving rise to the exponential band tails is produced by lattice vibrations, impurities, and other deviations from the perfect periodicity of the lattice. The effect of thermal and structural disorder on the electronic state of the hydrogenated amorphous silicon is investigated by *Cody*[12] *et al.* It is observed that the thermal and structural disorder are additive and suggest that the disorder is a fundamental factor in the optical band gap. In the case of crystalline semiconductors the width of the exponential tail is a direct measurement of the temperature independent component of Urbach edge. The presence of impurity levels or the dopants contributes to the optical absorption because they create charged defect and defect levels[13].

The density of states $\rho(E)$, of a particle, for example, has an electron interacting with charged centers which are randomly located in a highly

disordered material, is of utmost importance. The centers may be the host atom in an amorphous material, impurity ions randomly located in a heavily doped semiconductor or ions in a pure crystal with thermally created disorder. When the disorder is large, the edges of the allowed energy bands develop band tails reaching into the energy gaps. The form of these band tails can be expressed as[14]

$$\rho(E) \propto \exp(-E^n / E_0) \qquad 2.7$$

$n = 1$, for the Urbach tail where E is measured away from the band edge E_0.Since the absorption coefficient $\alpha(\omega)$ is proportional to $\rho(E)$, with $n = 1$. Here $E_0 = \hbar\omega_0$ plays the role of effective band edge energy. The review of the experimental data from the literature showed that the absorption coefficient varies as a few orders of magnitude within a small energy region near the absorption edge.

2.4 Theory of electrical conduction in plasma polymerised thin films.

The electrical resistance of plasma polymerised thin films show high values and hence the transport properties of these films are investigated using metal-polymer-metal (M-P-M) sandwich configuration across the film thickness. The prominent electrical conduction mechanisms found in plasma polymerised thin films are thermal or Schottky effect, tunneling, Poole-Frenkel effect and space charge limited conduction[15] (SCLC). The conduction takes place through the following processes. (i) through the conduction band, (ii) by tunneling (iii) through impurity bands (iv) space charge limited process and (v) by ionic transport. These effects are briefly explained in the following sections.

2.4.1 Tunneling

Tunneling is a quantum mechanical phenomena in which an electron passes through a potential energy barrier without acquiring enough energy to pass over the top of the barrier. The penetration probability of an electrode to the other through the insulator is much dependent on the applied electric field. The effect of image forces, temperature, dielectric constant, shape of the potential barrier and effective mass of electron in the conduction band play a role in determining the tunnel current.

In the metal-polymer-metal structure one of the electrodes is positively biased. The electrons can flow through the barrier between the conducting regions by quantum mechanical tunneling and the expression for current density in a tunneling process for a rectangular potential barrier of height ϕ_t with similar electrodes at high applied fields, is given by[16]

$$J = \frac{2.2e^3V^2}{8\pi h\phi_s^2}\exp\left[\frac{-8\pi s}{2.96\,heV}(2m)^{1/2}\phi^{3/2}\right] \qquad 2.8$$

where m is the mass of the electron, s is the inter electrode spacing, ϕ is the metal insulator work function and V is the applied field. This relation is analogous to the Fowler-Nordheim expression, which explains the direct tunneling. This involves the transfer of electrons from one electrode to the other through their Fermi surface levels. For a thin film under a high electric field the tunneling can be direct and according to Fowler-Nordheim[17] relationship. Then the current density *J* given by,

$$J = F^2\exp(-0.689\phi^{3/2}F) \qquad 2.9$$

where $F = V/d$, V is applied potential and 'd' is the film thickness. Here the current density *J* is independent of temperature according to Fowler-Nordheim expression. A plot of log *J* vs. 1/V will yield a straight line and is called the Fowler-Nordheim plot. For such a conduction mechanism the film thickness should be less than 100Å. Experimentally it is observed that the presence of traps can give rise to a strong temperature dependence of tunnel current contrary to that given by the Fowler-Nordheim expression.

2.4.2 Schottky effect

Schottky type mechanism of conduction is reported in many plasma polymers includes polyaniline[18], polypyrrole[19], polyfurfural[20], polythiophene[21] and the plasma polymers of some natural extracts like lemon grass oil and Eucalyptus oil[22]. In metal insulator interface region there is often a potential barrier and the electrons can overcome this and can flow from the metal electrode to the conduction band of the insulator under an applied electric field. This effect is known as Schottky effect and is a field assisted conduction process[23]. When an electron escapes from the metal surface, the later becomes polarized, and intern exerts an attractive force on the electron. Due to the

resulting image force, the potential step at the metal polymer interface changes smoothly. The potential energy of the electrons due to this image force is

$$\phi_i = -\frac{e^2}{16\pi\varepsilon\varepsilon_0 x} \qquad 2.10$$

where x is the distance of the electron from the electrode surface. Here ε is the high frequency dielectric constant of the material, e is the electronic charge and ε_0 is the permittivity of free space. The change in the barrier height due to the interaction with the image potential $\Delta\phi_s$ is given by

$$\Delta\phi_s = \left[\frac{e^3}{4\pi\varepsilon\varepsilon_0}\right]^{1/2} F^{1/2} = \beta_s F^{1/2} \qquad 2.11$$

where $\beta_s = \left[\frac{e^3}{4\pi\varepsilon\varepsilon_0}\right]$ is called the Schottky coefficient.

The flow of electrons does not follow the Richardson- Dushman relation

$$J = AT^2 \exp\left[-\frac{\phi}{kT}\right] \qquad 2.12$$

and this is to be modified by the potential barrier at the contact. The modified expression for current density in an electrode limited Schottky type mechanism is given by,

$$J = AT^2 \exp\left[-\frac{\phi_0 - \Delta\phi_s}{kT}\right] \text{ or} \qquad 2.13$$

$$J = AT^2 \exp\left[\frac{\beta_s F^{1/2} - \phi_0}{kT}\right] \qquad 2.14$$

where A is the Richardson coefficient, k Boltzmann constant and T is the temperature. In Schottky mechanism the current density J has an exponential dependence of the square root of the applied field, i.e, $F^{1/2}$. Since the film thickness is a constant, J depends exponentially on $V^{1/2}$. The electrode limited conduction process can change from Schottky to field emission as the temperature of the sample is lowered[24].

2.4.3 Poole-Frenkel effect

When an electric field is applied to a sample the potential barrier height caused by Coulombic forces of an atom will be reduced. This phenomenon is

known as the Poole-Frenkel effect[25]. For a traping center the potential energy of an electron can be given by the usual coulomb expression $\phi_c = -\frac{e^2}{4\pi\varepsilon_0 x}$, where x is the distance from the center. The lowering of Coulombic barrier will be twice that due to Schottky effect since the potential energy ϕ_c is four times that of the image force given in the Schottky mechanism. The Pool-Frenkel effect involves the emission of trapped electrons or holes. On applying an external electric field, the potential barrier of the trap is lowered and the carriers escape easily, giving rise to a bulk conductivity governed by the equation.

$$\sigma = \sigma_0 F \exp\left[\frac{\beta_{PF} F^{1/2} - \phi_c}{kT}\right] \qquad 2.15$$

σ_0 is the low field conductivity given by the expression $\sigma_0 = e\mu n$, here n is the number of charge carriers and μ is the mobility, ϕ_c is the ionization potential of the Pool-Frenkel centers. The Pool-Frenkel coefficient can be evaluated from the formula, $\beta_{PF} = \left[\frac{e^3}{\pi\varepsilon\varepsilon_0}\right]^{1/2}$ which will be twice that of the Schottky coefficient $\beta_{PF} = 2\beta_s$. The current density varies exponentially as the square root of the applied field similar to that in the Schottky mechanism. The following expression is applicable to both Schottky and Poole-Frenkel effect

$$J = J_0 \exp\left[\frac{\beta F^{1/2} - \phi}{kT}\right] \qquad 2.16$$

Where $\beta = \left[\frac{e^3}{a\pi\varepsilon\varepsilon_0}\right]$, the constant in the denominator and $a = 1$ for Pool-Frenkel effect and a= 4 for Schottky effect. In both cases the movement of carriers is facilitated by the application of an external electric field, which lowers the potential barrier for emission, in this case also the log J vs. $V^{1/2}$ is a straight line and generally referred to as a Schottky plot.

Comparison of the theoretical and experimental values of the β coefficient distinguishes both these mechanisms. The experimental value of β coefficient can be obtained from the slope of the log J vs. $V^{1/2}$ plots. The theoretical values can be calculated from the equations for both β_s and β_{PF} .To

confirms the dominance of either mechanism it is necessary to carry out the J-V studies in the asymmetric electrode configurations. In Schottky mechanism a change in the field polarity should bring about a shift in the current–voltage characteristics but this effect is absent in Pool-Frenkel type mechanism.

2.3.4 Space charge limited conduction (SCLC)

In the metal-polymer-metal (M-I-M) configuration where the contacts are ohmic the carriers can be injected from the metal electrode into the conduction band of the polymer under an applied electric field. If the amount of injected carriers is more than that which can be transported across the film, a space charge will be built up at the metal polymer interface. Electrons flowing through the system under an electric field will be impeded and controlled by the space charge collected at the metal polymer interface and this gives rise to the phenomenon known as space charge limited conduction[17] (SCLC). The space charge limited conduction shows a linear region occurs only at low bias voltages where the equation of conductivity will follow the ohm's law[26]

$$J = \mu n_0 e \frac{V}{d} \qquad 2.17$$

where e is the electronic charge, V is the voltage applied and d is the inter electrode distance or the film thickness of the insulator .Here the thickness of the film has a prominent role and J is given by

$$J = e\mu N_v \left(\frac{\varepsilon_r \varepsilon_0}{eP_k T_t} \right)^L \frac{V^{L+1}}{d^{2L+1}} \qquad 2.18$$

Here P is the trap density per unit energy range at the valence band edge, ε_o is the permittivity of the free space(8.85X10^{-12} F/M), ε is obtained by capacitance measurements, In the above equation, L = T_t/T where T is the ambient temperature and T_t is the temperature parameter describing the exponential trapping distribution. For voltages above V_c, the electron current strongly increases. The occurrence of an abrupt increase of the current at a certain critical voltage V_c is the characteristic of an insulator with traps. At this region, the current density switches to the SCLC. At higher voltages SCLC current density is given by the Mott-Gurney relation

$$J = \frac{9}{8}\varepsilon_0 \varepsilon_r \mu_p \frac{V^2}{d^3} \qquad 2.19$$

Where $\in_o \in_r$ is the permittivity of the polymer, μ_p the hole mobility and d is the thickness of the device. From the slope of the $logJ$-$log\sqrt{}$ plot we can observe that the current density J depends quadratically on the voltage V in this region which is characteristic of SCLC and after this region the quadratic dependence of J on V increases to a trap filled limit(TFL) with slope>2. The slope of the graph found in the high voltage region is about 3.The thickness dependence of the space charge limited current follows the relation $j \alpha d^{-n}$ where n is a parameter which depends on the trap distribution and is equal to or greater than three in the presence of traps. The dependence of current density on temperature is according to the relation

$$J = e\mu N_v \left(\frac{V}{d}\right) \exp\left(-\frac{E_a}{kT}\right) \qquad 2.20$$

where N_V is the effective density of states in the valence band, K is the Boltzmann constant, Ea is the activation energy

2.4.5 Hopping conduction

If two molecules are separated by a potential barrier in a metal-polymer-metal(M-I-M) structure, a carrier on one side can move to the other side either by tunneling through the barrier or by moving over the barrier via an activated state. The second process is called hopping. Though polymers are amorphous materials, short range order prevails in most of these materials, and the theory that is used to explain electronic band structure in amorphous material can be extended to the case of polymers too. If the spatial fluctuations of the interatomic distances are large, the correspondingly large and random fluctuations in the height or depth of the potential wells may lead to the localisation of states below a certain critical and well defined energy. When the carrier mobility is low and the mean free path is comparable with interatomic distance, the conduction can be expected to take place by a hopping process in the localized states. In hopping mechanism, only those carriers with an energy $\sim kT$ below the Fermi level have a significant probability of hopping. The expressions for conductivity in this case is given by[27]

$$\sigma = N(E_F)\alpha e^2 a^2 \nu_{ph} \exp\left(\frac{-w}{kT}\right) \qquad 2.21$$

where $N(E_F)$ is the density of states at the Fermi level, α is a parameter depending on the extent of overlap of localized states, e is the electronic charge , a is the number of electrons per unit volume, ν_{ph} is the phonon frequency and w is the activation energy for hopping. The conductivity thus shows exponential temperature dependence. Mott has shown that for strongly localized states, the conductivity at low temperature must follow a relationship, where b is a constant related to the hopping mechanism. At high temperatures the deviations from $T^{1/4}$ occurs, which can be understood in terms of interchain hopping. A carrier trapped in a chain, after detrapping thermally, may drift along the same chain, or may hope into an adjacent chain. In amorphous polymers the conduction occurs due to two distinct processes; a temperature dependent trap hopping and a comparatively less temperature dependent inter chain hopping in which the carriers hop from chain to chain.

2.5 Dielectric properties of plasma polymerised thin films

Dielectric constant can be evaluated by measuring the capacitance, thickness and the area of the sample using the formula, assuming a parallel plate configuration[28].

$$C = \frac{\varepsilon\varepsilon_r A}{d} \qquad 2.22$$

and the ac conductivity was then deduced from the measured dielectric loss, dielectric permittivity and frequency by employing the relation,

$$\sigma_{ac} = 2\pi f \varepsilon_0 \varepsilon_r \tan\delta \qquad 2.23$$

2.5.1 Capacitance and dielectric loss as a function of frequency and temperature

The low dielectric behaviour of ac polyaniline thin films[29] and the possibility of applying them as inter metallic dielectrics to reduce the time delay were reported. According to the basic theory of dielectric materials capacitance is frequency dependent at high temperatures and lower frequencies and

approach a constant value at higher frequencies. From the model described by Gosami[30] et al, the measured series capacitance C_s is given by the equation

$$Cs = C' + \frac{1}{\omega^2 R^2 C'} \qquad 2.24$$

this comprises of a frequency independent capacitate element C' in parallel with the resistance R , both in series with a low resistance at a frequency ω , Then the loss tangent $\tan\delta$ can be expressed as

$$\tan\delta = \frac{1 + r/R}{\omega R C'} + \omega r C' \qquad 2.25$$

where ω is the angular frequency. The thermal activation is given by

$$R = R_0 \exp\left(\frac{\Delta E}{k\mathrm{T}}\right) \qquad 2.26$$

R_0 is a constant and ΔE is the activation energy. The capacitance and the dielectric loss increases with temperature and decreases with increase in frequency.

The loss is given by the equation

$$\tan\delta = \frac{1}{\omega CR} \qquad 2.27$$

2.6 Spectroscopic ellipsometric studies

Spectroscopic ellipsometry is a sensitive technique for the determination of the dielectric functions and optical constants of thin films[31]. When plane polarized light is reflected from the surface of a material at some oblique angle of incidence, the reflected light is in general elliptically polarized. The degree of ellipticity is determined by the optical parameters *viz.* refractive index and absorption coefficient of the reflecting medium. Thus using an ellipsometer to determine the ellipticity enables a measurement of material parameters. From the ellipsometric parameters Ψ and Δ, the thin film parameters can be calculated.

Extracting useful information from ellipsometric data begins with the construction of an optical model for the polymer film on glass substrate. The optical model consists of: (i) surface roughness layer, (ii) the polymer film and (iii) the glass substrate.

The surface roughness layer in the optical model for the polymer film was analyzed with an Effective Medium Approximation (EMA)[32] model. The thickness of the polymer film was obtained by fitting the data in the highly transparent region of the spectrum using a Cauchy dispersion relation. Then the results for *n* in the transparent region obtained from Cauchy dispersion relation were used to perform a point-by-point fit starting from the transparent region, to extract approximate values of the optical functions. The error in the point-by-point fit, measured by a 90% confidence limit, was determined to check the quality of the *n* and *k* data. The optical functions thus obtained are called initial spectra and are close to the bulk dielectric response of the bulk film, free of substrate, interface, and surface roughness effects.

The initial spectrum can be fitted to a general oscillator model which uses a linear summation of Kramers-Kronig[33],[34] (KK) consistent oscillators to describe the various optical transitions. The fundamental transition can be modelled with parametric Gaussian Broadened Polynomial Superposition (GBPS) semiconductor oscillator. The electronic transitions at higher energies are also generally simulated using Gaussian oscillators. The strength, broadening and positions for these oscillators were adjusted to match the initial spectrum. In the next procedure, the expected ellipsometric parameters ψ and Δ of the multilayer structure were generated using this parametric dispersion layer in the optical model. The generated data are compared with the experimental data and fit to reduce the error using the Marquardt-Levenberg algorithm. In this procedure, the thickness and refractive index of the film are slightly adjusted. Also, non-ideal features like thickness and non-uniformity are introduced into the model to fit the depolarization measured using the auto retarder. The root mean square error (MSE) is used to quantify the difference between the experimental and predicted data. The MSE is calculated by:

$$MSE = \left\{ \frac{1}{2N - M} \sum_{i=1}^{N} \left[\left(\frac{\Psi_i^{\mathrm{mod}} - \Psi_i^{\mathrm{exp}}}{\sigma_{\Psi j}^{\mathrm{exp}}} \right)^2 + \left(\frac{\Delta_i^{\mathrm{mod}} - \Delta_i^{\mathrm{exp}}}{\sigma_{\Delta j}^{\mathrm{exp}}} \right)^2 \right] \right\}^{1/2} \qquad 2.28$$

where $\sigma_{\Psi_j,\Delta_j}^{\mathrm{exp}}$ is the standard deviation in the measured ellipsometry parameters Ψ and Δ, Ψ_i^{mod} and Δ_i^{mod} are the model generated ellipsometric parameters,

Ψ_i^{exp} and Δ_i^{exp} are the measured ellipsometry parameters , N is the number of measured parameters, and M is the number of fitted parameters. By using the experimental standard deviation as the weighting parameter in the fit, the contribution due to noise in the MSE is reduced significantly. The sequence of obtaining the point–by point fit, adjusting the oscillator strength and then fitting to reduce the MSE was repeated several times until a minimum value of MSE was obtained without significant parameter correlation. A good fit is obtained when MSE is close to unity[35].

2.6.1 Optical constants

The complex refractive index n can be represented as

$$\vec{n} = n - ik \qquad 2.29$$

where n and k represent the index of refraction (real) and the index of extinction (imaginary) respectively. The following equations can be employed for the calculation of the n and k through ellipsometric parameters Δ and Ψ and the angle of incidence φ for bare surfaces without the presence of any films or impurities at the surface.

$$n^2 - k^2 = n_0^2 \sin^2\varphi\left[1 + \frac{\tan^2\Psi\left(\cos^2 2\Psi - \sin^2\Psi \sin^2\Delta\right)}{\left(1 + \sin 2\Psi \cos\Delta\right)^2}\right] \qquad 2.30$$

and

$$2nk = \frac{n_0^2 \sin^2\varphi \tan^2\varphi \sin 4\Psi \sin\Delta}{\left(1 + \sin 2\Psi \cos\Delta\right)^2} \qquad 2.31$$

2.6.2 Dielectric constant calculation from spectroscopic ellipsometry

The complex dielectric function is given by

$$\vec{\varepsilon} = \varepsilon_1 + i\varepsilon_2 \qquad 2.32$$

where again ε_1 and ε_2 are the real and imaginary parts respectively. These values can be calculated by the equations[36,37]

$$\varepsilon_1 = n^2 - k^2 \qquad \text{and} \qquad \varepsilon_2 = 2nk \qquad 2.33$$

2.6.3 Optical conductivity

The complex optical conductivity[38] is

$$\tilde{\sigma} = \sigma_1 + i\sigma_2 \qquad 2.34$$

where σ_1 and σ_2 are real and imaginary parts, respectively and can be calculated from the values of dielectric constants.

$$\sigma_1 = \frac{\varepsilon_2 \omega}{4\pi} \text{ and } -\sigma_2 = \frac{\varepsilon_1 - 1\,\omega}{4\pi} \qquad 2.35$$

with the angular velocity $\omega = 2\pi\upsilon$ and $\upsilon = c/\lambda$ is the frequency in Hz

2.7 Nonlinear optical properties of materials

Nonlinear optics deals with various new optical effects and novel phenomena arising from interactions of intense coherent optical radiation with matter. Nonlinear optical effects could not be experimentally observed before the advent LASER, since the field strengths of conventional sources have been much too small to perturb the atomic and inter atomic fields. In terms of linear optics, the optical properties, such as the refractive index and the absorption coefficients are independent of the light intensity; the frequency of light cannot be altered by its passage through the medium; and light cannot interact with light; that is, two beams of light in the same region of a linear optical medium have no effect on each other[8].

However, after the LASERs were invented, the coherent property of the LASER beam enabled an examination of the behavior of light in optical materials at intensities higher than that in the case of conventional sources of light. Irradiation of a medium with high intensity LASER radiation is, in principle equivalent to the application of a large electric field to the material. Many experiments revealed that optical media exhibit nonlinear behavior. The following are the manifestation of the occurrence nonlinear optical property of a material.

1. The refractive index and consequently the speed of light in an optical medium does change with intensity
2. Light can alter its frequency when it passes through a nonlinear optical material
3. Light can control light; photons can be made to interact

With the advent of LASERs it is observed that the index of refraction of a material depends on the incident intensity. This phenomenon is observed for most type of materials whether they are isotropic or not. The effective index of refraction of a substance can then be described by[39]

$$n = n_0 + n_2 I \qquad 2.36$$

Where n_0 is the linear refractive index, I is the intensity of the optical beam, and n_2 is the non liner index of refraction or the second order index of refraction. The intensity is defined as the square of the time averaged electric field.

The nonlinear index of refraction gives rise to the self focusing or defocusing of the LASER beams. The time averaged electric field can be written as

$$E(t) = E(\omega)e^{-i\omega t} + Complex \quad .conjugate \qquad 2.37$$

The effective index of refraction as

$$n = n_0 + 2n_2 \left|E(\omega)\right|^2 \qquad 2.38$$

This equation implies a change in refractive index $\Delta n = 2n_2 \left|E(\omega)\right|^2$, which is called ac Kerr effect. It the refractive index of a material is changed by the application of a dc field it is known as DC Kerr effect or electro optic Kerr effect. In the polarization expansion the terms which affect the propagation of a beam of light through a nonlinear medium is

$$P(\omega) = 3\chi^{(3)} \left|E\right|^2 E \qquad 2.39$$

for a linearly polarized beam of light. Taking into account the linear and nonlinear terms the overall polarization is

$$P_{total} = \chi E + 3\chi \left|E\right|^2 E = \chi_{effective} E \qquad 2.40$$

The effective susceptibility of a medium is defined as

$$\chi_{effective} = \chi + 3\chi(\omega)\left|E\right|^2 \qquad 2.41$$

The general definition for refractive index is

$$n^2 = 1 + 4\pi\chi_{effective} \qquad 2.42$$

upon substitution we will get a relation in the form

$$\varepsilon_0 + 2n_2 \left|E(\omega)^2\right| = 1 + 4\pi\chi^{(1)} + 12\pi\chi^{(3)} \left|E(\omega)\right|^2 \qquad 2.43$$

When expanding the equation only terms up to the second power is to be retained the result will be

$$n_0 = \left(1 + 4\pi\chi^{(1)}\right)^{1/2} \qquad 2.44$$

The relation between n_2 and third order susceptibility can be obtained by solving this equation

$$n_2 = \frac{3\pi\chi^{(3)}}{n_0} \qquad 2.45$$

which is valid for a one beam type experiment. We can define the intensity as

$$I = \frac{n_0 c}{2\pi}\left|E^{(3)}\right|^2 \qquad 2.46$$

which is the averaged intensity of the optical field. Then

$$n_2 = \frac{12\pi^2\chi^{(3)}}{n_0^2 c} \qquad 2.47$$

I_s the relation between n_2 and third order susceptibility

2.7.1 Nonlinear optical absorption in polymers

The imaginary part of third order susceptibility is responsible for nonlinear absorption. Two photon absorption (TPA), saturable absorption (SA) and excited state absorption (ESA) are the most relevant types of nonlinear absorptive processes[40]. Optical transitions that involve one photon and transitions that involve two photons have different selection rules. Two photon processes involves, the simultaneous absorptions of two photons to excite a material. Saturable absorption (SA)[41] involves the saturation of a given transition, by populating an excited state of a material so that the material which initially absorbed at that wavelength becomes more transparent. Excited state absorption involves sequential proceeds in which a photon is initially absorbed and the molecule remains in an excited state for a finite length of time so that a second photon that arrives during that time is also absorbed to put the molecule into an even higher excited state. The basic difference between the two photon

and excited state transitions is that the former involve intermediate extremely short lived virtual states but the later involves intermediate real states whose life time is determined by the electronic structure of the molecules in the materials. Two photon absorption processes are dependent on the intensity of the incident light, where as excited state absorptions depends on the fluence (energy per unit area) of the incident light.

2.7.2 Nonlinear absorption by z-scan technique.

The z-scan technique is a single beam technique which allows the determination of the real and imaginary parts of the third order susceptibility. In the z-scan experiment, the transmittance of the nonlinear medium through a finite aperture in the far field is measured as a function of the sample position z- to determine the real part of the susceptibility[42]. The details of the experimental technique are given in chapter 3. In this experiment the transmittance of the nonlinear medium through a finite aperture in the far field is measured as a sample position z to determine the real part of the susceptibility. The transmittance of a nonlinear medium without an aperture is measured to determine the imaginary part of the susceptibility. The zero position for z is taken to be that of the focal plane. For a Gaussian beam (TEM_{00}) traveling in the +z direction is given by

$$E(z,r,t) = E_0(t)\frac{\omega_0}{\omega(z)}\exp\left[-\left(\frac{r^2}{\omega^2(z)}\right)-\left(\frac{ikr^2}{2R(z)}\right)\right]\exp^{-i\phi(z,t)} \quad 2.48$$

where $\omega^2(z) = \omega_0^2\left(1+z^2/z_0^2\right)$ is the beam radius, $R(z) = \left(1+z_0^2/z^2\right)$ is the radius of the curvature of the wave front at z, $z_0 = k\omega_0^2/2$ is the confocal parameter of the beam, $k = 2\pi/\lambda$ is the wave vector where λ is the LASER wavelength. If the sample length is smaller then the confocal parameter z_0, the sample can be considered as thin. Under such assumption the amplitude and the phase of an electric field as a function of z' are now governed in the slowly varying envelope approximation by a pair of differential equations.

$$\frac{d\Delta\phi}{dz'} = \Delta n(I)k \quad 2.49$$

$$\frac{dI}{dz'} = -\alpha(I)I \qquad 2.50$$

Here z' is the propagation depth in the sample. The absorption is $\alpha(I)$ is assumed to comprise linear and nonlinear absorption terms. By solving these equations we can calculate the complex electric field existing in the sample.

The normalized transmittance T(z) for measurements taken in the far field through a small aperture plotted verses the sample position exhibits a valley- peak trace for the positive refractive nonlinearity as the sample is translated across the focal plane from –z to +z and a peak–valley trace for a negative refractive nonlinearity. For large phase distortion the valley peak separation is nearly constant.

2.7.3 Theory of open aperture z-scan technique.

Nonlinear absorption of a sample is manifested in the open aperture z-scan. For example nonlinear absorption like two photo absorption (TPA) is present, it is manifested in the measurement as a transmission minimum in the focal point. On the other hand if the sample is a saturable absorber, transmission increases with increase in incident intensity and results in a transmission maximum in the focal region. It has been shown that the model originally developed by Bahae[43] *et al.* for pure TPA can also be applied to excited state absorption (ESA). ESA is a sequential TPA process, where two photons are successively absorbed.

In the absence of an aperture, transmitted light measured by the detector, in a z-scan experiment, is not sensitive to phase variation of the beam and hence it can be neglected and transmitted intensity need to be considered. The intensity dependent nonlinear absorption coefficient α(I) can be written in terms of the linear absorption coefficient α and TPA coefficient β as

$$\alpha(I) = \alpha + \beta I \qquad 2.51$$

The irradiance distribution at the exit surface of the sample can be written as

$$I_r(z,r,t) = \frac{I(z,r,t)e^{-al}}{1+q(z,r,t)} \qquad 2.52$$

where

$$q(z,r,t) = \beta I(z,r,t) L_{eff} \qquad 2.53$$

and L_{eff} is the effective length and is given in terms of the sample length *l* and the absorption coefficient α by the relation

$$L_{eff} = \frac{(1 - e^{-\alpha l})}{\alpha} \qquad 2.54$$

The total transmitted power P(z,t) is obtained by integrating the equation 2.52 over z and r. Then the equation for $I_r(r,z,t)$ and is given by

$$P(z,t) = P_1(t) e^{-\alpha l} \frac{\ln[1 + q_0(z,t)}{q_0(z,t)} \qquad 2.55$$

where $P_I(t)$ and $q_0(z,t)$ are given by the equations

$$P_I(t) = \frac{\pi \omega_o^{\,2} I_0(t)}{2} \qquad 2.56$$

$$q_0(z,t) = \frac{\beta I_0(t) L_{eff} z^2{}_0}{z^2 + z_0^{\,2}} \qquad 2.57$$

For a pulse of Gaussian temporal profile the transmission is given by

$$T(z, S = 1) = \sum_{m=0}^{\infty} \frac{\left[q_0(z,0) \right]^m}{(m+1)^{3/2}} \qquad 2.58$$

Saturable absorption (SA) occurs when the sample is excited to its resonant wavelengths. In this case, absorption in the sample decreases as input intensity is increased. Therefore, nonlinear absorption coefficient is considered as negative. SA takes place because of the depletion of the ground state population. This type of phenomenon is characterised by a parameter called saturation intensity I_s. The simplest model to explain the SA is a two level model. Assuming that SA occurs due to depletion of ground state population, steady state can be expressed by the equation[43]

$$\frac{dN}{dt} = \frac{\sigma I}{h\nu} \left(N_g - N \right) - \frac{N}{\tau} = 0 \qquad 2.59$$

Here N is the concentration of the excited sate molecules, N_g is the undepleted ground state concentration, σ is the absorption cross section, $h\nu$ is the photon energy and τ is the lifetime of the excited state. Absorption coefficient α is proportional to the ground state population which can be written as

$$\alpha = \sigma(N_g - N)$$

In the presence of SA, intensity dependent absorption coefficient[44]

$$\alpha(I) = \alpha_0 \frac{1}{1 + \frac{\sigma I}{h\nu}} = \alpha_0 \frac{1}{1 + I/I_s} \qquad 2.60$$

where $\frac{h\nu}{\sigma\tau} = I_s$, the saturation intensity and $\alpha_0 = \sigma N_g$. The case described by equation 2.60 is often referred to as homogeneous saturation .The presence of a bimolecular recombination of excited species will modify this equation. In the case of a two-level system with in homogeneously broadened states and hole burning, it has been found that the saturation can be described by the equation[45]

$$\alpha(I) = \alpha_0 \frac{1}{(1 + I/I_s)^{0.5}} \qquad 2.61$$

It can be seen that, (α / I_s) can be considered as equivalent to the TPA coefficient β. To a good approximation in the case of SA, (α / I_s) gives the nonlinear absorption coefficient. From the measured β value the imaginary part of the third order optical susceptibility can be calculated from the equation[45]

$$\mathrm{Im}[\chi^{(3)}] = \frac{\lambda \varepsilon_0 n^2 c \beta}{4\pi} \qquad 2.62$$

References

[1] Erica E.Johnston, Buddy D Ratner, *Journal of Electron Spectroscopy and Related Phenomena*. **81**,(1996) 303

[2] L.S.Hung, L.R.Zheng, and M.G.Mason, *Appl.Phys.Lett.* **78**, (2001),673

[3] R.Claude and M.Moisan, M.R.Wertheimer, Z.Zakrzewski, *Appl.Phys.Lett*, **50**,(1987),1797

[4] Yasuda H, *Plasma Polymerization*, Academic Press, (1985), Orlando.

[5] Donglu Shi, Peng He, *Rev. Adv. Mater. Sci.* , **7**, (2004), 97

[6] Donglu Shi S.XWang, Wim J.van Ooji, L.M.Wang,Jiangang Zhao and Zhou, Yu, *Appl. Phys. Lett*., **78**, (2001), 1243

[7] Seung J.Choi, and Mark J.Kushner, *IEEE transactions on Plasma Science*, **2**,(1994),138

[8] Donald L.Wise, Gary E.Wnek, Debra J.Trantalo, Thomas M.Cooper, Joseph D.Gresser, *Photonic Polymer Systems*, Markel Dekker, 1998, New York (book)

[9] S.Chakrabarti, D.Ganguli, S.Chodhuri, *Physica*, **E ,24**,(2004),333

[10] A.Irribarren, R.Castro-Rodriguez, V.Sosa, J.L.Pena, *Phys.Rev.**B***, **58**,(1998),1907

[11] K.Saito, and A.J Ikushima, *Phys.Rev.***B**,**62,**(2000),8584

[12] G.D.Cody,T.Tiedje, B.Abeles,B.Brooks, and Y.Golstein, *Phys,Rev.Lett*, **47**,(1981),1480

[13] D.S.Galvao, D.A.dos Santos,B.Laks, C.P.de Melo, M.J.Caldas, *Phys.Rev.Let*, **63**,(1989),786

[14] W.Sritrakool and V.Sa-yakanit, H.R.Glyde, *Phys.Rev.**B***, (1986),1199

[15] A.Gosami, *Thin Film Fundamentals*, New Age International Ltd, (1996), New Delhi,

[16] D.R Lamb, *Electrical Conduction Mechanism in Thin Insulating Films*, Methuens Monographs, Methun and Co Ltd, (1967)

[17] R.H.Fowler,L.Nordheim,*Proc.Roy.Soc.London*, **A,119**,(1928),73

[18] C.Joseph Mathai, S.Saravanan, , S.Jayalekshmi, S.Venkitachalam, M.R.Anantharaman, *Material Letters*, **57**,(2003),2257

[19] D.Sakthikumar,Kenji Nakamura, Satoko Nishiyama, Shingeru Ishii,Hiromichi Noguchi, Kunihiro Kashiwagi,and Yasuhino Yoshida, *J. Appl.Phys.* **93**,(2003),2705

[20] M.S.Silverstein,I.Visoly Fisher, *Polymer,***43**,(2002),11

[21] C.Joseph Mathai, M.R.Anantharaman, S.Venkitachalam, S.Jayalekshmi,*Thin Solid Films,* **16**, (2002), 10

[22] D.Sakthi Kumar, Kenji Nakamura, Satoko Nishiyama, Hiromichi Noguchi,Shigeru Ishii, Kunihiro Kashiwagi, Yasuhiko Yoshida, *J.Appl.Polymer Sci,* **90**,(2003), 1102

[23] W. Schottky,*Physik.Z*,**15**,(1914),872

[24] S.R.Pollack, *J.Appl.Phys*,**34**,(1963),877

[25] J.Frenkel, *Phys. Rev.* **128**,(1962),2088

[26] P.W.M.Blom,M.J.M.de Jong, and J.J.M.Vleggaar, Appl.Phys.Lett., **68**, (1996), 3308

[27] N.F.Mott, *Phil.Mag*.,**19**,(1969),835

[28] S.Saravanan, C.Joseph Mathai, S.Venkitachalam, M.R.Anantharaman, *New J.Phys,* **6**,(2004),64

[29] C.Joseph Mathai, S.Saravanan, M.R.Anantharaman, S.Venkitachalam, S.Jayalekshmi, *J.Phys.D.Appl.Phys.* **35**,(2002),240

[30] Gosami. A and Gosami A.P, *Thin Solid Films,* **16**, (1973),175

[31] L.Levesque, *Phys.Educ*, **35**, (2000), 359

[32] A.Fontcuberta I Morral and P.Roca J Cabarrocas and C.Clare, *Phys.Rev.***B** **69**,(2004),125307

---

[33] H.Fujiwara, Joohyun Koh, P.I.Rovira,and R.W Collins, *Phys.Rev.***B**,61(2000),10832
[34] C.Kittel, *Introduction to Solid State Physics*. 7th Ed. Chapter 11
[35] P.D Paulson, B E Mc Candless, R W Birkmire, *J.Appl.Phys*, **95**. (2004), 3010
[36] M.Tammer,R.W.T Higgins, A.P.Monkman, *J.Appl.Phys*, **91**,(2002),4010
[37] I.H.Campbell, D.L.Smith and J.P.Ferraris, *Appl.Phys.Lett*,**66**(1995),1175
[38] Kwanghee Lee, Reghu Menon, C.O.Yoon, and A.J.Heeger, *Phys.Rev.***B**, **52**,(1995),4779
[39] R.W,Boyd, Nonlinear Optics, Academic Press,(1993), New York
[40] K.P.Unnikrishnan, *Ph.D Thesis*, Cochin University of Science and Technology, 2003, India
[41] Takashige Omatsu, Naoyuki Hayashi, Hirofumi Watanabe, Akira Hasegawa,and Mistsuhiro Tadeda, *Optics Letters*, **23**,(1998),1432
[42] Mansoor Sheik-Bahae,Ali A.Said, Tai-Huei Wei, David J.Hagan, E.W.Van Stryland, *IEEE J. Quantum Electr.* **26**,(1990),760
[43] Tai-Huei Wei, Tzer-Hsiang Huang, Huang-Der Lin, and Sheng-Hsien Lin, *Appl.Phys.Lett.***67**,(1995),2266
[44] K.P.Unnikrishnan,J.Thomas,V.P.N.Nampoori, C.P.G.Vallabhan, *Appl.Phys.**B*** **75**,(2002),871
[45] M.Samoc, A.Samoc, B.L.Davies, H Hasai,H Reisch and U. Scherf. *Optics Letters*, **23**,(1998),1295

Chapter 3

Experimental Techniques

This chapter deals with the experimental techniques adopted during the present investigation. This includes the experimental methods employed for the preparation of plasma polymer thin films as well as various analytical tools for the characterisation at various stages. The techniques used for the preparation of thin film layers are rf and ac plasma polymerization. The rf plasma polymerization set up is modified for the deposition of ultra thin organic layers on alumina and iron oxide nanoparticles of different sizes. The characterization techniques such as low and high temperature dc conductivity, dielectric measurements, UV-Vis-NIR spectroscopy are employed for the measurement of optical absorption and band gap. The optical and dielectric parameters of polyaniline thin films are determined by spectroscopic ellipsometry (SE) and the non linear optical properties of the thin films were measured by open aperture z-scan technique.

This chapter is divided into two sections, Part I describes the preparation techniques of thin films, doping, preparation of thin films for thickness measurements, conductivity/dielectric measurements, ITO-polymer-Metal thin films structures for photoconductivity measurements, preparation of nanocomposites and passivation of their surface by rf plasma polymerisation and size reduction of the particles by high energy ball milling. Part II of this chapter describes various methods of characterisation employed at various stages.

Part I: Preparation of Samples

3.1 RF Plasma polymerisation for the preparation of polymer thin films

Plasma polymerised thin films from different monomer precursors were prepared by employing RF plasma polymerization technique[1,2]. It consists of a glass tube of length 50 cm and diameter around 8 cm, with provisions for admitting monomer vapours dopants for evacuation. A schematic of the experimental setup is shown in figure 3.1. Chemically and ultrasonically cleaned

glass substrates were placed inside the glass tube exactly under the space separated by the aluminum foil electrodes, which are capacitively coupled and wrapped around the glass tube, separated by a distance of 5 cm.

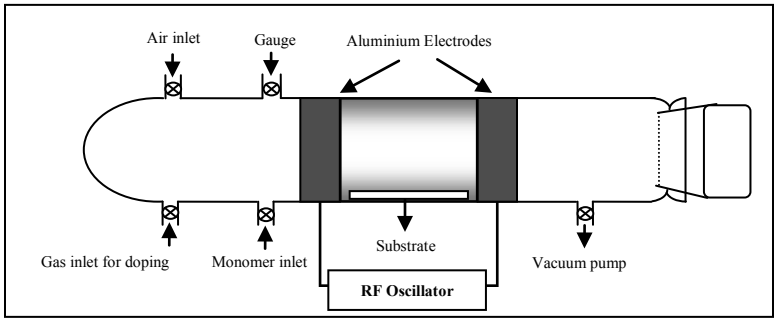

Figure 3.1: RF plasma polymerisation setup for the preparation of polymer thin films.

The chamber was evacuated and the monomer is allowed to get into the chamber. A glow discharge was obtained in between the electrodes by applying a radio frequency (rf) 9-13.5 MHz at a current of 60-80 mA. The flow rate of the monomer into the deposition cell is controlled by a needle valve and the deposition conditions were optimised. The monomer vapour pressure is maintained at 0.2 Torr. It has been found that good quality films can be obtained by optimising parameters like input power, pressure and temperature inside the chamber, monomer current, dimension of the glass chamber used for the plasma polymerisation, distance between the electrodes etc. Sandwiched films with metal electrodes were also fabricated and were employed for the studies involving conductivity and dielectric measurements.

3.2 AC plasma polymerisation technique

A schematic of the ac plasma polymerisation[3,4] unit for the preparation of polymer thin films is shown in figure 3.2. It consists of two parallel stainless steel electrodes of diameter 0.23m each and $2x10^{-3}$ m thick, which are 0.05 m apart. Chemically and ultrasonically cleaned glass substrates on which polymer films are to be deposited are kept on the lower stainless steel electrodes.

To obtain a sandwich type configuration, the glass substrates are pre-coated with Al/Au/Ag or purchased ITO electrodes and are masked appropriately so as to deposit the polymer film on a specific area. The whole set up is evacuated to 10^{-3} Torr by a rotary pump and the monomer is sprayed between the two electrodes by

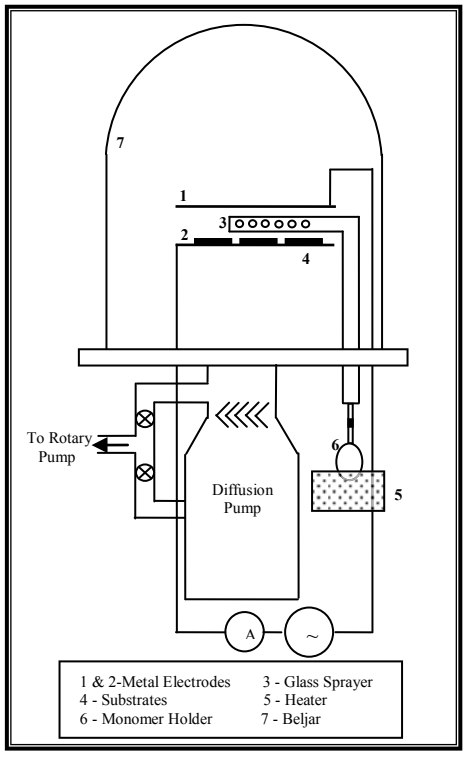

Figure 3.2: AC plasma polymerisation setup

means of a sprayer. By adjusting the roughing valve, the pressure inside the chamber is maintained at 0.08-0.2 Torr. Plasma discharge is obtained between the electrodes by applying a high ac voltage of 500-800 V by a step up transformer controlled by a current of 40-70 mA. Monomers introduced into the plasma are fragmented into small activated fragments called radicals and then the activated radicals are recombined. By repeated fragmentation and recombination larger molecules are formed and finally polymers are deposited

on the glass substrates kept on the lower electrode. The thickness of the films deposited on the glass substrates is controlled by the time of deposition. Parameters like input power, monomer flow rate and the time of polymerization can be varied to obtain polymer thin films with specific properties.

3.3 Insitu iodine doping of polymer thin films

Various electrical, optical and dielectric properties of polymers can be modified by doping. Incorporation of iodine is found to modify these properties. In this investigation doping of iodine is carried out *insitu* which ensures stability of iodine in the polymer matrix. The insitu doping of iodine is conducted using ac and rf both plasma polymerisation techniques. The iodine vapour is fed through the rf/ac plasma polymerisation chamber by means of a separate inlet in a controlled manner such that the introduction of the iodine vapor does not affect the pressure in the vacuum chamber. After deposition, the films are kept at a temperature of 330 K to expel the unreacted iodine from the film surface. The advantage of this method is that, the doped films are very stable.

3.4. Preparation of sandwich structures for conductivity and dielectric measurements.

The electrical conductivity as well as the dielectric properties of plasma polymer thin films is evaluated by employing a sandwich configuration having a metal-polymer-metal (M-P-M) structure. For this, pre-coated glass substrates

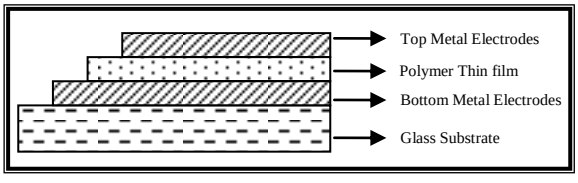

Figure 3.3 Cross sectional view of Metal-polymer-metal sandwich structure

with metal electrodes are coated with thin films and the top electrode is deposited on the polymer layer. The deposition of Al/Ag/Au thin films for preparing electrodes is made by vacuum evaporation in an ***Indovision -*** Vacuum evaporation Unit at a pressure of 10^{-5} Torr.

Suitably masked glass substrates are placed on the sample holder of the vacuum evaporation. The J-V Characteristics were studied in the sandwich configuration of M-P-M structure with an effective area 2.5×10^{-5} m^2. The lower and upper aluminum electrodes (99.99% pure) were deposited on to the glass substrate and the sample respectively.

Figure 3.3 shows the cross sectional view of a metal-polymer-metal sandwich structure on a glass substrate. The various steps involved in the fabrication of a sandwich layer of thin films are the following.

1. Appropriate masking of ultrasonically cleaned glass substrate
2. Vacuum evaporation to get a metal film of suitable thickness
3. By masking, expose only a part of the electrode for polymer film deposition
4. Vacuum evaporation of counter electrode.

In the case of ITO-polymer- Metal thin film deposition since the glass substrate is uniformly coated with ITO, a part of the film is masked to avoid the polymer deposition, and after polymer deposition a counter electrode is deposited by masking the exposed ITO portion and a part of the polymer layer.

The thickness of the electrode can be approximately estimated by the general formula $t = \frac{m}{2\pi\rho r^2}$, where r- is the source substrate distance, t- thickness of the film to be coated, ρ- density of the coating material, m-mass of the metal taken for evaporation.

3.5 Synthesis of magnetic nanoparticles by sol-gel method for surface modification by plasma polymerisation.

Pure γ-Fe_2O_3 nanoparticles were synthesized from the precursors of ferric nitrate Fe $(NO_3)_3.9H_2O$ (AR Grade) and ethylene glycol. Ethylene glycol is added to ferric nitrate and the solution is evaporated at a temperature of 70^oC. The product was finally gelated at an elevated temperature. This procedure was employed for the preparation of γ-Fe_2O_3 nanoparticles. The particle size of the above samples was reduced further by a '***Fritsch***

pulverisette P-7 planetary micro mill for different milling time. Nickel Ferrite nanoparticles were prepared by coprecipitation method and the preparation technique is described in the reference[5] .

3.6 Surface modification using plasma polymerization

The existing plasma polymerization set was modified for the surface modification of inorganic materials by organic coating[6]. The set up consists of the following elements.

1. Electric power source for the initiation and maintenance of glow discharge
2. Reaction chamber
3. Vacuum system

Control system of the monomer vapour flow the radio frequency plasma polymerization set up incorporates the deposition chamber, made up of borosilicate glass tube of about 0.5 m in length and of 0.035 m in diameter. The set up is evacuated to a pressure of about 10^{-2} Torr by using a vane type rotary pump with a pumping speed of 100 lit/min. The amplified output of an RF oscillator, constructed by using RCA 807 tetrodes, is capacitively coupled to the discharge tube, by means of two copper foils wrapped around the glass tube[7]. The plasma is produced in between the electrodes and the monomer is sprayed into the plasma discharge through a vacuum stopcock and a needle valve. The monomer gets polymerised inside the chamber and gets deposited on the nanoparticles surfaces stirred inside the bottom of a container connected to the bottom of the discharge tube.

A magnetic stirrer was used to stir the γ-Fe_2O_3 powder during the plasma polymerisation process. Nanoparticles of specific size are vigorously stirred in the glass container connected to the bottom of the glass tube in such a manner that the surface of the nanoparticles can be continuously renewed and exposed to the plasma for polymer deposition during the plasma polymerisation process. The particles of all the four different sizes, prepared by ball milling were also provided with a polymer coating of polyaniline by using the above

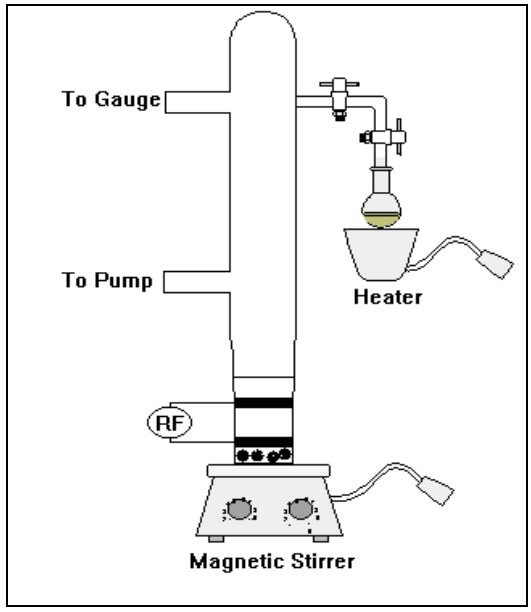

Figure 3.4: RF Plasma polymerization setup for surface modification of nanoparticles

technique. The nanoparticles belonging to the series $Ni_xFe_{1-x}Fe_2O_4$ were coated with polyaniline by this technique. This is then compacted by a pelletizer.

Part II: Characterisation techniques

3.7 Film thickness measurements.

3.7.1 Tolansky multiple beam interferrometry

Film thickness is estimated by employing tolansky multiple beam interferrometry[3]. The principle of this method is that when reflecting surfaces when brought to close proximity with a partially reflecting one, interference fringes are produced and from the measurements of the shifts and spacing of the fringes, the absolute film thickness can be calculated.

The experimental setup is shown in figure. Mercury vapour lamp with a green filter is used as the monochromatic source of light. Monochromatic light from the filter after collimation is made to fall on a glass plate, kept at an angle 45^0 with the incoming beam, so that the portion of light is reflected vertically

downward to the thin film sample holder assembly. The details are shown in figure.

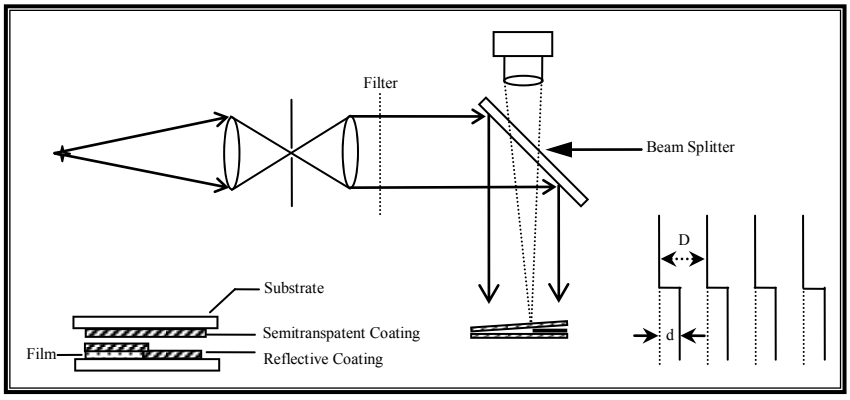

Figure 3.5: Setup for Tolannsky multiple beam interferrometry

The film whose thickness is to be measured is deposited on a glass substrate. The film is deposited with masks such that it will form a step on the glass substrate. A reflecting aluminum film is coated over the partially deposited polymer film. A semi reflecting film is placed above the film as shown in fig. and both these films are placed in the sample holder assembly. An air wedge is formed between the two surfaces and the distance can be altered to get a well defined system of fringes by adjusting the screws attached to the sample holder assembly. The displacement of the fringes at the film edge can be clearly observed through the vernier microscope. The readings for fringe shift and space can be evaluated. Then the film thickness is given by the formula

$$t = \frac{fringe\ \ shift\,(d)}{fringe\ \ spacing\ \ (D)}\,\frac{\lambda}{2}$$

where λ is the wavelength of the monochromatic light used. The entire experimental assembly for the measurements of thickness was fabricated in the laboratory.

3.7.2 Film thickness by thickness profiler

The film thickness is also calculated using ***Dektak 6M*** Thickness Profiler. The block diagram of the instrument is shown in figure 3.6

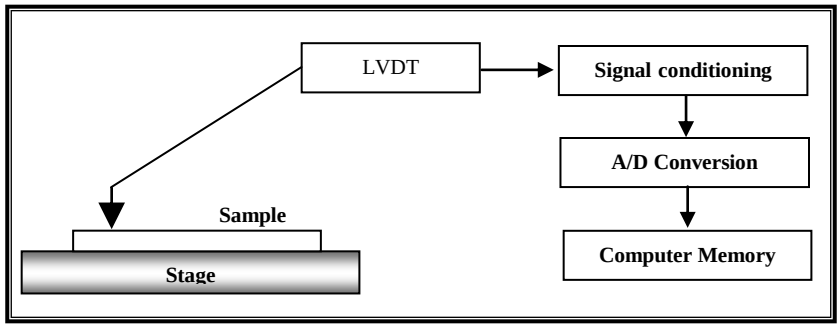

Figure 3.6: Block diagram of Dektak 6M stylus Profiler

Using this instrument thickness and the surface roughness of the films can be evaluated. The measurements are taken electromechanically by moving the sample beneath a diamond tipped stylus. The high-precision stage moves a sample beneath the stylus according to a user programmed scan length, speed and stylus force. The stylus is mechanically coupled to the core of an LVDT (Linear Variable Differential Transformer.)

As the stage moves the sample, the stylus rides over the sample surface. Sample variation causes the stylus to be transformed vertically. Electrical signals corresponding to stylus to movements are produced as core position of the LVDT changes. The LVDT changes the sample reference signal proportional to the position change, which is conditioned and converted to a digital format, through a high precession, integrating, analog-to-digital converter. The digitized signals obtained from a single scan are stored in a computer memory for display, manipulation and measurement.

3.8 Optical absorption studies using UV-Vis-NIR Spectroscopy

The absorption spectrum was recorded by a JASCO ***V-570***, spectrophotometer.

Light from the source is made to fall on a grating .The grating is made to rotate about an axis in such a way that the angle of incidence of the light beam from the source gradually changes. The output beam from the grating will contain different wavelengths, which are spatially separated. At a particular angle of the grating, only one wavelength will pass through the slit such that the output from the slit will be monochromatic. Different wavelengths are obtained in accordance with different angles of incidence. This beam is split by means of a beam splitter. One of the beams passes through the reference and the other beam passes through the sample for which the absorption is to be recorded. The phase and intensity of the transmitted beams from both the reference and the sample are detected (Radiation in the UV-visible region is detected using a PMT and that in the NIR region by a PbS crystal detector). By comparing these data using a phase sensitive amplifier the absorption spectrum of the sample is displayed and recorded.

The ultra-violet region is subdivided into two spectral regions. The range between 2000 and 4000 Å is referred to as the near ultra violet region. The region below 2000Å is called the far or vacuum ultra violet region.

There are two classes of spectra, namely emission and absorption spectra. An emission spectrum is obtained by analysing the light emitted by a luminous source. An absorption spectrum is obtained by the spectroscopic analysis of the light transmitted by an absorbing medium, which is placed between the light source and the detector. When light is incident on a sample, absorption takes place inside depending on the energy hν of the incident light and energy band gap (E_g) of the material[8]. When $h\nu < E_g$, the light passes through the material with little absorption. As the energy of the irradiation increases such that $h\nu \sim E_g$, a sharp increase or a rise in the absorption takes place.

The absorption coefficient is calculated from the spectrum by dividing the αd value by the thickness and it is plotted against the photon energy for pure and iodine-doped polymer thin films. The intercept of this plot on the photon energy axis gives the band gap of the polymer. The probable energies for the transitions were estimated from the Tauc plot by plotting the $(\alpha h\nu)^{1/2}$ vs $h\nu$ graphs. This graph is called Mott plot[9], here we assumes that the transition is indirect.

3.9 FTIR Analysis

The structural analysis of the thin films was carried out by recording the Fourier Transform Infra Red spectra using a ***Nicolet Avatar, 360 ESP-FTIR Spectrophotometer*** from 400 cm^{-1} to 4000 cm^{-1}.

FTIR stands for Fourier Transform Infrared, the preferred method of infrared spectroscopy. Infrared spectroscopy is a useful technique for characterizing materials and obtaining information on the molecular structure, dynamics and environment of a compound. In an infrared spectrum the absorption or transmittance peaks correspond to the frequencies of vibrations between the bonds of the atoms making up the material. From the characteristic peaks, different functional groups present in the compound can be identified. This aspect makes infrared spectroscopy quite useful in material characterization. A schematic diagram of an FTIR instrument is as shown in figure 3.7

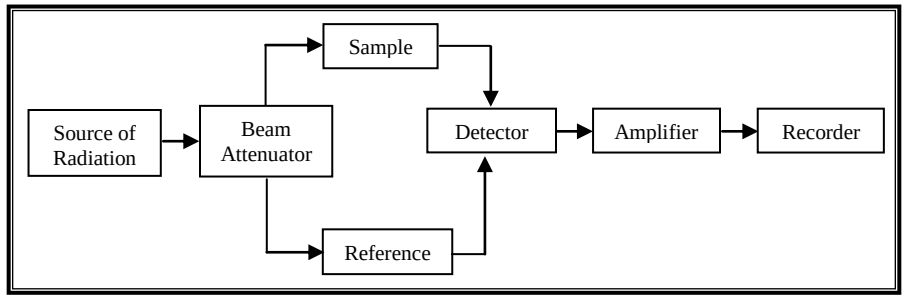

Figure 3.7: Schematic Diagram of FTIR Spectrophotometer.

3.10 TEM and AFM Analysis

A Joel JEM 2200 FS electron microscope (TEM) using an accelerating voltage of 200kV was used to characterise the morphologies and particle size distribution of nanoparticle, and AFM is taken by a Digital Nanoscope Instrument II.

3.11 Dielectric and impedance measurements

3.11.1 The cell for measuring the dielectric constant and ac conductivity

The schematic design of the cell employed for the electrical measurements is given in figure 3.9. The cell is made up of mild steel with a cylindrical stem having provisions for fixing various attachments such as electrical connections and vacuum gauges. The cell is connected to a rotary pump to maintain a pressure of 10^{-2} Torr inside the chamber. The inner diameter of the cell is about 18cm, and has a length of 30cm. The sample holder is fixed at the bottom of a one-end closed metallic tube to be embedded to the top flange. For the electrical conductivity and dielectric measurements the thin film sample is spring loaded to a sample holder and inserted into the conductivity cell

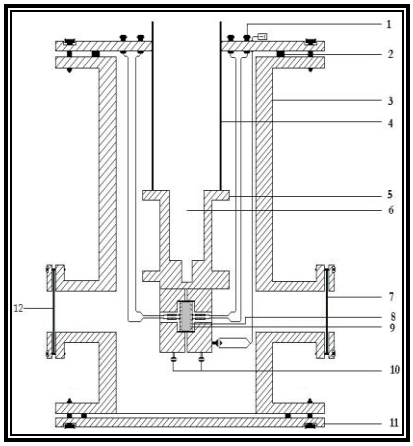

1. BNC
2. Neoprine O ring
3. MS Chamber
4. SS Pipe
5. Sample Holder
6. Liquid Nitrogen Cavity
7. Glass Window
8. Metal Electrodes
9. Sample
10. Heating Filament
11. MS Flange
12. To Vacuum Pump

Figure 3.8: Cell for the dielectric and conductivity measurements.

For bulk samples pellets are mounted on the sample holder consisting of two copper disc electrodes in between which the pelletised samples are loaded. The sample holder can be heated using a temperature-controlled heater. The details of the dielectric/conductivity cells are depicted in figure 3.8.

3.11.2 Method of measurements of dielectric constant and ac conductivity

The dielectric constant measurements of the samples at low and high frequencies, *viz*, from a few Hz to 8MHz were carried out by a Hewlett Packard 4192A LCR meter which is automated and controlled by a virtual instrumentation package called LAB View supplied by National Instruments. The temperature variation studies are also carried out. The theory involved in estimating the ac conductivity are described elsewhere[10].

The dielectric constant of the sample can be calculated using the equation

$$\varepsilon_r = C\, d\, /\varepsilon_0 A \qquad 3.1$$

and the ac conductivity by the formula,

$$\sigma_{ac} = 2\pi\, f\, \varepsilon_0\, \varepsilon_r \tan\delta, \qquad 3.2$$

Where $\tan\delta$ is the loss factor.

In addition to the dielectric measurements, the complex ac impedence Z is also be calculated for the thin films at room temperature, in the $|Z|/|Y|$ mode. In this measurement the complex impedance and the phase is obtained and Z can be expressed as $Z = Z' - jZ''$ with Z' is the real and Z'' is the imaginary parts. For a pure capacitor with capacitance C the impedance is given by[11],

$$\log Z'' = -\log 2\pi C - \log f \qquad 3.3$$

Where ω is angular frequency of the ac signal used in the impedence measurement. Thus the $1/f$ dependence of the Z'' vs. Z' .where ω is the angular frequency of the ac signal used in the impedance measurement. The theoretical description and the model for the dielectric and impedance measurements are already provided in chapter 2.

3.12 DC conductivity measurements

For the measurement of electrical conductivity of thin films the metal-polymer-metal sandwich samples are placed in a home made conductivity cell to investigate the dependence of current density on voltage and temperature. A bias voltage in the range 1-60 V (step 0.5 V-interval 0.5 s between two measurements) is applied and the current flowing through the films was measured using an automated Keithley 236 SMU Source Measurement Unit. (This voltage range and step is changed for different samples), to enable measurements, the samples were loaded in a conductivity cell which is evacuated with a diffusion pump to a vacuum of 2x 10^{-5} Torr. The SMU was automated to a data acquisition system using Interactive Characterization Software (ICS) Version 3.4.1 developed by Metrics Technology Inc. (1997).

To measure the conductivity of the polymer nanocomposites, pelletised surface modified nanocomposites of the samples are placed in the home built conductivity cell in which the temperature can be varied from 300 K to 423 K by a digital temperature controller and the temperature is measured by a Fe-K thermocouple kept on the sample. A bias voltage in the range 0-60V is applied and the current flowing across the sample is measured under dynamic vacuum conditions as explained above.

3.13 Spectroscopic Ellipsometry measurements

3.13.1 Principles of the Method

Spectroscopic Ellipsometry measures the change in polarization state of light reflected from the surface of a sample. The measured values are expressed as $\Psi$and Δ. These values are related to the ratio of Fresnel reflection coefficients, R_p and R_s for *p* and *s*-polarized light, respectively.

$$\tan(\Psi)e^{i\Delta} = \frac{R_p}{Rs} \qquad 3.4$$

Because ellipsometry measures the ratio of two values, it can be highly accurate and very reproducible The ratio is seen to be a complex number, thus it contains "phase" information contained in Δ, which makes the measurement very sensitive. A linearly polarized input beam is converted to an elliptically

polarized reflected beam. For any angle of incidence greater than 0° and less than 90°, *p*-polarized light and*s*-polarized will be reflected differently. A schematic of the experimental setup is shown in figure 3.11

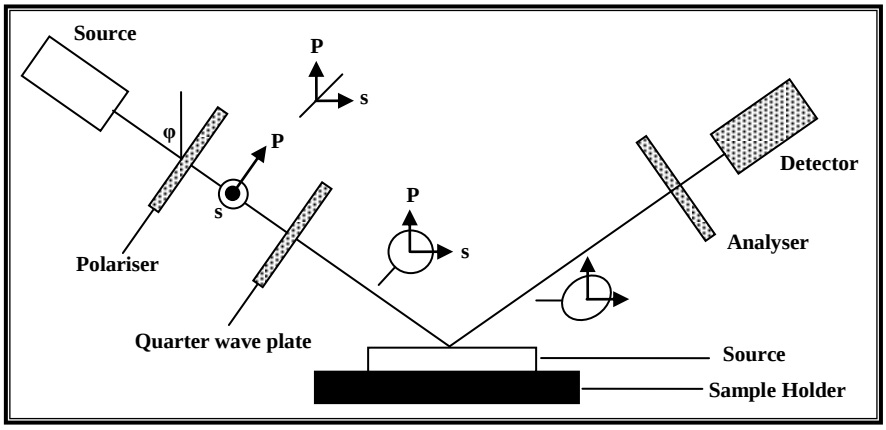

Figure 3.9: Schematic of the geometry of an ellipsometry experiment.

The coordinate system used to describe the ellipse of polarization is the *p*-*s* coordinate system. The *s*-direction is taken to be perpendicular to the direction of propagation and parallel to the sample surface. The *p*-direction is taken to be perpendicular to the direction of propagation and contained in the plane of incidence.

3.13.2 Determination of optical constants

The optical constants define how light interacts with a material. The complex refractive index is a representation of the optical constants of a material, it is represented by

$$\tilde{n} = n + ik \qquad 3.5$$

The real part or index of refraction, *n*, defines the phase velocity of light in material $v = c / n$, where *v* is the speed of light in the material and *c* is the speed of light in vacuum. The imaginary part or extinction coefficient, *k*, determines how fast the amplitude of the wave decreases. The extinction coefficient is directly related to the absorption of a material and is related to the absorption coefficient by:

$$\alpha = \frac{4\pi k}{\lambda} \qquad 3.6$$

The characterization of the optical constants and thickness of thin films prepared by plasma polymerisation is a major part of our research, and Ellipsometry is the primary method of determining these quantities. The instrument used is a Variable Angle Spectroscopic Ellipsometer (VASE©) ellipsometer made by J.A. Woollam Co. Ellipsometry is sensitive to several material characteristics, such as

- Layer thickness
- Optical constants (refractive index and extinction coefficient)
- Surface roughness
- Composition and
- Optical anisotropy

3.13.3 Experimental conditions

Spectroscopic Ellipsometric measurements were carried out using a J.A. Woollam variable angle spectroscopic ellipsometer (VASE)[12]. The VASE is a rotating analyzer ellipsometer equipped with an auto-retarder, which is useful in measuring the depolarization caused by reflection from the glass backside and thickness non-uniformity. Measurements were carried out at room temperature immediately after peeling with the sample under argon flow to reduce possible surface contamination. VASE measurements were carried out between 0.725 eV to 4.6 eV with an energy step of 12.5 meV energy step. The data acquisition and modeling were performed with the help of WVASE 32™ software supplied by J. A. Woollam Company. The Optical modeling and the related theoretical details are provided in chapter 2.

3.14 The z-scan experiment

3.14.1 The z-scan experimental setup

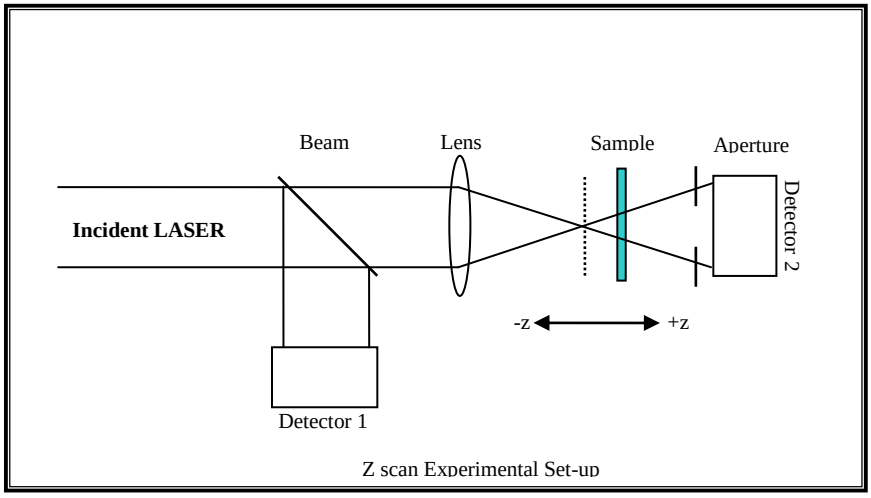

Figure 3.10: Z- scan set up.

This technique is used to study the non linear optical properties of plasma polymer thin films[13]. The z-scan technique was originally introduced by Sheik Bahae[14] et.al which is a sensitive and single beam technique to measure the sign and magnitude of the real and imaginary parts of the third order nonlinear. Susceptibility, $\chi^{(3)}$, in the original experiment the transmittance of the sample is measured , as the sample is moved along the propagation direction of a focused Gaussian laser beam. A laser beam propagating through a nonlinear medium will experience both amplitude and phase variations. The figure 3.10 shows the experimental setup for the z-scan measurement.

In a typical experimental setup, a lens initially focuses a laser beam with a transverse Gaussian profile. The sample, the thickness of which is kept less than the Rayleigh range, is then moved along the axial direction of the focused beam in such a way that it moves away from the lens, passing through the focal point. At the focal point, the sample experiences the maximum pump intensity, which will progressively decrease in either direction of motion from the focus. A suitable light detector is placed in the far field and the transmitted intensity is measured as a function of the position of the sample, to obtain the open aperture z-scan curve. Then an aperture of suitable S value is placed closely in

front of the detector, and the experiment is repeated to obtain the closed aperture z-scan. The absorptive nonlinearity is first determined from the open aperture data, and then the refractive nonlinearity can be determined from the closed aperture data. In the present study the open aperture z-scan is performed.

3.14.2 Open aperture z-scan

Nonlinear absorption of a sample is manifested in the open aperture z-scan measurements. For example if non linear absorption like two photon absorption (TPA), it is manifested in the measurements as a transmission minimum at the focal points. If the sample is a saturable absorption (SA), transmission increases with increase in incident intensity and results in a transmission maximum at the focal region. In materials arising from either direct multiphoton absorption, saturation of the single photon absorption, or dynamic free carrier absorption have strong effects on the measurements of non linear refraction using the z-scan technique. Clearly, even with nonlinear absorption, a z-scan with a fully opened aperture (S=1) is insensitive to non-linear refraction.

In the Open Aperture z-scan Technique, the sample transmission for different z values is measured as before, but the aperture is removed from the set up. The absorptive non-linearity will be a maximum at the focal plane. For example, in the case of two-photon absorption, the transmittance will be a minimum and in the case of saturable absorption, the transmittance will be a maximum. The open aperture z-scan curve is symmetrical about the focus (z=0).

3.14.3 The instrument specifications used in z-scan

Specifications of the laser sources, photodiodes and laser energy meters used for making the Z-scan measurements are given below.

Pulsed Nd:YAG laser

Model and make	:Quantaray GCR. GCR:170
Wavelength	:532 nm
Pulse energy (maximum)	:450 mJ
Pulse width	:6-7 ns
Pulse repetition frequency	:10 Hz

Spatial Mode	:Gaussian (70%)
Photo diodes	
Model and make	: New port 818 UV
Spectral range	: 190-1100nm
Active area	: 0.1 cm^2
Model and make	: Melles Griot, 13 Das 007
Active area	:0.1 cm^2
Spectral range	: 350-1100nm
Breakdown voltage	:20 V
Dark current (at 1V)	:10nA
Energy meter	:Rjp-7620 Energy ratio meter
Detector head (pyrro electric)	: Rjp-735

3.15 Structural Characterisation of nanoparticles by X-Ray Diffraction

The structural analysis of the nanoparticles analysis is based in X-ray diffraction measurements. The XRD spectrums of the samples were recorded on the X-ray diffractometer (Rigaku Dmax-C) using Cu Kα radiation (λ=1.5406Å), which has energy of 8.04keV.

Lattice parameter was calculated assuming cubic symmetry by employing the relation[15]

$$d_{h,k,l} = \frac{a}{\sqrt{h^2 + k^2 + l^2}} \qquad 3.7$$

The lattice parameter 'a' can be calculated from the equation

$$a = \frac{\lambda}{2 Sin\,\theta}\sqrt{h^2 + k^2 + l^2} \qquad 3.8$$

The average particle size was determined from the measured width of their diffraction curves by using Debye Scherrer's formula.

$$D = \frac{0.9\lambda}{\beta \cos \theta} \qquad 3.9$$

Here λ is the wavelength of Cu K_α radiation (λ = 1.5406Å), β is the angular width which is equal to the full width half maximum[i]

[i] The Spectroscopic Ellipsometry measurements were carried out at, Institute of Energy Conversion, University of Delaware, USA.

ii The Z-Scan measurements were carried out at International School of Photonics, Cochin University of Science and Technology, Cochin-22

References

[1] S.Saravanan, *Ph.D Thesis*, Cochin University of Science and Technology, 2003, India

[2] S.Saravan, C.Joseph Mathai, S.Venkatachalam, M.R.Anantharaman, *New J.Phys,* **6**,(2004), 64

[3] C.Joseph Mathai, *Ph.D Thesis*, Cochin University of Science and Technology, 2002, India

[4] Joseph Mathai.C, Anantharaman.M.R,. Saravanan.S, Venkitachalam.S, Jayalekshmi. S, , *J.Phys.D, Appl. Phys*.**35**, (2002), 240

[5] V.S. Abraham, S. Swapna Nair, S. Rajesh**,** U.S Sajeev and M.R Anantharaman, *Bull. Mater. Science,* **27** (2), 2004,

[6] Vijutha Sunny, T.N.Narayanan, U.S.Sajeev, P.A.Joy, D.Sakthi Kumar, Yasuhiko Yoshida, and M.R.Anantharaman, *Nanotechnology,* accepted for Publication (2006)

[7] D.Sakthi Kumar, *Ph.D Thesis* , Mahatma Gandhi University, Kottayam, (1999). India,

[8] Tauc J, Menth A, Wood. D.L, *Phys.Rev.Lett*,**25**,(1970)749

[9] Silverstein M.S and Visoly Fisher I, *Polymer*,**43**, (2002), 11

[10] Joseph Mathai.C, Anantharaman.M.R,. Saravanan.S, Venkitachalam.S, Jayalekshmi. S, *J.Phys.D, Appl. Phys*.**35**, (2002), 240

[11] Nora E.Hill, Worth E.Vaughan,.Price A.H and Mancel Davies, , *Dielectric Properties and Molecular Behaviou*r, Van Nosttrand Reinhold Co, 1961 London

[12] P.D Paulson, B E Mc Candless, R W Birkmire, *J.Appl.Phys*, **95**. (2004), 3010

[13] K.P.Unnikrishnan, *Ph.D.Thesis* , Cochin University of Science and Technology , (2003), India

[14] Mansoor Sheik-Bahae,Ali A.Said, Tai-Huei Wei, David J.Hagan, E.W.Van Stryland, *IEEE J. Quantum Electr.* **26**,(1990),760

[15] C Suryanarayana and M Grant Norton, *X-Ray Diffraction,* (1998), Plenum Press, New York.

Chapter 4

Structural and optical properties of plasma polymer thin films

Plasma polymerisation results in a polymer chain which is entirely different from that of the polymers prepared by other conventional chemical routes. Most of the properties exhibited by the polymers are structure dependent too[1]. The optical and structural properties of a polymer are strongly interdependent. Insitu doping of plasma polymersed thin films is achieved by incorporating iodine in the polymer chain. The role of iodine is to enhance the conductivity and to modify the optical properties[2]. The effect iodine doping can be investigated by evaluating the structural and optical properties. In order to achieve these motives FTIR and UV-Vis-Spectroscopy are used as analytical tools. The details of the experimental techniques are described in chapter. 3.

Further more, it is well known that the electrical properties of the polymers are largely dependent on their structure. In order to arrive at a possible mechanism of conduction in a polymer thin film, the knowledge of its structural parameters is essential. In a simplistic model, the optical properties of any polymer originates from the infinitely long one dimensional arrangements of pi-electrons. The Highest of the Occupied Molecular Orbit (HOMO) and the Lowest Unoccupied Molecular Orbit (LUMO)[3], bands merge in the polymer, behave like a synthetic metal. However when a polymer is doped with a halogen, the localized modes and the resulting disorders due to doping contributes to the optical properties. These disorders produce an absorption edge different from that of the pristine sample. Thus the evaluation of the optical band gap is important in asserting these changes. In this chapter the structural and optical studies carried out on plasma polymerised thin film samples are given in detail. Based on the FTIR and UV-Vis-NIR studies, the optical and structural properties of plasma polymerised thin films are explained. The polymers employed for these studies are polyaniline (PANI), poly phenyl hydrazine (PPPH) and plasma polymerised films of tea tree oil (TTO).

4.1 Plasma polymerised phenyl hydrazine thin films

4.1.1 FTIR spectroscopic studies on rf and ac plasma polymerised thin films.

The structure of phenyl hydrazine in its monomer form is given by C_6H_5-NH-NH_2 .The structure of phenyl hydrazine is depicted in figure 4.1

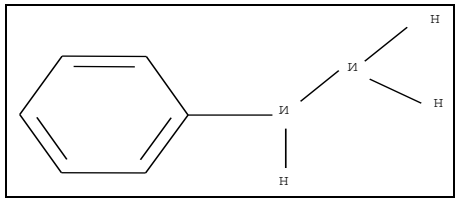

Figure 4.1: Phenyl hydrazine –monomer

The FTIR spectra of the monomer as well as the pristine and doped phenyl hydrazine prepared by rf and ac plasma polymerisation techniques are charted and are depicted in figure 4.2. The functional groups present in the monomer and the polymer were identified with the help of standard charts and are tabulated in table 4.1. It can be seen that the FTIR spectra of the plasma polymer of phenyl hydrazine in its pristine and doped form exhibit considerable differences. It is noticeable from the table that the peaks corresponding to 1248 cm^{-1} is absent in the FTIR spectrum of the rf pristine and doped rf plasma polymerised phenyl hydrazine thin films[4]. It is the peak corresponds to the C-C deformation vibration of the C-C skeleton. The peak at 1248 cm^{-1} can also emerge from the symmetric deformation of the NH-NH-C=O. This is a strong possibility since the phenyl hydrazine contains an NH-NH_2 group associated with the benzene ring.

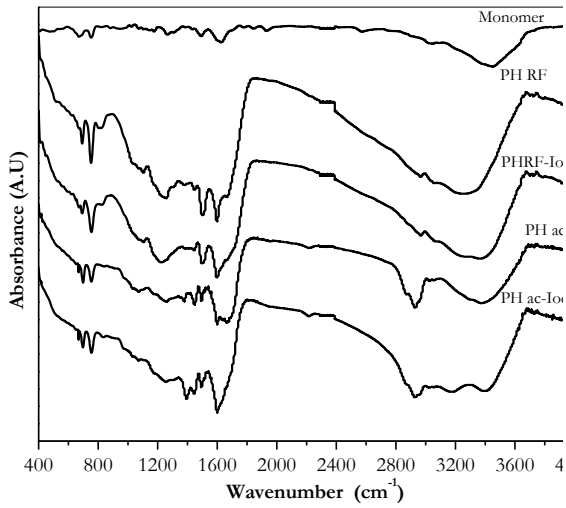

Figure 4.2: FTIR spectrum of plasma polymerised phenyl hydrazine thin films. The spectrum of monomer is also given.

From the table it is clear that in the case of doped rf plasma polymerised phenyl hydrazine, there exists no signature corresponding to the chemical bonding of iodine, which is usually observed in the short wave number region (400-500 cm^{-1}). However the relative intensities of the peaks corresponding to various vibrations changes considerably between rf and ac plasma polymerised samples. The abstraction of the $NH\text{-}NH_2$ is another possibility which leads to the formation of a C=O group. The peak at 1661 cm^{-1} corresponding to conjugated C=C, C=O, or C=C stretching vibration and, are present in the ac plasma polymerised phenyl hydrazine but is not observed in the rf plasma polymers in both pristine and in iodine doped forms. The reason for such a result may be the abstraction of theses groups, due to the high energy of plasma species evolved during the rf plasma polymerisation mechanism.

Monomer (cm^{-1})	RF Pristine (cm^{-1})	RF Iodine (cm^{-1})	AC Pristine (cm^{-1})	Ac Iodine (cm^{-1})	Assignment of frequencies
661	696	696	691	692	Aromatic ring substitution.
			1069	1069	C-H out of phase vibration
	1237	1217	1248	1237	CN Stretching ,
1480	1488	1498	1442,	1452	Aromatic ring , phenyl radical.
1646	1595	1605	1661,1595	1595	Band for aromatic ring, N=N Stretching, C=C Conjugation
3010	absent	absent	2917	2932	N.H asymm. stretch. (aromatic)
3430	3234	3254	3162	3162	NH_3 Stretching
		3382	3397	3397	NH Stretching vibration

Table 4.1: Assignment of frequencies of FTIR spectrum of phenyl hydrazine

Significant information obtained from the FTIR spectra suggest that the intensity of the characteristic aromatic absorption (1500cm^{-1}) present in the monomer spectrum is totally reduced in the polymer form in both pure and doped cases. The 1598 cm^{-1} and 1599 cm^{-1} peaks present in the polymer film clearly point to intense aromatic ring opening mechanisms[5]. This will result in aliphatic unsaturated and free radical structure as reported in the case of plasma polymerised polyaniline by Paterno[6] *et al.* This is further substantiated by the presence of an FTIR peak at 1381 cm^{-1}. These FTIR results substantiate the conclusion that the plasma polymerisation process modifies the structure of the polymer considerably, and thus the polymer obtained in this way differs from that of the chemically synthesized conducting polymers. The polymers formed under the iodine atmosphere or iodine doped samples show considerable difference in their structure with respect to the pristine samples[7].

Strong absorptions at 3449 cm^{-1}(monomer), 3263 cm^{-1} (pristine) and 3372 cm^{-1}(iodine doped) can arise from free NH stretching of amides. The shifting of these peak positions is due to different structures obtained in the polymerisation process. The presence of these peaks rules out the abstraction of nitrogen species present in the monomer. Eventhough the ring opening is observed, the significance of the presence of benzene ring was also observed in the polymer spectra. The indication of N=O stretching at 1256 cm^{-1} in pristine and 1224 cm^{-1} in the iodine doped form may be due to the formation of N=O by the photochemical reaction of phenyl hydrazine when exposed to oxygen.

It is to be noted here that in the case of iodine doped plasma polymerised phenyl hydrazine films, there were no significance changes in the FTIR spectrum corresponding to the possibility of iodine binding with any functional group. Further it has been found that *insitu* iodine doping of phenyl hydrazine resulted in thermally stable films without any indication of iodine escape. In the case of ac plasma polymerised thin films the FTIR spectra of pristine and iodine doped samples exhibit considerable difference from their rf counterparts. One of the main differences of the ac films with that of the rf plasma polymerised films is the change in the relative intensity of spectral peaks corresponding to different functional groups. It is evident from the FTIR data that there is not much structural difference noticed in the case of plasma polymerised phenyl hydrazine thin film samples prepared by two different techniques *viz* ac and rf. The incorporation of iodine in the polymer matrix by doping has give rise to charged defects[8]. This can result in the formation of intermediate energy levels and these additional levels changes the electronic structure of these polymers. These changes can be investigated by conducting the optical absorption studies and is described in the next section.

4.1.2 UV-Vis-NIR absorption studies on rf and ac plasma polymerised phenyl hydrazine thin films

The optical absorption graphs of ac and plasma polymerised phenyl hydrazine in the pristine and iodine doped forms are shown in figure 4.3, and figure 4.5. Since the structure of the polymer is highly amorphous, the optical transition is assumed to be indirect[9] and is calculated from the $(ah\nu)^{1/2}$ vs. photon energy graph or Mott plot[10,11]. The Mott plot for ac and rf films of phenyl hydrazine are shown in figure 4.4 and figure 4.6 respectively.

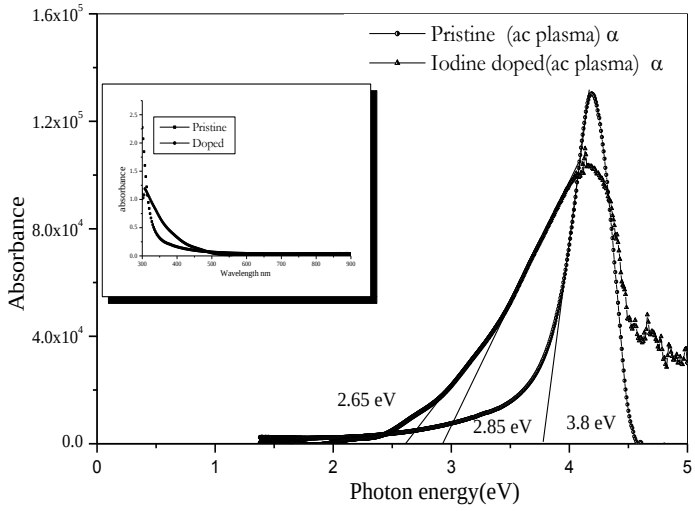

Figure 4.3: Absorbance vs. Photon energy graph of ac plasma polymerised phenyl hydrazine in its pristine and iodine doped form

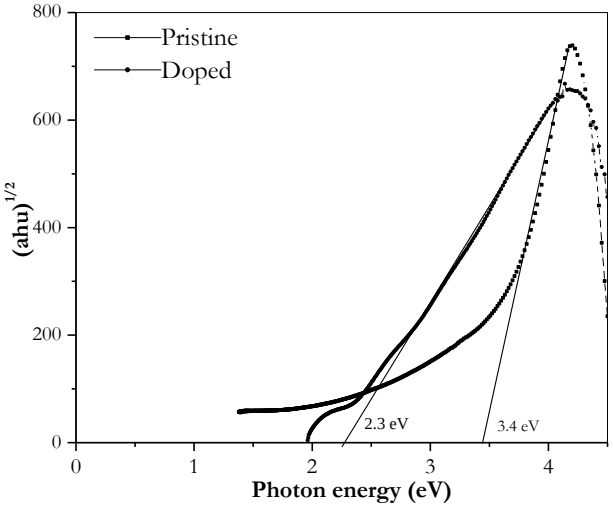

Figure 4.4: $(ah\nu)^{1/2}$ vs. photon energy graph of ac plasma polymerised phenyl hydrazine in its pristine and iodine doped form

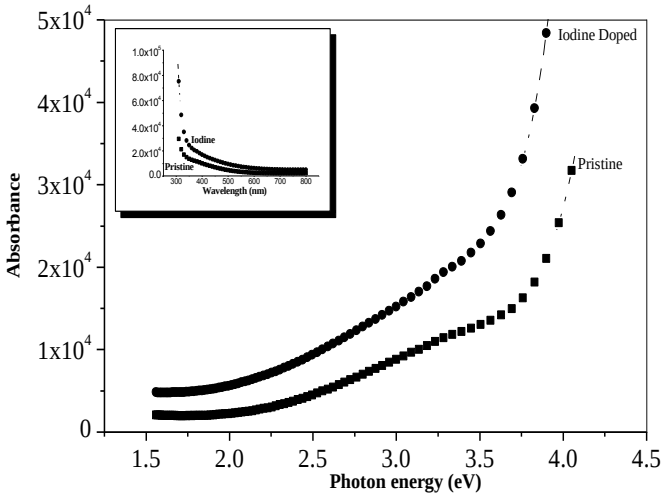

Figure 4.5: Absorbance vs. Photon energy graph of rf plasma polymerised phenyl hydrazine in its pristine and iodine doped form

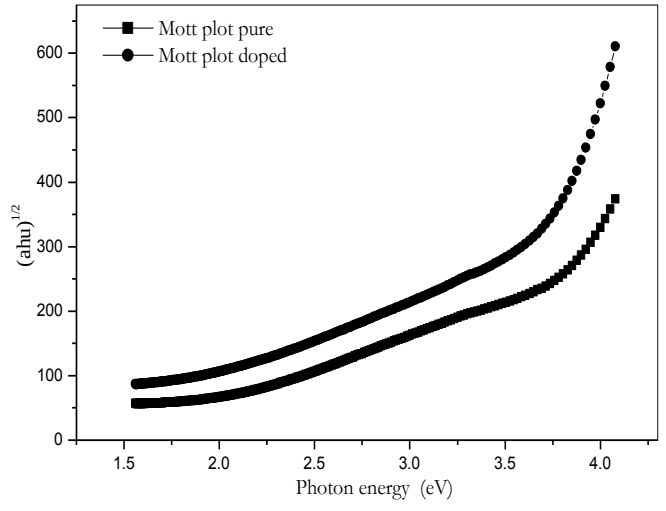

Figure 4.6: $(ah\nu)^{1/2}$ vs. Photon energy graph of rf plasma polymerised phenyl hydrazine in its pristine and iodine doped form.

It can be seen that doping of iodine decreases the band gap of the thin film considerably. The decrease in the band gap in a polymer can be attributed to the increase in the number of the n-type charge carriers and can result in the formation of the sub band polaronic states. The $\pi - \pi$ transition gap size can also be confirmed by the enhancement of the conductivity by a few orders. Similar conclusions were drawn from PL studies carried out by Xu[2] *et al.*

Furthermore plasma polymerised phenyl hydrazine thin films prepared by two different techniques namely rf and ac exhibit altogether different optical absorption characteristics. Here it is to be noted that the technique of rf and ac produce entirely different environment for plasma. It is noteworthy that in the case of rf plasma polymerised phenyl hydrazine samples the band gap is 4.2 eV in its and in the ac plasma polymers the band gap is 3.8 eV. In the RF sample it is also seen a transition at 3.6 eV in their pristine form.

The absorption at 4.2 eV is characteristic of the absorption from the benzene ring and the one at 3.6 eV corresponds to a $\pi - \pi^*$ interband transition[12]. This intrinsic absorption loss in the near UV-region (4.2 eV) in the pristine film is associated with electronic excitations of chromophores in the repeating units of the polymer and the presence of strong UV-absorbing groups, like include carbonyl, nitro, etc. The presence of these groups in the polymer chain as evidenced from the FTIR spectra. Absorption in this energy range corresponds to the optical transition of $n \rightarrow \sigma^*, n \rightarrow \pi^*, \pi \rightarrow \pi^*$, with n representing a non-bonding orbital. In the case of the iodine doped films the shift in the band gap can be correlated to the opening of the benzene ring. It must be note worthy that the structural changes inducted in the polymer film by iodine doping produces changes in the absorption spectra[13]. For this, complementary evidence exists in the IR spectrum. Structurally induced optical transitions are reported in the literature in the case of some oligomers and polymers with different backbone structures

4.1.3 Urbach tail analysis of phenyl hydrazine thin films

ln α vs. photon energy graph of plasma polymerised thin films of phenyl hydrazine prepared under different polymerisation conditions are shown in figure 4.7 and in figure 4.8, Structural disorder frozen in amorphous materials is an important factor to determine their physical properties[14]. For example structural disorder from the form of localized states in the amorphous materials causes changes of their optical and electrical properties. The amount of disorder is crucial to control the physical properties of the amorphous

solids[15]. The effect of structural disorder in the electronic structure of amorphous solids is clearly recognized at the band edges.

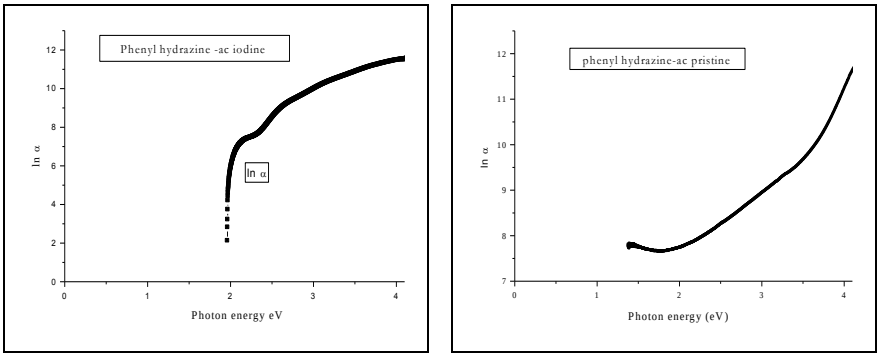

Figure 4.7: ln α vs. Photon energy graph of plasma polymerised thin films of phenyl hydrazine prepared under AC plasma polymerisation.

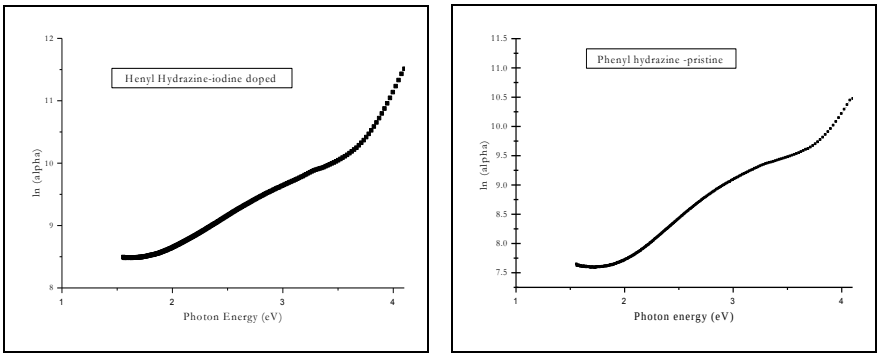

Figure 4.8: ln α vs. Photon energy graph of plasma polymerised thin films of phenyl hydrazine prepared under rf plasma

The band tails extent into the band gap generally shows an exponential behavior, appreciable in the low-energy region of luminescence spectra and absorption profiles[16]. The band tails are characterized by the band tail parameter E_0 as

$$\alpha(h\nu) \infty \exp\left(\frac{h\nu}{E_0}\right) \qquad 4.1$$

where α is the absorption coefficient $h\nu$ is the photon energy. The band tail parameter E_0 depends on the carrier concentration n, p or temperature T and the structural disorder. E_0 is the sum of the interactive and structural

contributions and its value can be calculated from the slope of the absorption edge $E_0 = \frac{d(h\nu)}{d(\ln \alpha)}$ which is a strong function of temperature.

It is found that the iodine doping reduces the band gaps considerably in ac and rf plasma polymerised thin films. The effect of iodine doping on phenyl hydrazine samples can be explained as follows. The iodine doping of polymer results either in the charge transfer complexes or molecular aggregates[17], and this affects the properties of the free volume holes. Iodine may enters into the polymer chain substitutionally or reside in the crystalline amorphous boundaries and in the amorphous regions. Due to its high electronegativity, iodine interacts with the lattice and produces distortions and stress with in the crystallites, leading to structural modification. The structural modification induced defect levels in the doped samples, indicated by the exponential tail with decrease in photon energy below the band gap. The broadening of the Urbach tail increases with increase in defect states of the films[18]. From the inverse of the slope of the $\ln\alpha$ vs. $h\nu$ plot the value of tail width E_0 (eV) can be calculated. It reflects the defect content in the film. The E_0, of the films prepared under various conditions are given in the table 4.2. The width of the exponential edge and the optical gap were controlled by the amount of disorder, which is a function of the structural and thermal properties of the material. According to Cody $E_0(X,T)$[19] can be written as

$$E_0(X,T) = \frac{k_B\theta}{2\sigma_0} + \frac{k_B\theta}{\sigma_0}\left[\frac{1}{\exp(\theta/T)-1}\right] + \frac{k_B\theta X}{2\sigma_0} \qquad 4.2$$

k_B is the Boltzmann constant X is a dimensionless parameter called structural disorder parameter , θ is related to the Debye temperature of the material, θ_D by $4\theta/3 = \theta_D$. The second term in the equation for $E(X,T)$ represents the contribution of electron-phonon and exciton-phonon interactions and the third term originates due to the mean square deviation of the atoms from a perfectly ordered lattice due to the structural disorder.

Poly phenyl hydrazine	Band gap (eV)	Indirect absorption (eV)	Urbach tail width eV
rf pristine	3.6 , 4.2	3.2,4.2	0.165
rf iodine	3.6	3.8	0.295
ac pristine	3.8	3.9	0.251
ac iodine	2.6	3.4	0.973

Table 4.2: Comparison of band gap, direct and indirect transition and the Urbach tail width of phenyl hydrazine thin films prepared by plasma polymerisation under different deposition conditions.

Here in this case it is found that the degree of disorder of the iodine doped films exhibited high values when compared to their pristine counterparts both in the case of rf and ac plasma polymerised thin films.

4.2 Studies on polyaniline

4.2.1 FTIR spectroscopic studies on rf and ac plasma polymerised thin films

The FTIR spectrum of plasma polymerised thin films of polyaniline is given in figure 4.9

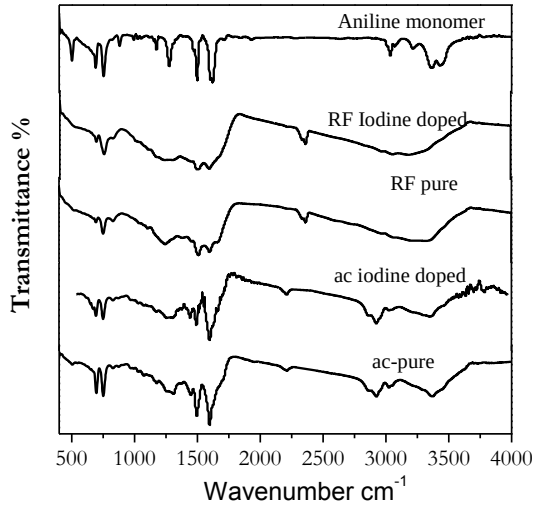

Figure 4.9: FTIR spectrum of plasma polymerised polyaniline

The frequency assignment of the rf and ac plasma polymerised polyaniline thin films were carried out and tabulated (table 4.3). The structural difference noticed when polymerisation is carried out in iodine atmosphere is also brought out in the table.

Mono mer	RF pure	RF Iodine doped	ac Pure	AC Iodine doped	Assignment of the frequencies and the comments
691	693	692	703	676	CH Out of Plane vibration
753	750	753	740	740	Aromatic ring substitution , C-H out of plane vibration
878	829	823			C-N Stretching
1180	1105				C-N Stretching
1270	1244	1239	1176	1170	CH In plane deformation
1490	1381				C-N Stretching
	1455	1449	1326	1300	C-N Stretching, aromatic primary amine
		1500			C-C Skeletal vibration,
			1451	1451	Aromatic ring, C-C skeletal vibration
1610	1598	1592	1480	1488	CN Stretching and C-N_In plane bending.
			1600	1606	Aromatic stretching , Benzene ring
			2850	2850	NH_3 Stretching, methyl group.
3050		2969	2921	2929	OH stretch band.
3380	3319	3056			CH Stretching, NH3 stretching,
3430		3182	3385	3385	NH2 group.

Table 4.3: Assignment of FTIR spectrum of polyaniline prepared at various conditions

The FTIR peaks obtained in all samples in the 750 cm^{-1} can result from the out of plane stretching of the NH bond[20]. A quick comparison between the spectra of ac and rf thin films exhibit marked structural difference between the polymers evolved by both polymerization routes namely rf and ac. It is observed that NH stretching (3220 cm^{-1}) is not very prominent in the ac plasma polymerised samples but its presence is seen in the rf samples. A peak at 3038 cm^{-1} corresponding to the CH stretching observed in the monomer, is retained in the polymerised samples. The peak at around 2960 cm^{-1} corresponding to NH asymmetric stretching in the monomer is found at 2928 cm^{-1} in ac and 2970 cm^{-1} in rf samples respectively. The CH in-plane deformation (1175cm^{-1}) is found to be retained in the ac samples but is seen shifting to 1105 cm^{-1} in rf samples. The FTIR studies and further analysis establishes the fact that structural difference in the ac and rf plasma polymerised aniline thin films samples do exist. It can also

be seen that doping with iodine modifies the bond length and facilitates shifting of functional groups[21]. The assignment of frequencies also line shows shifting of most of its peaks. It can also be seen that doping with iodine modifies the bond length and facilitate the shifting of functional groups. The polyaniline in its plasma polymerised form involves several infrared active molecular groups such as NH, C=O, SO_3H, CH_3, CH_2, CH. The coexistence of the 1590 cm^{-1} and the 3380-3430 cm^{-1}shows the OH bending[22].

4.2.2 UV-Vis-NIR absorption studies on rf and ac plasma polymerised polyaniline thin films

UV-Vis-NIR spectra of rf and ac plasma polymerised thin films of polyaniline in its pristine and iodine doped forms are given in figure 4.10 and 4.12. The band gap and the optical transition energy of the thinfilms are calculated from the Mott-plot (figure 4.11 and 4.13)

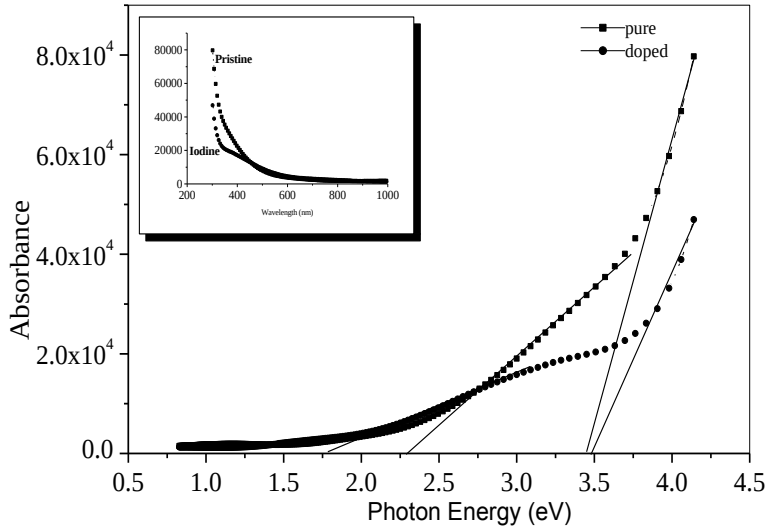

Figure 4.10: Absorbance vs. photon energy graph of ac plasma polymerised aniline in its pristine and iodine doped form

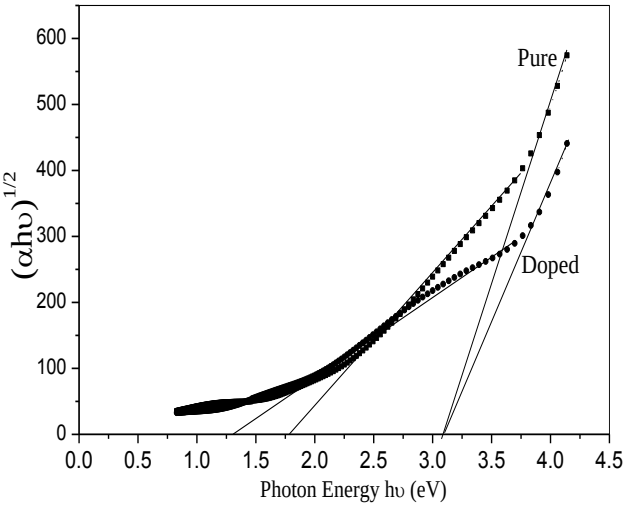

Figure 4.11: $(ah\nu)^{1/2}$ vs. photon energy graph of ac plasma polymerised aniline in its pristine and iodine doped form

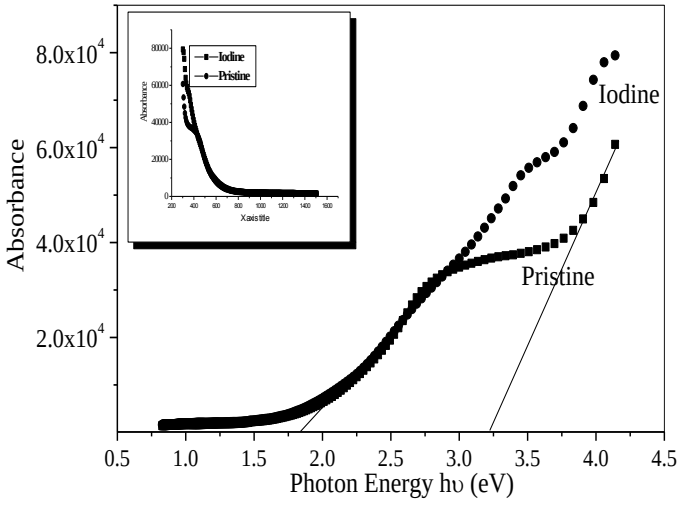

Figure 4.12: Absorbance vs. photon energy graph of rf plasma polymerised aniline in its pristine and iodine doped form

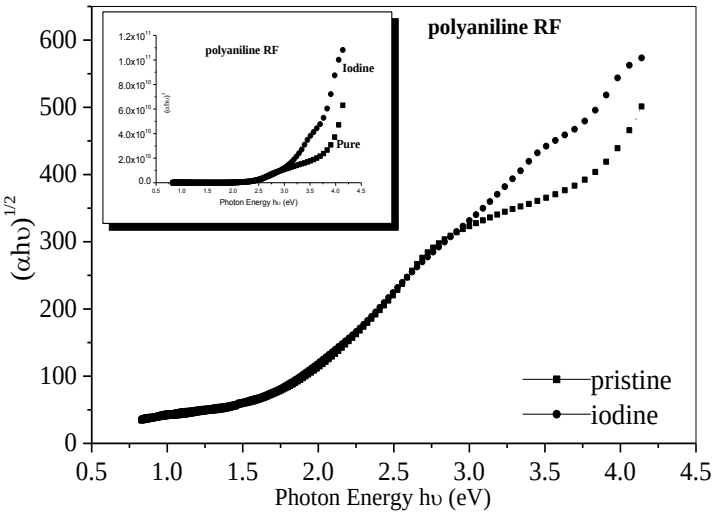

Figure 4.13: $(ah\nu)^{1/2}$ vs. photon energy graph of rf plasma polymerised aniline in its pristine and iodine doped form.

The optical transition energies (optical band gap) corresponding to the thin films prepared under various deposition conditions is given in table 4.4. It can be seen that the optical transition energies of rf polyaniline films are considerably different with respect to its ac counterpart. It is also evident from the table that the iodine doping decreases the optical band gaps from 3.6 eV to 2.8 eV and 2.2eV to 1.9 eV respectively in the case of rf plasma polymerised thin films. A second optical transition is also observed in the plasma polymer films. A reduction of 0.8 eV and 0.3 eV in the optical transition energies are noticed with respect to pure and doped rf plasma polymerised samples. However in the case of ac plasma polymerised thin film polyaniline samples, the optical transition found at 3.4 eV is shifted to 3.6 eV as a result of iodine doping where as the optical transition found at 2.3 eV reduced to 1.8 eV. The reduction in the optical band gap is probably due to the modification of the polymer structure.

The reduction of band gap in the rf polymerised samples arises out of extended conjugated structure evolved in the rf polymerization mechanism. Doping induces a structural ordering of the polymers due to the incorporation of the charged species. There are signatures supporting these changes in the UV-

Vis-NIR and FTIR spectra. Such an ordering in the plasma polymer thin films are reported earlier by Silvestein[11] et al.

Polyaniline	Optical transition energies (eV)			
	Pristine		Iodine Doped	
	First transition	Second transition	First transition	Second transition
RF plasma polymerised	2.2	3.65	1.9	2.8
AC plasma polymerised	2.3	3.4	1.8	3.6

Table 4.4: Comparison of optical transition energies of polyaniline samples prepared by rf and ac plasma polymerization.

4.2.3 Urbach tail analysis of polyaniline thin films

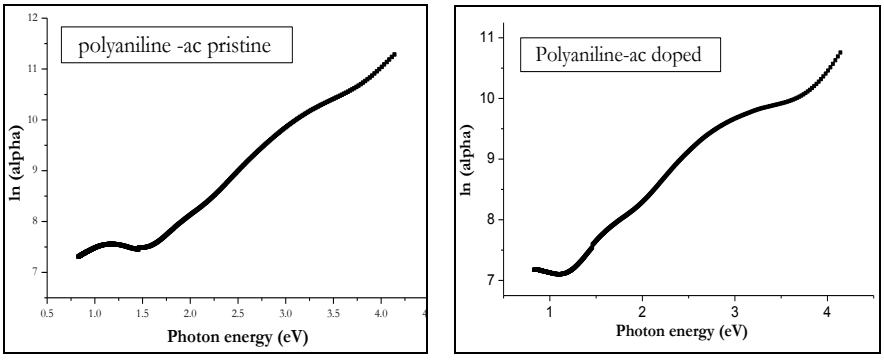

Figure 4.14: ln a vs photon energy graphs of ac plasma polymerised aniline in the pure and doped forms

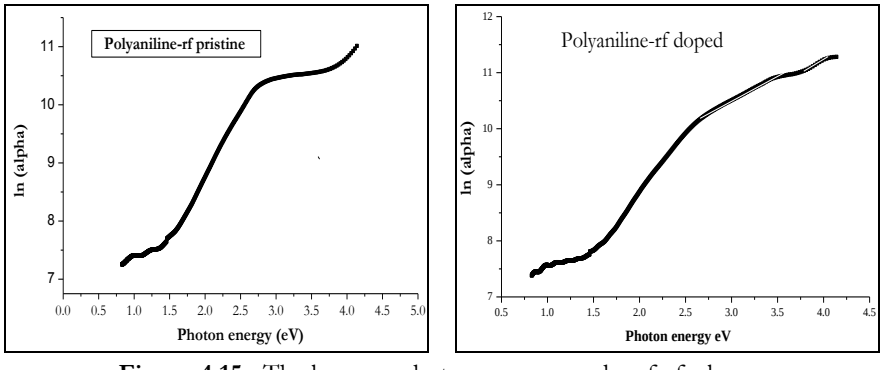

Figure 4.15: The ln a vs photon energy graphs of rf plasma polymerised aniline in the pure and doped forms

The the band tail parameter E_0,for the plasma polymerised thin films of aniline were calculated from the ln α vs photon energy graphs figure 4.14 and figure 4.15, in the case of ac and rf plasma polymerised thin films. Here also it is found that the iodine doping reduces the band gaps considerably in ac and rf plasma polymerised thin films.

Polyaniline	Band gap (eV)	Indirect absorption (eV)	Urbach tail width eV
rf Pristine	3.4, 2.0	2.7. 1.75	0.479
rf Iodine	2.9, 2.2, 1.65	2.4, 1.5	1.097
ac Pristine	3.6, 2.4	3.1,1.8	0.506
ac Iodine	3.5, 1.6	3.1,1.3.	0.453

Table 4.5: Comparison of band gap, direct and indirect transition and the Urbach tail width of polyaniline thin films prepared by plasma polymerisation under different deposition conditions.

There is a considerable variation is found in the case of the E0 values of the polyaniline films prepared by rf and ac plasma polymerisation. It can be seen that, the E_0 value decreased in the iodine doped form of ac plasma polymerised thin film. It indicates a decrease in the defect levels when the polymerisation carried out in the presence of iodine vapour. It is found that the value of E_0 is enhanced considerably in the case of the doped film of polyaniline prepared by rf plasma polymerisation when compared to its pristine form. This is an evidence for the enhancement of defect levels.

4.3 Studies on tea tree oil

4.3.1 FTIR spectroscopic studies

Good quality thin films of tea tree oil, which are pinhole free and optically transparent were prepared by rf plasma polymerization at a frequency of 13.56 MHz. The film thickness ranges from 100nm to 240nm for the deposition time of 5~15 minutes at a constant monomer flow rate. FTIR spectra of these thin films were recorded and the spectra are compared to that of the precursor monomer[23]. The chemical structures of the major components present in the monomer are given in figure 4.16.

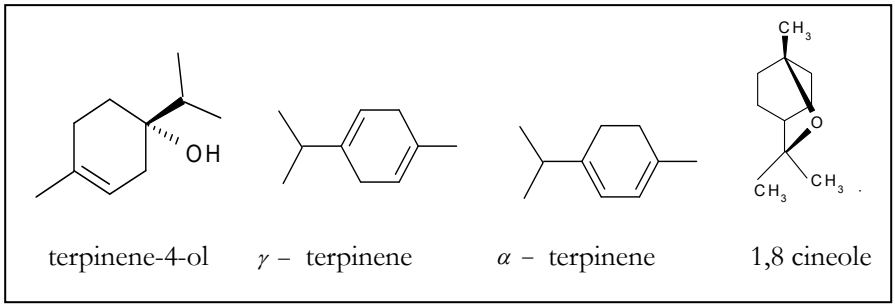

Figure 4.16: The chemical structure of the major components of tea tree oil.

The structural characterization of tea tree oil is tedious because the complexities of the structure of tea tree oil. The main component of tea tree oil is **terpinen-4-ol** (typically 30-40%) with Molecular formula: $C_{10}H_{18}O$, the other components are p-cymene, 4-iso propyl toluene. Para methyl cymene. The FTIR Peak assignment of the tea tree oil is given in table 1.

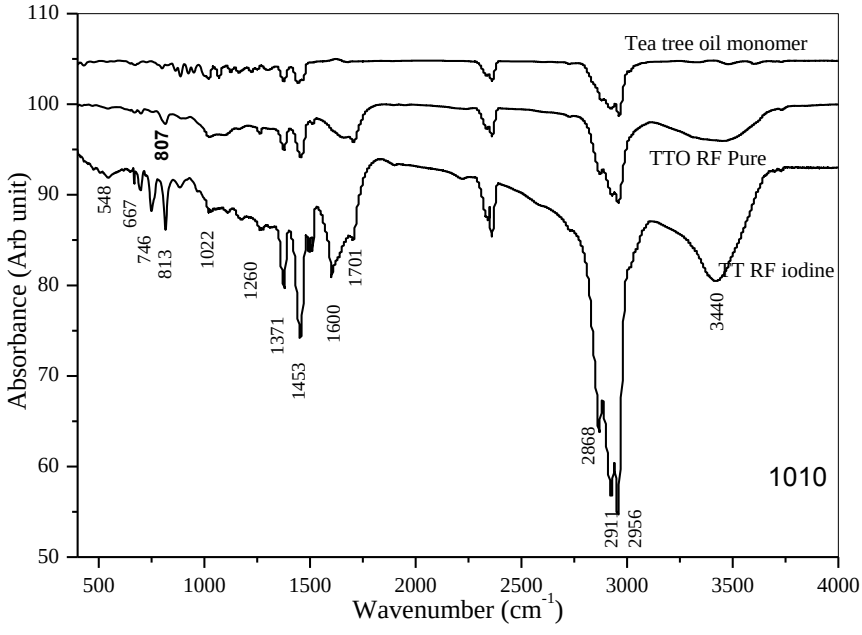

Figure 4.17: The FTIR spectrum of plasma polymerised thin film of tea tree oil in the pure and doped films prepared by rf plasma polymerisation

The assignment of frequencies of plasma polymerised tea tree oil by FTIR analysis is a laborious process since the monomer itself containing a large number of compounds in various proportions. Since the complexity of the structure of the tear tree oil in its monomer form it self it is not possible make a complete characterisation of the tea tree oil thin film formed under various plasma conditions.

Monomer	Pure	Iodine doped	Assignment	Comments
672	668	686	NH out of plane bending, aromatic substitutions	
782		745	O-H deformation and C-O stretching interaction	Abstracted in the pristine form but appears in the iodine doped form.
890	824	803	Skeletal vibration of ≺ CH3(2)	Shifting of the frequency due to the streric repulsion in the presence of iodine
948	910	882	Skeletal vibration of ≺ CH3(2	Considerable shift is observed in this peak.
1027	1023	1035	Presence of Methyl benzenes	Persistence of aromatic ring and substitutes.
1370, 1457	1364, 1457	1348, 1457,	OH deformation, NH benzene	Shifting is more prominent in iodine doped samples
	1707	1594	C=O stretching	Suppressed in the iodine doped form, shifted to 1594 cm^{-1}
2954(vs)	2962(vs)	2873, 2925(vs)	NH^2 stretching vibration	Persisted in polymerisation but strongly shifted in the iodine doped samples
3491(m)	3431(s)	3426(s)	NH stretching vibration	Relative intensity of the peaks enhanced in the polymerised and further enhanced in iodine doped

Table 4.6: Assignment of frequencies of plasma polymerised tea tree oil

The peaks at 803 cm^{-1}, 891cm^{-1}, 920 cm^{-1}, 950 cm^{-1} and 1068cm^{-1} of the monomer and 810 cm^{-1}, 906 cm^{-1}, 1060 cm^{-1} of the polymer are, the peaks corresponding to the C-H in plane bending. These peaks can be also attributed as the aromatic substitution[24]. Peaks corresponding to C-O-C asymmetric

stretching present at 1126 cm^{-1}, 1163 cm^{-1} and 1209 cm^{-1} , were absent in the polymer. The peaks at1290 cm^{-1} and 1253 cm^{-1} represents the C-C stretching vibration[25]. Peaks at 1370 cm^{-1} and 1451 cm^{-1} in the monomer and 1363 cm^{-1} and 1474 cm^{-1} in the polymer indicates that ring stretching of the monomer has not been affected very much in the polymerised structure.

The enhanced peak centered at 1724 cm^{-1} in the polymer than that of the peak observed at 1650 cm^{-1} in the monomer indicates that the benzene ring is intact and the functional groups associated with the aromatic ring were altered in the plasma atmosphere. The peaks for the C-H stretching mode of the hydrogen atom bonded to a benzene ring 2929 cm^{-1} and 2946 cm^{-1} found in the monomer are unaffected in the polymer also. The peaks at the above wave numbers can be also attributed to the signatures of CH_3 and CH_2 groups. The spectra peaks corresponding to the NH stretching[26] is present at 3339 cm^{-1}, 3487 cm^{-1} and 3612 cm^{-1} present in the monomer is considerably enhanced and combined together. A strong band centered at 3616 cm^{-1} is observed in the polymer. The broadening of this peak in the polymer is an indication of hydrogen bonding.

These results are indicative and does not purport to a complete identification of the possible groups or the polymer structure of PPTTO. A very elaborate study employing FTIR and NMR spectroscopy is necessary to identify the functional groups that are retained and are prominent in the plasma polymerised tea tree oil thinfilms. The identification of various functional groups is rather difficult and tedious and an exclusive systematic study is recommended for the evaluation of the structure of PPTTO.

4.3.2 UV-Vis-NIR absorption studies on plasma polymerised tea tree oil thin films

The UV-Vis-NIR absorption spectra of plasma polymerised tea tree oil in its pristine and iodine doped form is given in figure 4.18. It is observed that, the thin films are transparent to the visible region, in their pristine form, but are visibly absorbing when it is doped with iodine. An additional peak at 2.3 eV is observed in the spectrum of iodine doped samples.

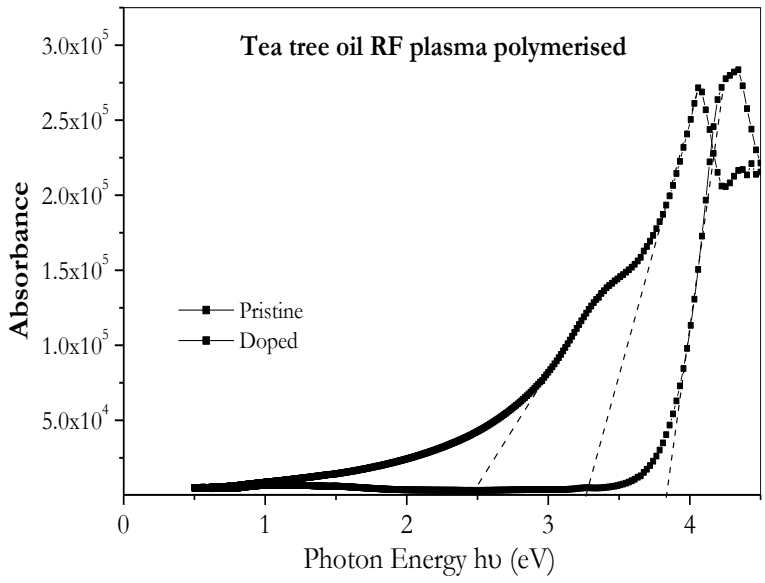

Figure 4.18: Absorption Spectrum of rf plasma polymerised tea tree oil thin films

The band gap is calculated from the α vs. photon energy ($h\nu$) graph using the Tauc[27] relation

$$\alpha h\nu = B(h\nu - E_{opt})^n$$

Where α is the absorption coefficient, B is a constant and the n is an index determining the probability of optical transition, which is related to the distribution of density of states. From the value of n it is possible to understand the type of optical transition occurring in the sample.

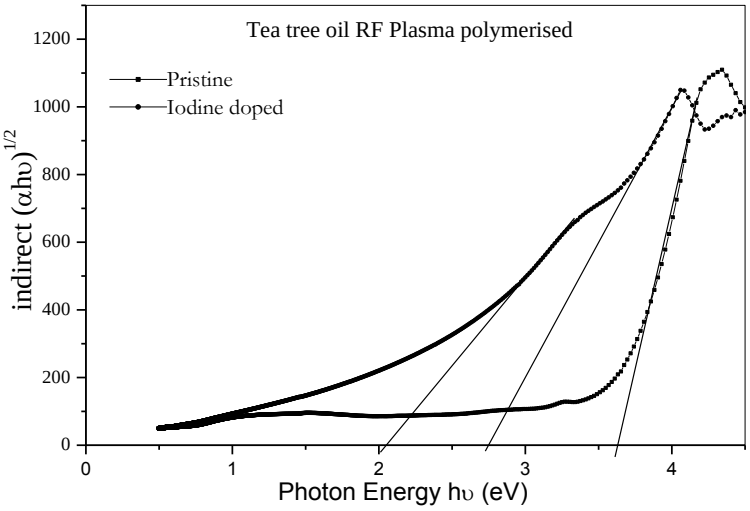

Figure 4.19: $(\alpha h\nu)^{1/2}$ vs photon energy of rf plasma polymerised tea tree oil thin films

The absorption spectra of iodine doped samples exhibit a considerable difference form that of the pristine samples. The Absorption maximum of the iodine doped samples is red shifted to 370 nm, and an additional absorption peak at 447nm appeared in the absorption spectra. The absorption around 447 nm observed, in the doped films is possibly due to the localised polarons or intermediate levels created by iodine doping[5]. Absorption in polymers is due to intrinsic and extrinsic losses, and the details are already given in section 4.1.2. The coupling of the electronic and the vibrational modes of such groups relax the dipole selection rule and the, transition occurs. In the case of $\pi \rightarrow \pi^*$ transition, the absorption in the UV region of the chromophore is not completely restricted in the UV region but decays exponentially with increasing wavelength. This phenomenon is observed in the sample. The results shown in the case of ac plasma polymerised samples are similar to that of the tea tree oil thin films in the rf plasma polymerisation.

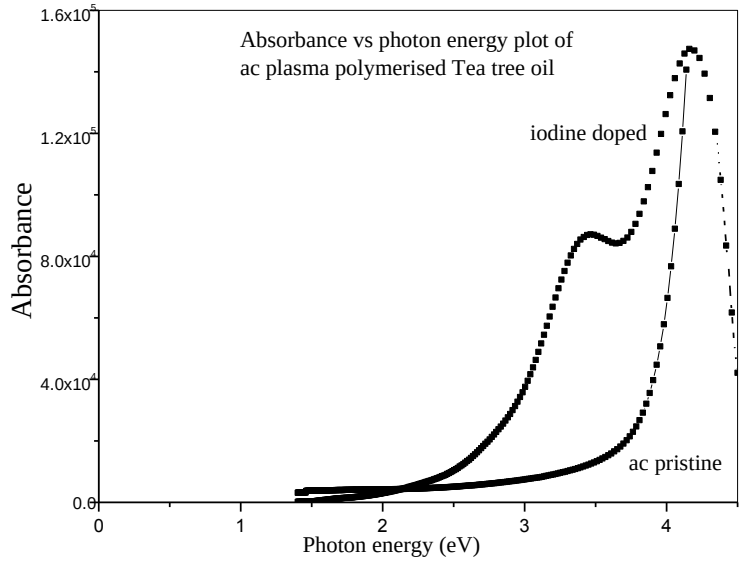

Figure 4.20: Absorbance vs photon energy of ac plasma polymerised tea tree oil thin films

The estimation of defect levels in the plasma polymerised thin films of tea tree oil is calculated from the $\ln \alpha$ vs photon energy plot of the samples (not given), the enhanced value of the E_0 is observed in both rf and ac plasma polymerised forms.

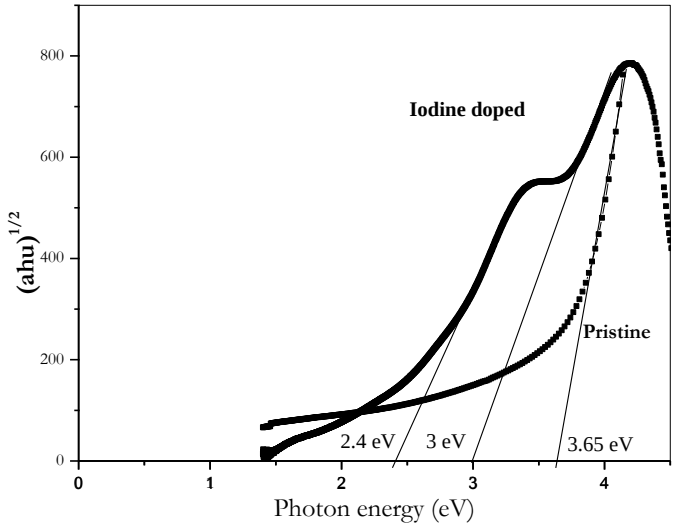

Figure 4.21: $(\alpha h\nu)^{1/2}$ vs photon energy of ac plasma polymerised tea tree oil thin films

Tea tree oil	Band gap (eV)	Indirect absorption (eV)	Urbach tail width eV
RF Pristine	3.8	3.5	0.184
RF Iodine	3.2,2.4	2.8,2.	0.867
AC Pristine	3.8	3.6	0.188
AC Iodine	3.4, 2.8,2.4	2.8,2.2	0.661

Table 4.6: Comparison of band gap, indirect transition and the Urbach tail width of tea tree oil thin films prepared by plasma polymerisation under different deposition conditions.

It is found that due to the incorporation of iodine, the defect states of the polymers increased considerably. This enhancement of the charged defect states reflects in the other properties of the plasma polymers, and described in the consecutive chapters.

Conclusion

Structural characterisation of plasma polymerised thin films of polyaniline, phenyl hydrazine and tea tree oil were carried out by FTIR spectroscopic studies. Since in the plasma polymerised form of the polymers is highly cross linked and complex, a complete elucidation of the structure is not possible by this technique only. However the structural difference, and the functional groups present were estimated from the FTIR spectroscopy. From the UV-Vis-NIR studies the band gap and the indirect transition energy of the plasma polymers in the pristine and doped forms were calculated. It is found that the structural change is introduced in the polymer chain when the polymerisation is taking place in the iodine atmosphere. This induces charged defect states in the polymer structure and as a result intermediate energy levels/trap levels are created by iodine doping and these defect levels were estimated by the Urbach tail analysis.

Chapter 4

References

[1] S.H.Cho, Z.T Park, J.G.Kim,J.H.Boo, *Surface and Coating Technology*, **174**,(2003),1111.

[2] Xu.B, Jaewu Choi, Carus A.N. and Dowben.P.A, *Appl.Phys. Lett.* **80**, (2002) , 4345.

[3] Hideki Shirakawa., *Current Appl. Phys.* **I** (2001), 281

[4] Sharma Y.R, , *Elementary organic Spectroscopy, Principles and Chemical Applications*, S.Chand and Co,(1998), New Delhi

[5] Guofeng Li, Mira Josowicz, and Jiri Janata and Klaus Mullen, *J.Phys.Chem.* **B**, **105**,(2001),105

[6] Paterno L.G.,.Manolache.S and Denes.F ,*Synthetic Metals*, **130**, (2002), 85

[7] Vickie Pan.Y Ernesto.Z.Barrios, Denice D.Denton, *Appl. Phys. Lett.* **68**,(1996), 3386

[8] A.K.mukharjee and Reghu Menon, *Pranama*, **58**,(2002),233

[9] Tauc J, Menth A, Wood. D.L, 1970, *Phys.Rev.Lett*,**25**,749

[10] Mott N.F and. Davis E.A, 1971, *Electronic Process in Non Crystalline Materials*, (Clarenndon Press, Oxford)

[11] Silverstein M.S and Visoly Fisher I, *, Polymer*,**43**,(2002),11

[12] Donald L.Wise, Gary E. Wnek, Derbra J.Trantolo, Thomas M.Cooper, Joseph D. Gresser, *Photonic Polymer Systems*, Marcel Dekker, (1998) ,New York

[13] F. Huang and AG mac Diarmid, B.R. Hsieh., *Appl. Phys.Lett*. **71**,(1997)-2415.

[14] A.Irribarren, R.Castro-Rodriguez, V.Sosa, J.L.Pena, *Phys.Rev.B*, **58**,(1998),1907

[15] D.S. Galvao, D.A.dos Santos, B.Laks, C.P. de Melo, M.J.Caldas, *Phys.Rev.Lett*,**63**(1989),786

[16] W. Sritakool, V. Sayakanit, and H.R.Glyde, *Phys.Rev.**B*,**33**, (1986).1199

[17] Paolo Coppo, Raoul Schroeder, Martin Grell, Michael L.Turner, *Syntetic Metals*, **143**,(2004),203

[18] S.Chakrabarti, D.Ganguli, S.Chodhuri, *Physica*, **E** ,**24**,(2004),333

[19] G.D.Cody,T.Tiedje, B.Abeles,B.Brooks, and Y.Golstein, *Phys,Rev.Lett*, **47**,(1981),1480

[20] U.S.Sajeev, C.Joseph Mathai, S.Saravanan, Rajeev.R.Ashokan, S.Venkatachalam, M.R.Anantharaman *Bull. of Mater. Sci.* **29**, (2006), 159

[21] Bellami L J,1962 , *Infrared spectrum of complex molecules,* (New York) John Willy and Sons,

[22] C. Nastasea,, D. Mihaiescub, F. Nastasea, A. Moldovanc, Ioan Stamatina, *Synthetic Metals* **147** (2004) 133–138

[23] Brophy Joseph J, Davies Noel W, Southwell Ian A, William Lyall R,*Journal of Agricultural and Food Chemistry*, **37**, (1989), 1330

[24] X.Y. Gong, L.M. Dai, A.W.H. Mau, H. J. Griesser, *J. Polym. Sci. Polym. Chem. Ed.* **36,** (1998) 633.

[25] S.K. Dhawan, D.C. Trivedi, *Polym. Int*. **25** (1991) 55.

[26] H. S. Nalwa (Ed.), Handbook of Organic Conductive Molecules and Polymers, Conductive Polymers: Synthesis and Electrical Properties, **2**, third ed., 1997,Chichester

[27] Tauc J.C, *Optical Properties of Solids,* 1972, (North Holland, Amsterdam).

Chapter 5

Electrical conductivity studies of plasma polymerised thin films

This chapter deals with the electrical conduction of the plasma polymerised thin films. In the present study the electrical conductivity of various plasma polymerised thin films prepared by rf and ac plasma polymerisation techniques were measured. Plasma polymers of aniline (PANI), phenyl hydrazine (PH) and tea tree oil (TTO) were subjected to conductivity studies. The mechanism of conduction of plasma polymers is elucidated and the dependence of electrodes, film thickness and temperature on conductivity is also investigated. Generally, plasma polymers exhibit space charge limited conduction (SCLC) under bias. The mobility and the carrier density of the films are calculated and a plausible explanation for this mechanism is provided.

5.1 Electrical conductivity studies on polyaniline

The experimental set up for the measurement of conductivity of the plasma polymerised polyaniline thin films is described in chapter 3. The device in the present study consists of a single polymer layer sandwiched between two metal electrodes. Al-polymer- Al (M-I-M) structures were employed for the evaluation of the J-V characteristics. The dependence of the electrical conduction is studied using, gold and silver as the upper electrodes and aluminum as the base electrode. ITO-Polymer-Metal (Al, Au & Ag) is also utilized for the dc conductivity measurements. Under normal circumstances, the mechanism of conduction in the polymerised thinfilms fall under three categories. They are Schottky[1,2], Pool-Frenkel and Space Charge Limited Conduction (SCLC).

5.1.1 J-V studies on rf plasma polymerised aniline thin films.

The J-V characteristics of the *Al-RFPANI-Al* thin film is shown figure 5.1(a). Since the reverse and forward characteristics of the film are identical, double log plot of (J-V) in the forward direction is drawn and shown in figure 5.1(b).

At very low voltage region the current density exhibits an ohmic dependence with the applied voltage described by the relation

$$J = \mu n_0 e \frac{V}{d} \qquad 5.1$$

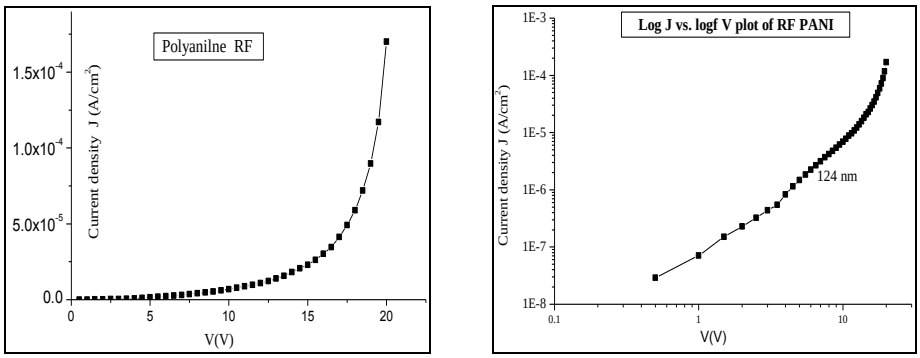

(a) (b)

Figure 5.1: (a) J-V plot of RF plasma polymerised aniline thin film of thickness 124 nm (Al-Polymer-Al). (b) The graph shows double log plot of (J-V)

It is clear from the graph 5.1b that, up to a voltage of (3.6 V), the slope of the graph is found to be 2 which indicates space charge limited conduction (SCLC)[3]. In this region the current density is governed by the Mott-Gurney[4] relation

$$J = \frac{9}{8}\varepsilon_0 \varepsilon_r \mu_p \frac{V^2}{d^3} \qquad 5.2$$

Where $\epsilon_o \epsilon_r$ is the permittivity of the polymer, μ_p the hole mobility and d is the thickness of the device. From the slope of the *logJ-logV* plot, it can be seen that the current density J varies quadratically with the voltage V in this region[5,6], which is characteristic of SCLC and beyond this region the quadratic dependence of J on V increases to a trap filled limit(TFL) with slope >2. The slope of the graph of rf plasma polymerised thin films in the high voltage region is found to be 4, which is an indication of the presence of traps.

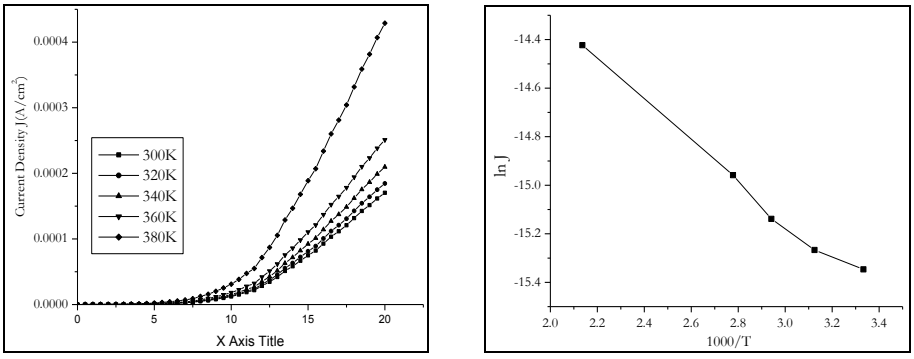

(a) (b)

Figure 5.2: (a) The temperature dependence of the J-V characteristics of RF plasma polymerised aniline thin film (124 nm). (b) The log J vs 1000/T plot. The activation energy calculated is 0.81 eV

The temperature dependence of the J-V characteristics of the rf plasma polymerised aniline thin film (124 nm) is shown in figure 5.2. The temperature dependence of current density J obeys the relation.

$$J = e\mu N_v \left(\frac{V}{d}\right) \exp\left(-\frac{E_a}{kT}\right) \qquad 5.4$$

This expression is characteristic of an exponential trap distribution, where N_V is the effective density of states in the valence band, k is the Boltzmann constant, E_a is the activation energy which can be obtained from the ln J against the 1/T plot given in figure 5.2.

The activation energy thus obtained is *Ea*=0.81 eV. Here the trap distribution obeys a Mayer-Neidel[7] observation and with in the SCLC region the current density J is given by the relation

$$J = e\mu N_v \left(\frac{\varepsilon_r \varepsilon_0}{ePkT_t}\right)^L \frac{V^{L+1}}{d^{2L+1}} \qquad 5.5$$

Where P is the trap density per unit energy range at the valance band edge, ε_0 is the permittivity of the free space, ε_r is the relative permittivity of the sample. For rf polyaniline thin films, $\varepsilon_r = 2.2$ is the relative permittivity. The value of ε_r is obtained from the dielectric measurements and further confirmed by spectroscopic ellipsometry (SE). Here L is a ratio T_t / T, where T is the ambient temperature and T_t is the temperature parameter described by the trap distribution. The exponential trap distribution may be described in terms of T_t as

$$P_{(E)} = P \exp\left(\frac{-E}{kT_t}\right), \qquad 5.6$$

Where $P_{(E)}$ is the trap concentration per unit energy range at an energy E above the valance band edge. The total concentration of the traps are given by the equation[8]

$$N_t = PkT_t, \qquad 5.7$$

The complete characteristic shown in figure 5.1 is determined by four parameters. They are the carrier mobility μ, the equilibrium density of carriers n_o, the trap density N_t and the trap distribution parameter T_t. From the slope of the double log plot given in figure 5.1, in the TFL regime T_t is obtained and equal to 900K since the slope of the trap filled region is 4.

In the Space Charge region described by the Mott-Gurney relation (equation5.2), the mobility can be calculated directly from the current density .It is found that the mobility in the SCLC region is in the order of 3×10^{-14} $m^2/V.s$. At low voltages, the mobility is a constant and independent of the electric field and carrier density, but a function of temperature. At high voltages it is observed that the current increases more steeply than a quadratic relation. This increase in current density is due to an electric field induced enhancement of the mobility of the carriers.

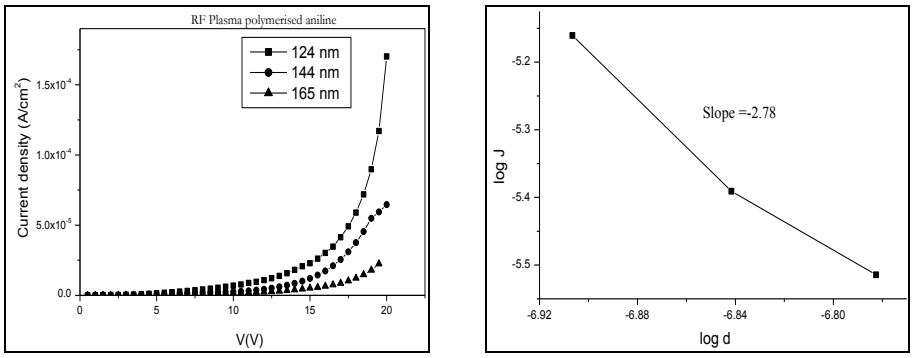

(a) (b)

Figure 5.3: (a) J-V plot of rf plasma polymerised aniline thin films for different thickness. (b) The log J vs log d plot. Here the slope of the log J-log d plot is 2.35 shows a space charge limited current.

5.1.2 Thickness dependence of conductivity of rf polyaniline thin films.

The thickness dependence of conductivity in the SCLC is governed by equations 5.1, 5.2, and 5.3 Here in these sample the in the *log J* vs. *log d* graph has a slope of 2.35 which clearly discards the possibility of a Schottky or Pool-Frenkel mechanism in rf plasma polymerised aniline thin films[9].

The various aspects of conduction mechanisms in a polymer thin film are explained in chapter 2. To check the plausibility of a Pool-Frenkel or Schottky type mechanism, the log J vs. $V^{1/2}$ graph of the asymmetric electrode configuration of rf-polyaniline films were plotted and given in figure 5.6. The graph is not a straight line and thus it is found that the mechanism of conduction is not Schottkey or Pool-Frenkel type but the chances for a space charge limited conduction is evident here[10,11]

5.1.3 J-V studies on asymmetric electrode configuration of rf polyaniline

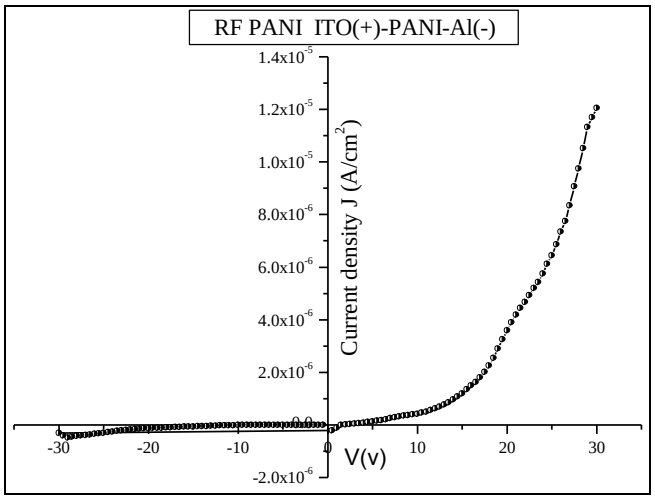

Figure 5.4: J-V plot of rf plasma polymerised aniline thin films ITO-PANIRF-Al structure.

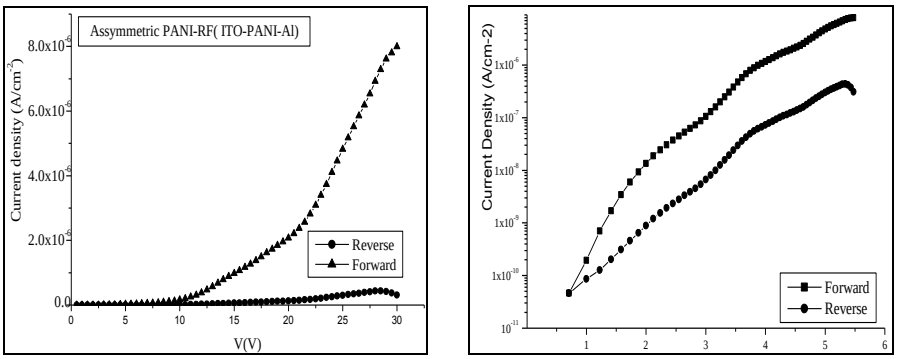

(a) (b)

Figure 5.5: (a) J-V plot of rf plasma polymerised aniline thin films. (b) The log J vs log V plot for reverse and forward bias.

Here the overall slope of the graph is 3 for reverse bias and 3.45 for forward bias condition. Forward bias (Al-) , and reverse bias(Al+). Slope of the log J log V plot is shows a space charge current. The reverse J-V characteristics give information about the metal semiconductor contact. Figure 5.6 shows the reverse bias data plotted in the form of ln J vs. $V^{1/2}$. From the slope of this graph the Schottky and Pool-Frenkel field lowering coefficients can be calculated.

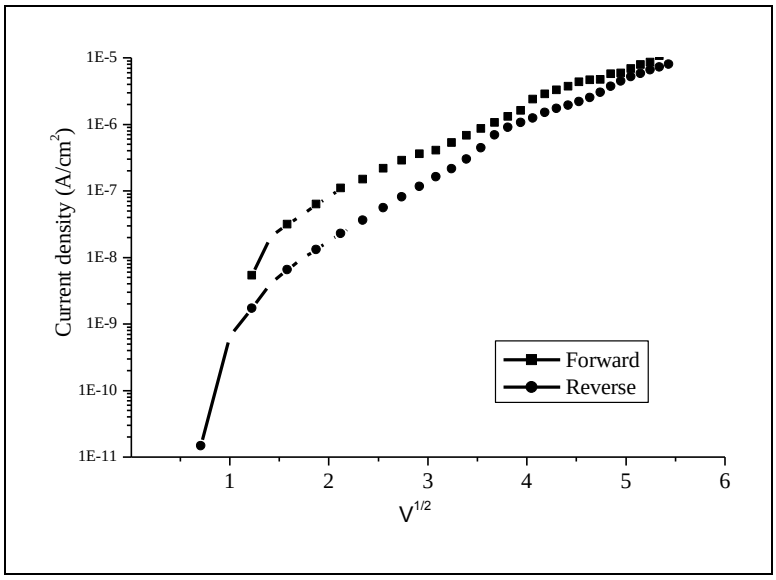

Figure 5.6: log J vs $V^{1/2}$ plot of rf plasma polymerised aniline thin films in asymmetric electrode configuration.

In the J-V characteristics of the asymmetric electrode configuration having ITO-PANI-Al structure (figure 5.4), it is found that the J-V characteristics exhibits a diode like behaviour. This is similar to the behaviour exhibited by pthalocyanine and other organic composites. The reason for this asymmetry could be the difference in work function of the two electrodes and the ionization potential of the organic film.[12] The work function difference

arises due to the difference in work function in the case of ITO (4.7 eV) and aluminum (4.2 eV). The figure 5.5 shows a rectification curve with considerable rectification ratio.

This rectification behaviour is obtained at the low field bias condition which results from the Schottky junction at the interface of PANI/Al, and the ohmic contact at PANI/ITO junctions for the asymmetric electrode configuration. Here from the plot we can see that the rf plasma polymerised PANI is p-type, and the conduction in the asymmetric electrode configuration is as follows. At the Schottky junction, electrons are presumed to transfer from Al to the p type semiconductor of PANI until the electronic potentials reach equilibrium due to the difference in work functions of Al and PANI. The electron transfer fills the p-type acceptors and forms an insulating depletion layer, resulting in the formation of negative space charge and built in field at the depletion layer[13,14].

It is possible to explain the difference in the J- V characteristics of the forward and reverse biased conditions from the above explanation. It can be seen from figure that the slope of the *logJ-logV* plot have a considerable difference at low electric fields and the variation of current with voltage is almost same when the applied field is enhanced. A possible reason for that is after a particular biasing voltage the, electrode independent SCLC[15,16] mechanism dominates over the electrode dependent Schottkey or ohmic contacts formed at the electrode/polymer interface[17].

5.1.4 Electrical conductivity studies on ac plasma polymerised polyaniline thin films

AC plasma polymerised aniline[7] thin films were deposited on glass substrates by employing an MIM configuration with Al electrodes. The DC conductivity of these films was measured using a Keithley 236 SMU. It is found that in ac plasma polymerised polyaniline thin films the dependence of current density on the electric field E is according to the relation.

$$J = J_0 \exp\left[\frac{\beta E^{1/2} - \phi}{kT}\right] \qquad 5.1$$

with ϕ is the electrode-polymer interface barrier height. β is a parameter, depends on the conduction mechanism of the thin film. The experimental value of β is compared with the theoretical values of schottkey and Pool-Frenkal parameters $\beta_s = \left(\frac{e^3}{4\pi\varepsilon_0\varepsilon_r}\right)^{1/2}$ and $\beta_{PF} = \left(\frac{e3}{\pi\varepsilon_0\varepsilon_r}\right)^{1/2}$. The experimental value of β, $\beta_{\exp} = \left(\alpha kTd^{1/2}\right)$, here α is calculated from the slope of the *logJ* vs. $V^{1/2}$ plot.

Film thickness in nm	β_s -Coefficient (eV $m^{1/2}V^{1/2}$)		Theoretical β_{PF} (eV $m^{1/2}V^{1/2}$)
	Experimental	Theoretical	
135	$3.21X10^{-5}$	$2.82X10^{-5}$	$5.64 X 10^{-5}$

Table 5.1: The comparison of the theoretical values of schottkey and Pool-Frenkal parameters for PANI ac films[18].

5.2 Electrical conductivity studies on phenyl hydrazine thinfilms

5.2.1 J-V studies on ac plasma polymerised phenyl hydrazine thin films

Preparation of phenyl hydrazine thin films using any of the existing methods are not found in literature and not much study exist out on plasma polymerised phenyl hydrazine thin films. The sandwich layer of Al-PPH-Al fabricated on a glass substrate by employing the ac plasma polymerisation technique and for the deposition of metal electrodes vacuum evaporation was employed. The details are cited elsewhere.

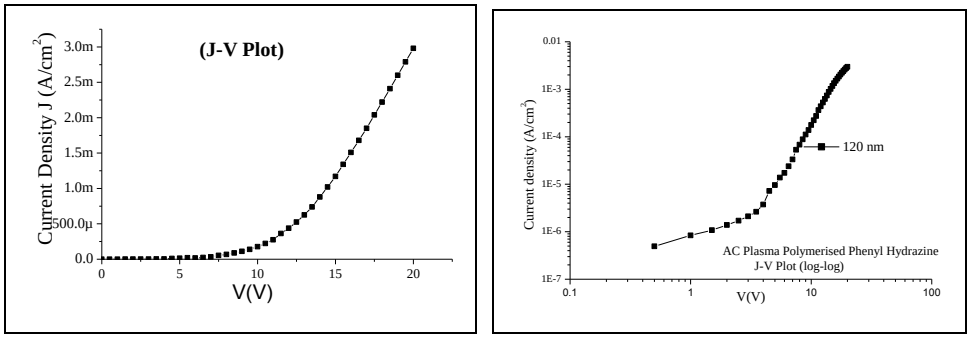

(a) (b)

Figure 5.7: (a) J-V plot of plasma polymerised phenyl hydrazine thin film of thickness 122 nm (Al-Polymer-Al). (b) The graph shows the double log plot of (J-V)

The J-V characteristics of the Al-PHAC-Al thin film is plotted and shown in figure 5.7. From the double log plot of (J-V) in the forward direction is drawn in figure 5.7b, it is clear that, up to a voltage (3.6 V) the slope of the graph is found to be 1.03 which agrees with the ohmic conduction described by the equation 5.3.

Beyond 3.6 V, the slope of the graph increases considerably. At the region between 4 V and 10 V the slope has an average value of 2 which indicates the possibility of a space charge limited conduction (SCLC) and is in accordance with the Mott-Gurney relation described by equation 5.2. From the slope of the log J-log V plot it can be seen that, the

current density J varies quadratically on the voltage V in this region which is a characteristic for SCLC and after this region the quadratic dependence of J on V increases to a trap filled limit (TFL) with slope >2. The slope of the graph found in the high voltage region is about 3.

5.2.2 Temperature dependence of conductivity of phenyl hydrazine thinfilms.

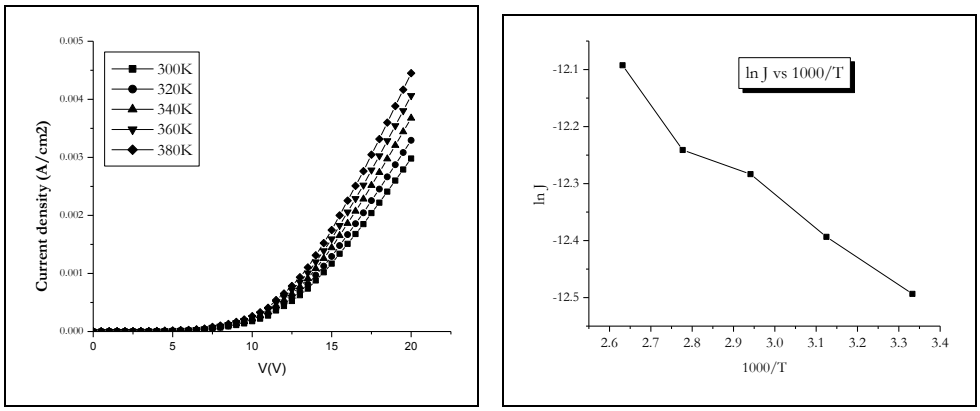

(a) (b)

Figure 5.8: (a) Temperature dependence of J-V characteristics of Al-PHAC-Al thin film. (b) The log J vs 1000/T plot showing the temperature dependence of J-V characteristics of Al-PHAC-Al thin film.

From the ln J versus the 1/T graph, the activation energy is evaluated and as Ea=0.56 eV. As in the case of RF PANI the trap distribution obey a Mayer-Neidel relation. Here in the SCLC region, the current density J as per the equation 5.5 can be applied. ε_r is the relative permittivity of the sample and here it is $\varepsilon_r = 3.2$. The relative permittivity of the sample obtained from dielectric measurements. T_t is the temperature parameter describing the exponential trap distribution given in equation 5.6. The slope of the double log J-V plot at the trap filled region is 3, and L=2. The ambient temperature is taken as 300K and from this data T_t is calculated and its value is 600 K.

In the JV characteristics of PHAC films unlike in other plasma polymerised films a sharp increase in current in the trap filled region is not observed. This is indicative of the hole transport in the PH AC thin films and the films can be assumed to be free of traps[12]. At high voltages a deviation from the square law is observed, probably due to the increase in carrier mobility. This demonstrates that the hole current in this thin film is bulk limited and not injection limited[12,19]. The carriers in the PH thin films are identified as holes from the J-V characteristics of the asymmetric Au-PHAC-Al configuration. From the slope of the ohmic region of the characteristics $n_0\mu$ can be calculated. Assuming $\mu_n = \mu_h$, at 2 V, n_0 is calculated and found to be =1.0x 10^9, here the mobility is in the order of 10^{-13} $m^{-2}/V.s$ in the low voltage regime.

In the space charge region described by the Mott-Gurney relation, the mobility can be calculated directly from the current density and it is found that the mobility in the SCLC region is in the order of 3x 10^{-13} $m^2/V.s$. At low voltages, the mobility is a constant and independent of the electric field and carrier density, but a function of temperature. But at high voltages it is observed that the current increases more rapidly than a quadratic relation with the voltage since field induced mobility is assumed.

5.2.3 Thickness dependence of conductivity in ac plasma polymerised phenyl hydrazine thin films.

The J-V characteristics of ac plasma polymerised phenyl hydrazine thin films with different thickness are given in figure 5.9. Here in this sample the log J vs. log d graph (figure 5.10) has an average slope of 2.35 which clearly discards the Schottky and Pool-Frenkel conduction mechanism in ac plasma polymerised phenyl hydrazine thin films and suggestive of a SCLC type of conduction.

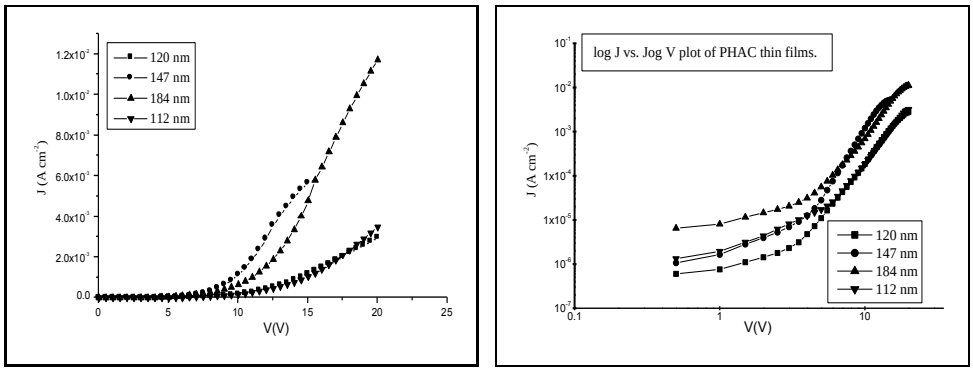

(a) (b)

Figure 5.9: (a) J-V characteristics of ac plasma polymerised phenyl hydrazine thin films. (b) log current density vs. log thickness plot. Here the slope of the log J- log d plot is 2.35 shows a space charge limited current.

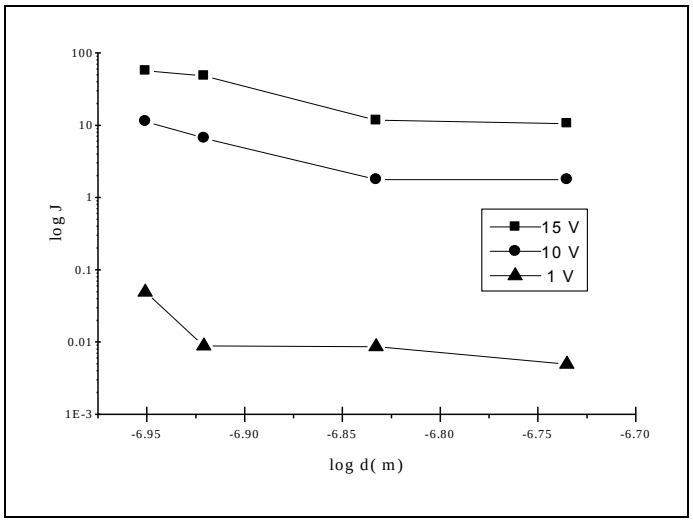

Figure 5.10: log J vs. log d of ac plasma polymerised PH thin films.

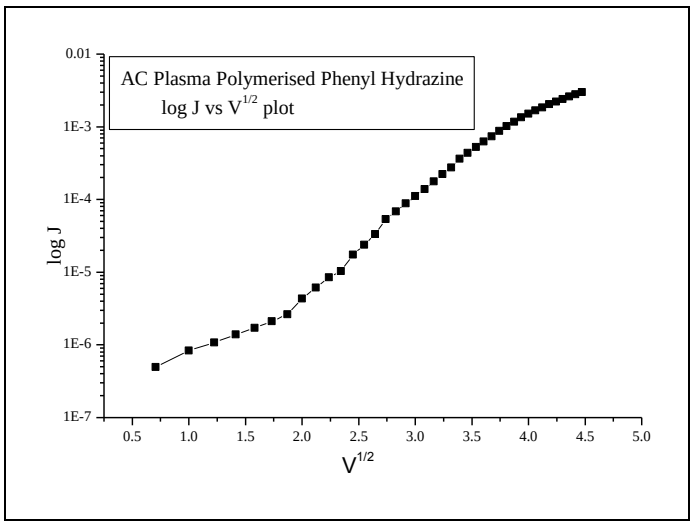

Figure 5.11: log J vs $V^{1/2}$ plot of PHAC thin film

The log J vs. $V^{1/2}$ graph of ac PPH is plotted. It is found that this graph is not a straight line and thus it is found that the mechanism of conduction is not Schottky or Pool Frenkel type[20].

5.2.4 J-V studies on the asymmetric electrode configuration of PHAC thin films

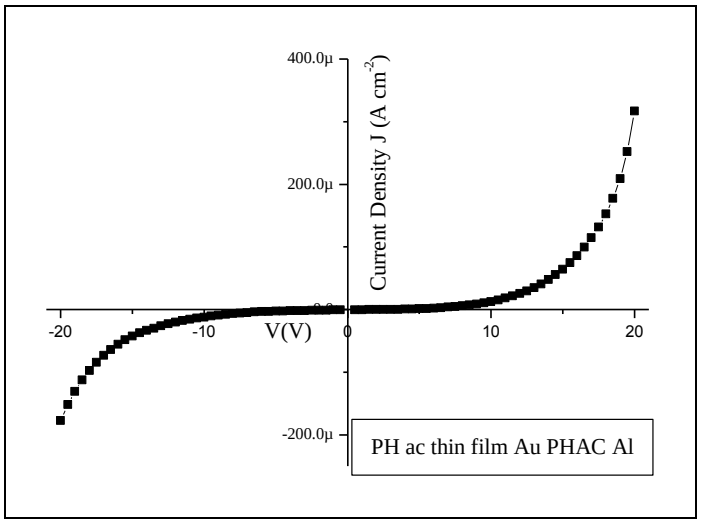

Figure 5.12: J-V plot of ac plasma polymerised phenyl hydrazine thin film asymmetric electrode configuration

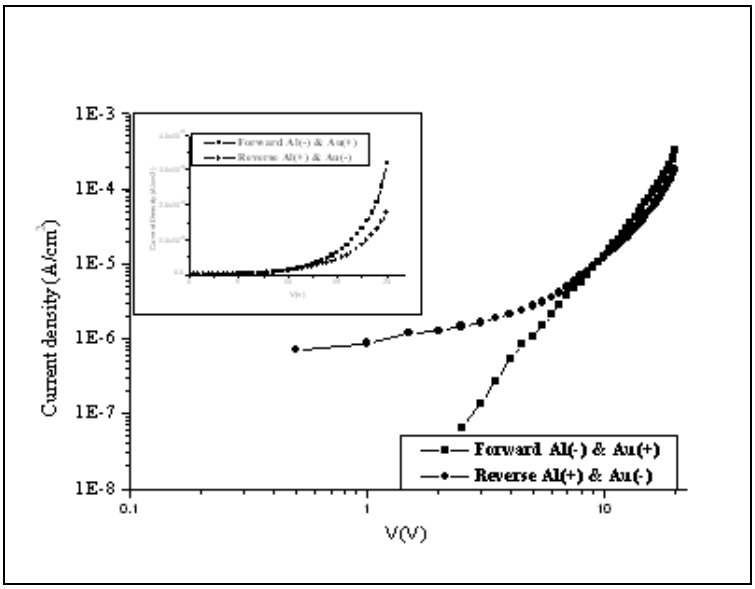

Figure 5.13: log J vs log V plot of ac plasma polymerised phenyl hydrazine thin films (Al-PHAC-Au). Forward bias (Al-), and reverse bias(Al+). Slope of the log J log V plot is shows a space charge current.

The J-V characteristics of ac plasma polymerised thin films of phenyl hydrazine are prepared in the form of Al-ACPPH-Au sandwich structure and given in figure 5.12. The forward and reverse characteristic of the asymmetric electrode configuration is different as in the case of RF plasma polymerised phenyl hydrazine. The double log plot of J-V of Al-ACPPH-Au configuration is given in figure 5.13

The results on the asymmetric electrode configuration of the ac plasma polymerised phenyl hydrazine thin films is similar to that in the case of rf plasma polymerised polyaniline described in the previous section. Here the electrodes used are Au (work function-5.2 eV) and Al instead of ITO and Al. The difference in work functions of these metals affects the conduction in the low field region and after the Schottky barrier is crossed, the reverse and forward characteristics show similar behaviour and the slope of the graphs becomes almost identical[21].

5.2.5 JV Studies on rf plasma polymerised phenyl hydrazine

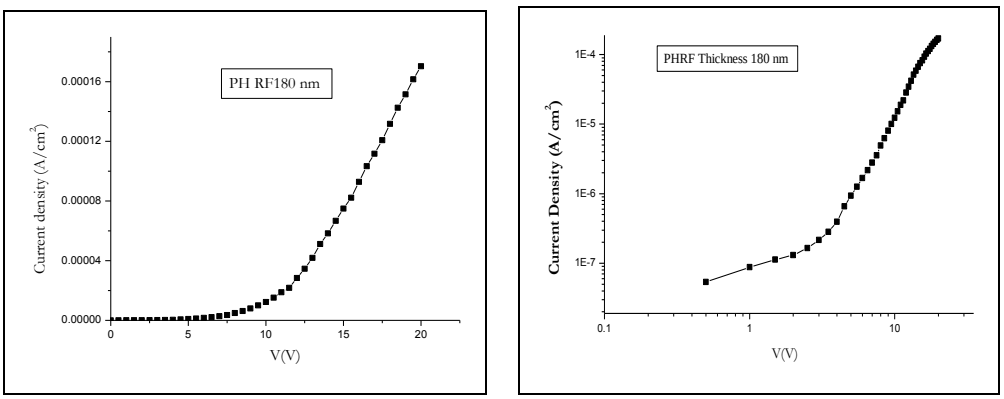

(a) (b)

Figure 5.14: (a) log J-logV plot of plasma polymerised phenyl hydrazine thin film of thick ness180 nm (Al-Polymer-Al). (b) The graph shows the double log plot of (J-V) and the inset shows the J-V characteristics.

A comparison on the J-V characteristics of rf plasma polymerised phenyl hydrazine with the ac plasma polymerised phenyl hydrazine is carried out. The forward characteristics of the PH RF film are given in figure5.14. The charge transport in rf plasma polymer shows a SCLC mechanism as observed in the plasma polymerised in the RF PANI and PHAC thin films. In the low field region the slope of log J log V plot is found to be 0.8 which corresponds to the ohmic conduction and as the field increases the current density increases with a power dependence of 3.9 which corresponds to a Tt=870K. The activation energy E_a is calculated as 0.668 eV. The mobility of the carriers at the low voltage (ohmic region) is calculated at 2.5 V, as 6.5 x 10^{-14} $m^2/V.s$

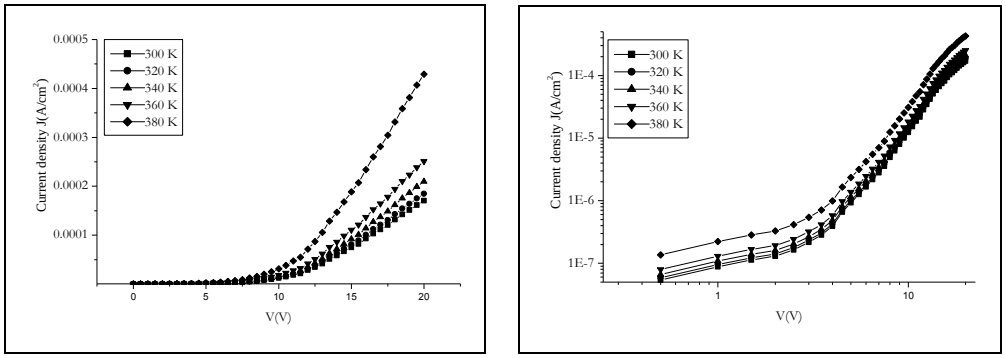

(a) (b)

Figure 5.15: Temperature dependence of log J-log V characteristics of Al-PHRF-Al thin film. Inset shows the J-V characteristics of Al-PHRF-Al thin film.

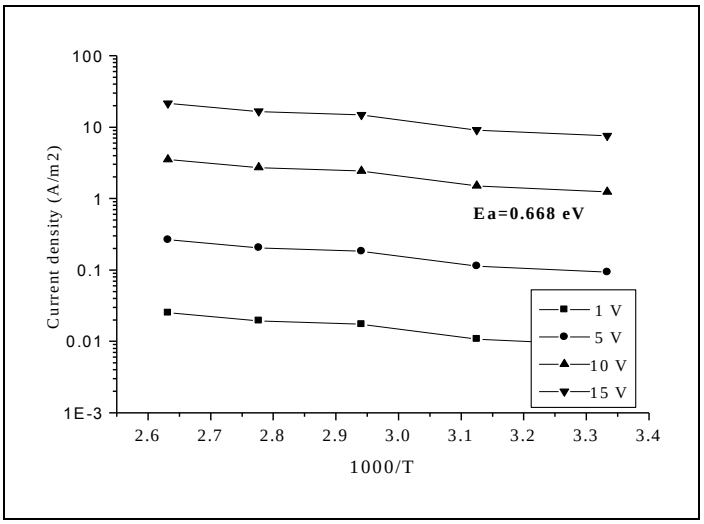

Figure 5.16: log J Vs 1000/T plot of RF PH thin film

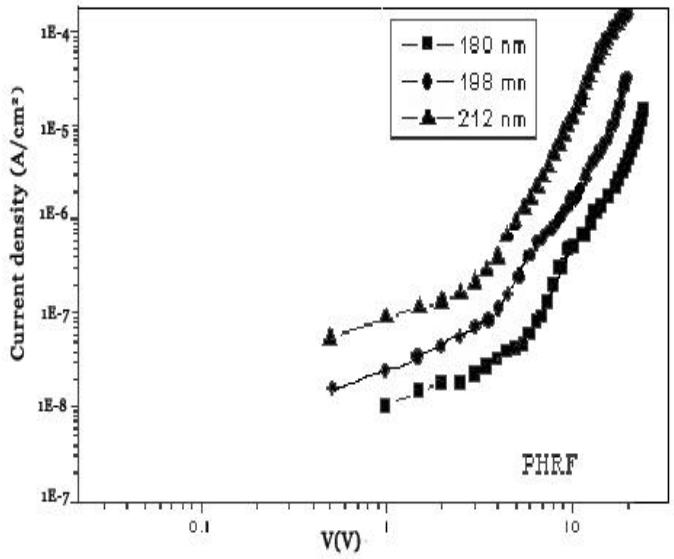

Figure 5.17: log J-log V plot of dependence of J on thickness of the thin films of rf plasma polymerised phenyl hydrazine.

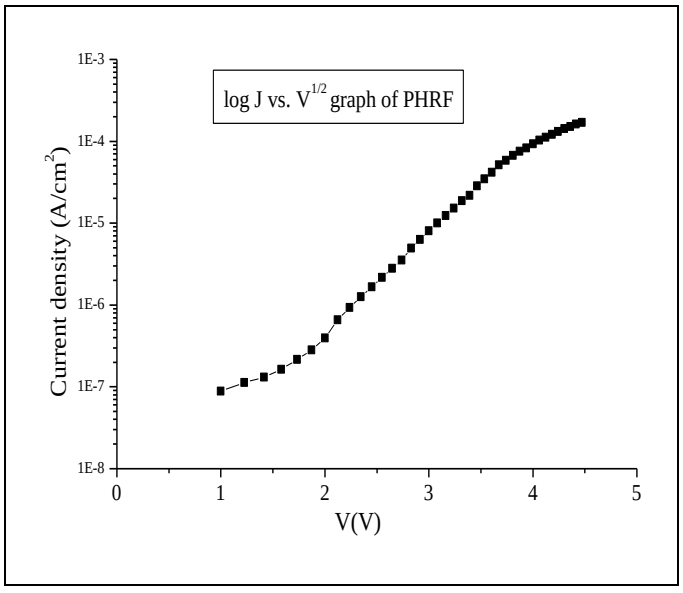

Figure 5.18: log J vs $V^{1/2}$ plot of rf plasma polymerised PH thin films.

5.2.6 J-V studies on asymmetric electrode configuration of rf polymerised phenyl hydrazine thinfilms.

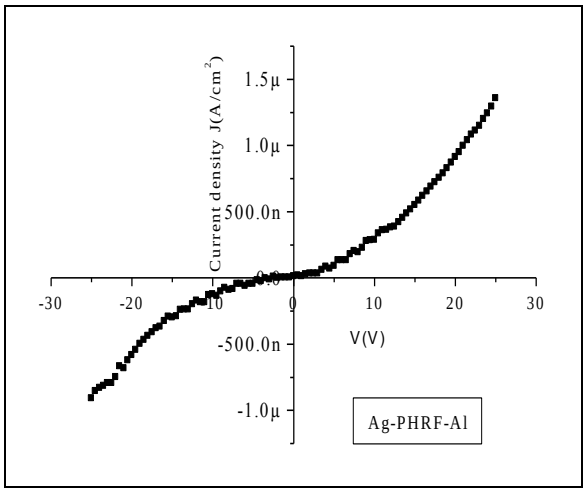

Figure 5.19: Asymmetric electrode configuration of PHRF thin films of thickness 224 nm. The Configuration is Ag-PHRF-Al.

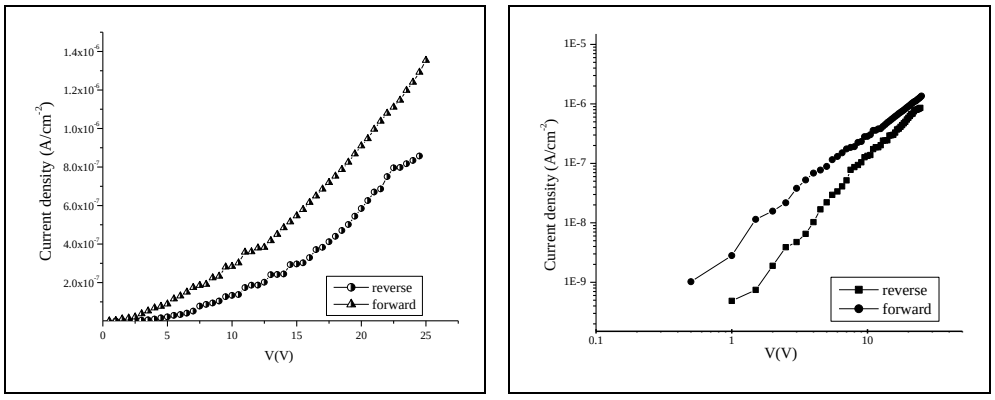

(a) (b)

Figure 5.20: (a)J-V plot for Asymmetric electrode configuration of PHRF thin films of thickness 224 nm. The Configuration is Au-PHRF-Al. Forward bias configuration Al(-ve), and Ag (+ve) (b) log J-log V plot.

The J-V characteristics of the asymmetric electrode configuration of the rf plasma polymerised PH thin film is shown in figure 5.20. This also exhibits a diode like behaviour but the rectification is not as prominent as in the case of the other two samples (RF PANI/ACPPH). A plausible explanation is that Ag and Al electrodes have a similar work function values. Here also it can be seen that in the upper voltage region the current density dependence in both the reverse and forward bias cases are the same as expected, where the electrode independent SCLC mechanism dominates at high electric fields[22].

5.3 Electrical conductivity studies on tea tree oil thin films

Tea tree is a native plant found in parts of Australia and New Zeeland and is widely grown in this continent[23]. The oil is extracted from the leaves of the tea tree and is known by the name tea tree oil and widely used in the pharmaceutical industry world wide. Tea tree oil consists of a mixture of numerous components and recent studies on this oil enabled to identify around 97 components. Among these components terpinen-4-ol (40.1%), has been found to be the most abundant .Prominent groups or components among the rest belong to the class of various mono and sesqui terpenes as well as aromatic compounds which are γ – Terpinene (23.0%), α – terpinene (10.4%), 1,8-cineole (5.1%), terpinolene (3.1%), p-cymene(2.8%), α – terpineol (2.4%), α – pinene(2.6%) and the rest are in trace amounts[24]. The natural content of the individual terpenes in tea tree oil may vary considerably depending on the climate, leaf maceration, the age of the leaves and the duration of the distillation. The literature is replete with reports on the various applications of plasma polymerised organic thin films. However reports on the employment of the techniques for the preparation of thin films based on organic products are limited, a survey of the literature reveals that studies have been limited to the growth of the film based on natural product like eucalyptus oil[25]. The primary motivation of this investigation is to explore the possibility of converting tea tree oil product in to an electronic grade material. With this objective in mind, thin films based on tea tree oil have been prepared and the structural, electrical and optical properties of these films have been evaluated with a view to understanding the possible mechanisms of conduction process occurring in these films.

5.3.1 J-V studies on rf plasma polymerised tea tree oil

Thin film of tea tree oil is prepared by the methods described in chapter 3. The J-V characteristics of rf plasma polymerised tea tree oil given in figure 5.22. The charge transport in RF plasma polymerised tea tree oil shows a SCLC mechanism as observed in the previous results of plasma polymerised rf PANI and rf and ac phenyl hydrazine thinfilms. In the low field region the slope of the log J vs log V plot is 1.2. This corresponds to the ohmic region and as the field increases the current density increases with a power dependence of 4.1, which corresponds to Tt=930K. The activation energy Ea is calculated as 0.77 eV. The mobility of the thin films in the SCLC region is calculated and is in the order of 10^{-14} $m^2/V.s$.

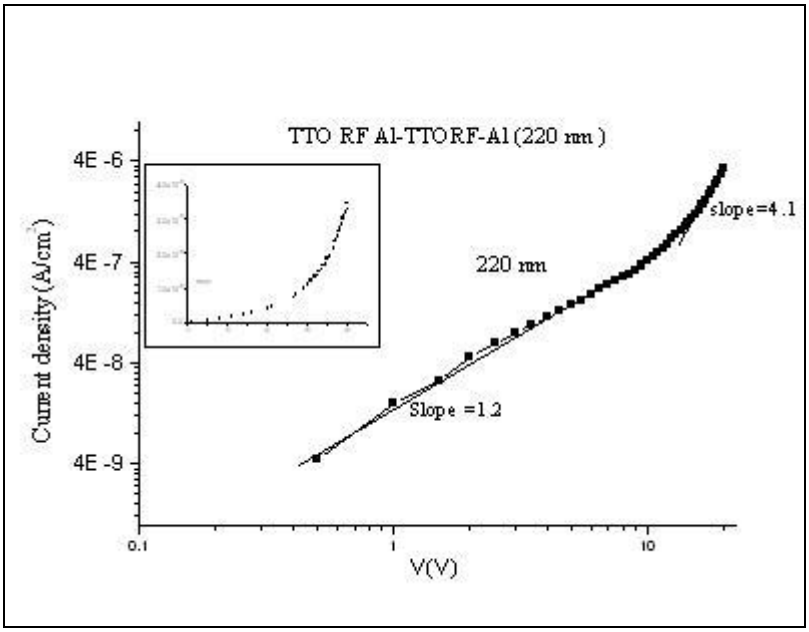

Figure 5.22: J-V plot of rf plasma polymerised TTO thin film of thick ness 220 nm (Al-Polymer-Al). The graph shows the double log plot of (J-V) and the inset shows the J-V characteristics.

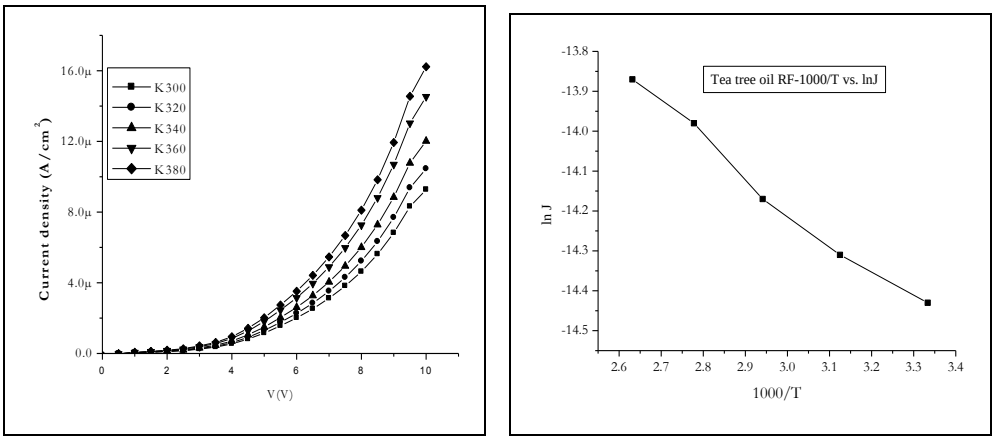

(a) (b)

Figure 5.23: (a) The temperature dependence of the J-V characteristics of rf plasma polymerised TTO thin film (220 nm). (b) log J vs 1000/T plot. The activation energy is calculated as 0.77eV

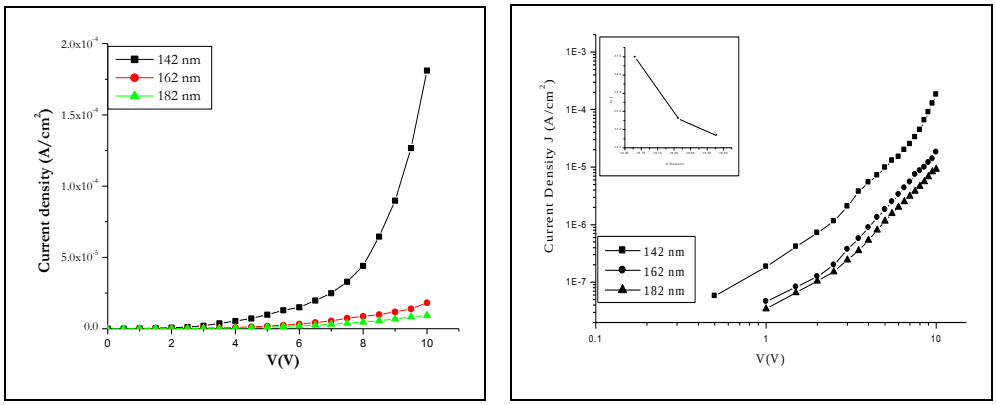

(a) (b)

Figure 5.24: (a)J-V plot of rf plasma polymerised TTO thin films for different thickness. (b) log J vs log V plot. Inset shows the log J- log d plot. The slope is 3.4, which shows a space charge current.

5.3.2 J-V studies on plasma polymerised tea tree oil thin films (asymmetric Electrode Configuration).

Figure 5.25 gives the J-V plot of RF plasma polymerised TTO thin films in its asymmetric electrode configuration. This J-V characteristic exhibits a diode like behaviour.

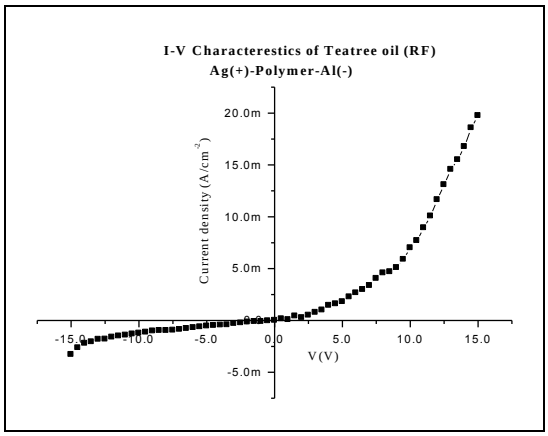

Figure 5.25: J-V plot of rf plasma polymerised TTO thin films. Ag-TTORF-Al Forward bias (Al-), and reverse bias(Al+).

Figure 5.26 (a) shows the J-V plot of the asymmetric Ag-TTORF-Al thin film. Figure 5.26 (b) shows the log J vs log V plot for reverse and forward bias. Here the overall slope of the graph is 3 for reverse bias and 3.45 for forward bias condition. Forward bias (Al-), and reverse bias(Al+). Slope of the log J log V plot is shows a space charge current.

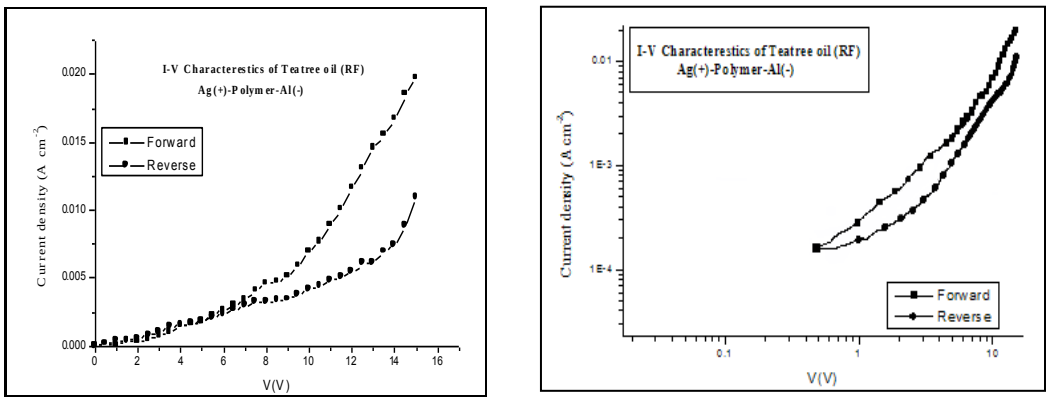

(a) (b)

Figure 5.26: J-V plot of rf plasma polymerised TTO thin films. (b) log J vs log V plot for reverse and forward bias. Here the overall slope of the graph is almost same for both bias conditions. Forward bias (Al-), and reverse bias (Al+). Slope of the log J log V plot is shows a space charge current.

The asymmetric electrode configuration of the rf plasma polymerised tea tree oil thin films thin films are given in figure. This also shows a diode like behaviour but the rectification is not so prominent as in the case of the other samples. In the high voltage region, the current density dependence in both the reverse and forward bias cases is the same as expected, where the electrode independent SCLC mechanism dominates at high electric fields.

Conclusion

Studies on conducting properties of plasma polymerised thinfilms of aniline, phenyl hydrazine and tea tree oil were carried out inorder to elucidate the possible conduction mechanism of these polymer thin films. It is found that the dominant conduction mechanism found in rf plasma polymerised aniline, phenyl hydrazine and tea tree oil is space charge limited conduction (SCLC), where as the ac plasma polymerised form of aniline exhibited Schottkey type conduction mechanism. Conductivity of all the plasma polymers subjected to the J-V measurements were found in the semiconducting regime.

References

[1] D.Sakthikumar,Kenji Nakamura, Satoko Nishiyama, Shingeru Ishii,Hiromichi Noguchi, Kunihiro Kashiwagi,and Yasuhino Yoshida, *J. Appl.Phys.* **93**,(2003),2705

[2] C.Joseph Mathai, M.R.Anantharaman, S.Venkitachalam, S.Jayalekshmi,*Thin Solid Films,* **416**, (2002), 10

[3] Blom.P.W.M,de Jong M.J.M, Van .Munster M.G,1997-II, *Phys. Rev.B* .**55**, (1997) 656

[4] M.A.Lampert, *Phys.Rev.***103**,(1956),1648

[5] B.Thomas, M.G.krisna Pillai and S.Jayalekshmi, *J.Phys.D*,**21**,(1988),503

[6] J.Tyczkowski, M.Kryszewski,*Thin Solid Films*, **55**,(1978),253

[7] F. Schauer, S.Nespurek, H.Valerian, *J.Appl.Phys.***80**, (1996),880

[8] T.S. Shafai and T.D Anthopoulos, *Thin Solid Films*, **398/399,**(1997), 361

[9] K.L.Chopra*, Thin Film Phenomena*,(Mc Graw-Hill, (1969), New York.

[10] C.Joseph Mathai, S.Saravanan, , S.Jayalekshmi, S.Venkitachalam, M.R.Anantharaman, *Metirials Letters,* **57**,(2003),2257

[11] D.Sakthi Kumar,*J.Mater.Sci.* **35**,(2000),4427

[12] M.G. Mason, L.S.Hung, C.W.Tang, S.T.Lee, A.W.Wong, and M.Wang, *J.Appl.Phys.* **86**,(1999), 1688

[13] Keiichi Kaneto, Kazuhisa Takayama,Eataru Takashima, Takeshi Endo, Masahiro Rikukawa, *Japan J.Appl.Phys.*,**41**(2002).675

[14] M.Koehler, M.G.E da Luz, I A Hummelgen, *J.Phys.D:Appl.Phys.***34**,(2001),1947

[15] M.A.Lampert, and A Mark, *Current Injection in Solids,Academic Press*,(1970), New York

[16] P.W.M. Blom, de Jong M.J.M,and J.J.M Veggaar *Appl.Phys.Lett.* ,**68,**(1996),3308

[17] K.Limouni, C.Legrand and A Chapton, *Synth.Metals.***97**,(1998),151

[18] C.Joseph Mathai, *Ph.D Thesis,* Cochin University of Science and Technology, (2002)

[19] P.W.M.Blom, M.C.J.M Vissenberg, *Phys.Rev.Lett*, **80**,(1998),3819

[20] H.S.Kang, K.H.Kim, M.S.Kim, K.T.Park, K.M.Kim,T.H.Lee, J.Joo,K.Kim,D.H.Lee,J.I.Jin, *Current Appl.Phys.***I** (2001),443

[21] V.D.Mihailethi, P.W.M.Blom, J.C.Hummelen and M.T.Rispens, *J.Appl.Phys.***94**, (2003),6849

[22] J.H.Park, H.Y.Yu, J.G.Park, B.Kim, S.H.Lee, L.Olofsson, S.H.M.Persson, Y.W.Park, *Thin Solid Films*, **393**,(2001),129

[23] Hammer A.A, Carson C.F and Riley T.V, 2004, *Journal of Antimicrobial Chemo Therapy*, **53**, 1081.

[24] Brophy Joseph J, Davies Noel W, Southwell Ian A, William Lyall R, *Journal of Agricultural and Food Chemistry*, **37**, (1989), 1330

[25] D.Sakthikumar,Kenji Nakamura, Satoko Nishiyama, ,Hiromichi Noguchi, Shingeru Ishii, Kunihiro Kashiwagi,and Yasuhino Yoshida, *J. Appl.Polym.Sci* **90**,(2003),1102

Chapter 6

Dielectric and Impedance characterization of plasma polymerised thin films

The dielectric properties of plasma polymerised thin films assume significance not only from application point of view, but also from a fundamental point of view. Recently extensive investigations are on to replace low-k (low permittivity) materials based on silica with newer materials based on organic polymers[1,2]. This is because low k materials with appropriate thermal stability can easily be integrated into the ICs. These low-k materials serve as ideal interlayer dielectric and thus reduce the RC time constant[3]. The low-k values have a direct influence on the capacitance and the RC time constant is reduced[4].

Researchers have been trying to incorporate porosity in silicon, there by reducing the permittivity[5]. However the low-k characteristics exhibited by polymer thinfilms do not owe their low-k to porosity, instead they probably acquire these characteristics because of the nature of bonding, presence of dangling bonds in the matrix apart from a variety of other factors contributing to these parameters. Hence research on the preparation and characterisation of the plasma polymer thin films are in the forefront of research[6]. The employment of ac or rf plasma polymerisation offers many advantages as stated earlier like ease in preparation, pinhole free films etc. Many materials based on plasma polymerised thinfilms have been found to be exhibiting low-k characteristics[7]. In that some of theses films exhibit low-k values up top certain frequency under the influence of an ac electric field and there after displays anomaly. These are unexplained in our earlier investigations and hence this is an attempt to delve into the mechanisms that govern the dielectric properties over a wide range of frequencies and offer a plausible mechanism.

In the earlier chapters we have dealt with the electrical conducting properties of many plasma polymerised thin films of aniline, phenyl hydrazine

and tea tree oil. This chapter takes a look at the dielectric properties of these films. Attempts will be made to offer a plausible mechanism to the conduction phenomenon under the influence of an ac electric filed.

6.1 Dielectric permittivity studies on plasma polymerised aniline (PANI) thin films

In our laboratory, investigations are underway on the low-k properties of plasma polymerised thinfilms. Preliminary investigations were carried by Saravanan[6] et al and Joseph[1] et al and it has been found that both pristine and iodine doped plasma polymerised aniline exhibited low-k characteristics over a wide range of frequencies. The thermal stability of these films was also a subject of study and it was found that they are thermally stable up to a temperature of 400K.

The low-k properties of these thinfilms are also investigated in the optical frequency regime employing spectroscopic ellipsometry (SE) and there was excellent correlation between these experiments. The details of these findings are cited in the chapter 7.

An automated LCR meter was used to evaluate the capacitance and then the dielectric permittivity employing the principle of parallel plate capacitor. The impedance of these films were also estimated and the results are analysed. Sandwich configurations (M-I-M) were used to evaluate all these parameters. The ac conductivity was deduced using the formula from the loss tangent.

$$\sigma_{ac} = 2\pi f \varepsilon_0 \varepsilon_r \tan \delta \qquad 6.1$$

The entire experiment was carried out under dynamic vacuum and in the frequency regime of 100Hz to 10 MHz. The details are cited in Chapter 3.

Polyaniline thin films were prepared by employing both rf and ac plasma polymerisation (using the optimized parameters).The thickness of these thinfilms were determined by utilizing Dektac 6M stylus profiler. A metal-insulator-metal (M-I-M) sandwich configuration was employed to evaluate the capacitance and subsequently the dielectric permittivity ε_r. The frequency (in logarithmic scale) vs. dielectric permittivity of these thinfilms were plotted and

are depicted in figure 6.1. It can be noticed that, both films made using ac and rf technique display almost similar characteristics. The dielectric permittivity values at low frequency are ~ 4.5 for rf-PANI and around 3.75 for ac-PANI. These values by and large remain a constant up till a frequency of 100 KHz, and there after decrease steeply. The permittivity values exhibited by this film are in the low-k regime, beyond the frequency limit of 100 KHz.

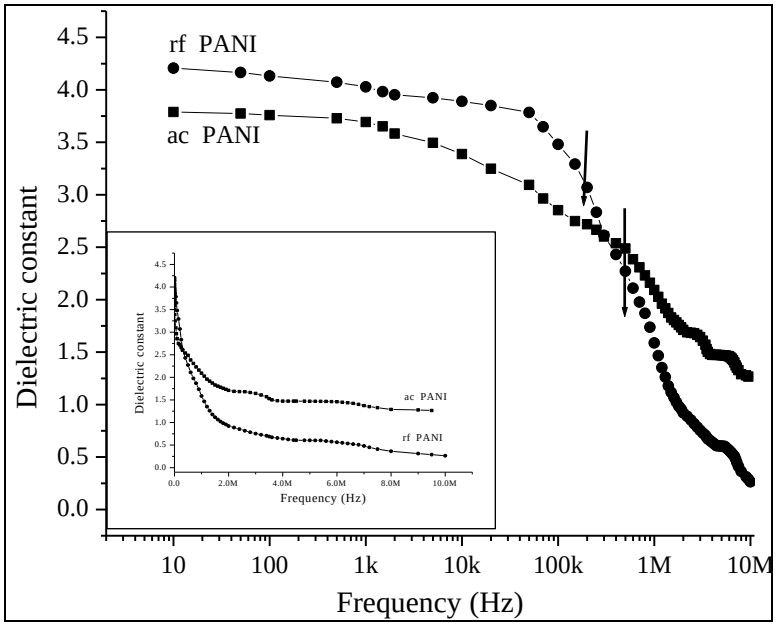

Figure 6.1: Dielectric permittivity vs. frequency (in log scale) Plot of ac and rf plasma polymerised polyaniline thin film of thickness rf 169nm, ac163nm prepared at a plasma current of 60 mA. Inset shows the dielectric constant vs frequency graph (frequency in the linear scale)

This variation pattern of dielectric permittivity for PANI films is typical of a Maxwell-Wagner type of interfacial polarization[8]. This type of behaviour is most often found in solid dielectrics, were it is assumed to be consisting of two types of grains , one a conducting grain separated by a non conducting grain. The influx point is noted here and an additional evidence for this dispersion is to be procured from the other measurements. This $\tan \delta$ vs. log F has plotted and the ac conductivity was evaluated and this was plotted along the y axis and log F

along the x axis. These graphs are shown in figure 6.2. It can be seen that the frequency at which the dielectric permittivity decreases matches with that of the peaks at which the ac conductivity begins to increase sharply.

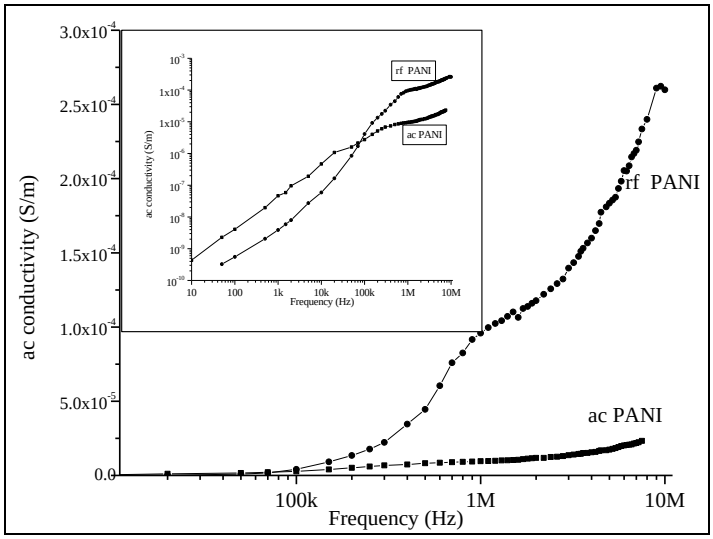

Figure 6.2: ac conductivity vs frequency (in log scale) of plasma polymerised aniline thin films. The inset shows log $\sigma(ac)$ vs. log f plot of rf and ac plasma polymerised PANI

Earlier studies on dc conductivity of these samples established the fact that it is the space charge limited conduction (SCLC) which is predominant in these films. These details are cited in chapter 5. These conclusions led to the presumption that the space charge accumulation at the structural interfaces of a inhomogeneous dielectric material is responsible for the interfacial polarization. So it can be intuitively inferred that the characteristic dependence of dielectric permittivity with frequency is because of interfacial polarization which is a direct consequence of the space charge accumulation.

An equivalent circuit for this system of inhomogeneous dielectric is essential to deduce ε_s and the capacitance Cs. Gosami and Gosami[9] has proposed a model, according to which the total series capacitance *Cs* is given by

$$C_S = C' + \frac{1}{\omega^2 R^2 C'} \qquad 6.2$$

According to this model, a capacitor system is assumed to be comprised of a frequency independent capacitive element C' in parallel with a discrete-temperature-resistive element R. Both are in series with a constant low voltage resistance R. The dielectric constant is evaluated from the capacitance as $C = \frac{\varepsilon_0 \varepsilon_r A}{d}$, where d is the film thickness, C is the measured capacitance of the sample and A is the surface area of the sample. ε_r is the relative permittivity at the frequency at which the capacitance is measured.

The probable reason for the "breakdown" in the dielectric constant after a frequency range about 2 MHz is the inter electrode tunneling occurring in PANI thin films in the ac and rf plasma polymerised films. In ac films such a breakdown of dielectric does not occur even at 8 MHz frequency, but in the rf plasma polymerised films the dielectric behaviour of the film is lost and the film becomes conducting at a lower frequency when compared to that of the ac plasma polymerised films. This can be explained in terms of the electric field induced polarisation. At higher frequencies the mobility of the carriers, driven by the applied field increases and the hopping between different grains becomes more prominent. This can be explained based on the field induced polarization[10].

Here it is assumed that, the total dipole moment of a polymer molecule is the vector sum of the moments of the constituent monomer units and this depends on the configuration which the monomer assumes, since the molecular configuration is constantly changing when a frequency dependent electric field is applied, dependent on the temperature and molecular environment. The effective moment is the statistical moment of the polymer chain which is dependent on the molecular structure.[11]. This will reduce the ac impedance of the thin films and at that frequency, the film acts as a good semiconductor with low resistance/impedance at high frequencies.

6.2 AC conductivity studies on PANI thin films

The evaluation of ac conductivity (σ_{ac}) from the dielectric loss ($\tan\delta$),values gives valuable information on the nature of conduction occurring in these films. The ac conductivity σ_{ac} was evaluated for a wide range of frequencies and is plotted and is depicted in figure 6.2. In the case of plasma polymerisation it is a well known fact that, a single molecule alone is responsible for the conduction, but the conduction process is dependent on the interchain interaction of the polymer[12]. The ac conductivity σ_{ac} is frequency independent at low frequencies, but increases with a frequency above a critical value. Such a behaviour is found among materials with a disordered structure. The disordered materials are assumed to be composed of disordered low conductive matrix, and conductive islands[13]. The conduction occurs via electronic hopping transport probably involving phonon assisted tunneling- sprinkled with conductive islands[14].

After a particular frequency, the ac conductivity σ_{ac} increases with increase in the frequency. The ac conductivity increases rapidly at higher frequencies when compared to lower frequencies[15]. This can be empirically expressed as $\sigma(\omega) = A\omega^n$, where ω is the frequency and n is an index which is used to understand the type of conduction mechanism in amorphous materials. Here A is a constant. Here in this case the value of n determined from the $\ln\sigma - \ln\omega$, graph (figure 6.2- inset) lie between 0.3 to 0.92, and this value is in accordance with the theory of hopping conduction in amorphous materials. It agrees with the same parameter calculated by Joseph Mathai *et al* in their earlier studies (0.334)[1].According to a model based on *Mott and Austin*[16], the dependence of ac conductivity at lower temperatures is given by the relation [3]

$$\sigma_{ac} = A\left(\frac{e^2}{\alpha^5}\right)\left(\left\{\Delta E_F{}^2\right\} kT\omega\left[\ln\frac{\upsilon_{ph}}{\omega}\right]\right)^4 \qquad 6.3$$

when differentiating this equation with respect to ω we get,

$$\frac{d\ln\sigma_{ac}(\omega)}{d\ln\omega} = 1 - \frac{4}{\ln\left(\nu_{ph}/\omega\right)} \qquad 6.4$$

The term in the left hand side is determined by the slope of the $\ln \sigma - \ln \omega$, graph and $\omega = 2\pi f$. The slope of the log-log plot (ac conductivity vs. frequency) of rf polyaniline gives different values at different frequency regions. The overall slope of the graph (from the liner fit) is found be 0.39281. In the low frequency region (10 Hz -10KHz) the slope is 0.86, from 10KHz to 1M slope is 0.304 and 1M-10M , the slope is) 0.92. The phonon frequency corresponding to these slopes in the ac and rf plasma polymerised films lies in the range of 10^{10}-10^{14} Hz.

The strong dependence of ac conductivity with frequency indicates a frequency induced hopping conduction mechanism in plasma polymerised thinfilms[17],[18] Here the applied electric field between the electrodes is responsible for the hopping conduction mechanism. As the frequency increases, the hopping between the charge centers and the electrodes increases and as a result the ac conductivity increases sharply and the material becomes conducting. At this stage, an inter electrode tunneling of the carrier occurs and this will result in a frequency dependent reversible "breakdown" of the dielectric property of the material. The reports on plasma polymers by *M.S.Silverstein et.al*[19] support these findings. Silverstein proposed a model for this behaviour and he assumed that the plasma polymer thin film consists of two types of grains, an insulating island and a semiconducting one. In such a structure it is assumed that, with in the wider network of the insulating matrix, the semiconducting islands are sprinkled all over. This behaviour is also observed in polymers prepared by chemical synthesis[20],[21].

It can be noticeable from figure 6.2 that, at low frequencies up to a critical frequency ω_c, the conductivity is frequency independent and after that σ is a strong function of frequency. Here in this case for rf-PANI and the ac-PANI ω_c is 100 KHz. The conduction mechanism at higher frequencies can be assumed to be hopping in a disordered medium having random free energy barrier between the residence sites[22]. The jumping frequency between a minimum and a maximum frequency $\gamma_{\min}$ and $\gamma_{\max}$ is governed by the equation

$\gamma = \gamma_0 \exp(E/kT)$ where γ_0 is the frequency factor depends on the distance between the dopant sites and E is the energy of activation.

6.3 Impedance analysis on polyaniline thin films

Evaluation of impedance is a very good alternative to arrive at the nature of the conduction occurring in these types of films. This not only provides additional supports to the hypothesis that beyond a certain frequency and under an applied electric field, the apparent "breakdown" of the dielectric is a possibility and here onwards the accumulated charges gains mobility and they tunnel between the grains[23]. The complex ac impedance is measured and is given by the relation

$$Z = Z' - jZ'' \qquad 6.5$$

where Z' and Z'' are the real and imaginary part of the ac impedance[24]. Here, in our analysis only the real part of Z is taken into account. Equivalent circuit for the impedance is arrived at, based on a model suggested by [25,26] Mills *et.al.* According to this model, Z' can be calculated from the equation

$$Z' = R_0 + R_b / \left(1 + \omega^2 R^2 C_b{}^2\right) \qquad 6.6$$

In the case of plasma polymerised PANI thin films R_0 is very small, of the order of few ohms. R_b is many orders higher magnitudes when compared to R_o at lower frequencies. As the frequency increases, the second term in equation 6.6 decreases. The frequency dependence of ac conductivity enables the estimation of R_0 for different polymers used in this study. This model is generally applicable to a polymer having a disordered structure. It can be seen that, beyond a critical frequency the conduction is via a hopping transport and the tunneling is assisted by phonon.

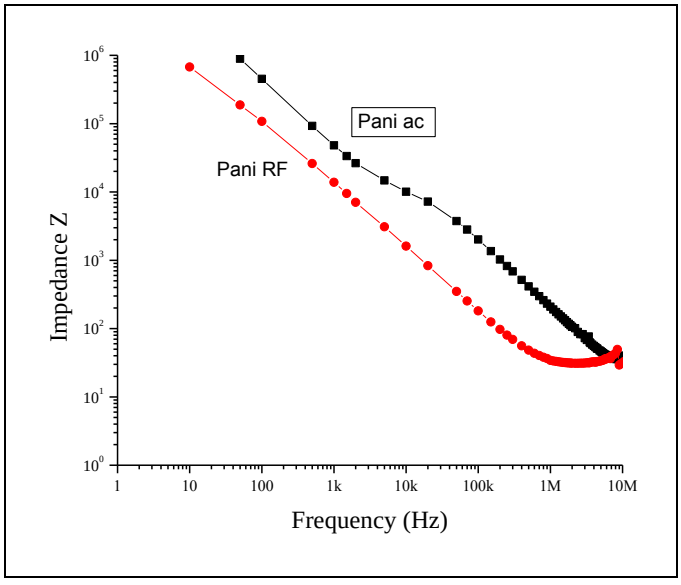

Figure 6.3: Impedance Vs frequency of ac and rf plasma polymerised polyaniline thin films.

At high frequencies the rapid increase of ac conductivity associated with decrease in ac impedance is probably due to the increase of carrier mobility at higher driving frequencies. At a frequency of 5 MHz the AC conductivity is of the order of 0.01 S/cm and impedance of the order of 20 ohms. In the plasma polymerised thin films as the frequency increases, the bulk impedance decreases[27]. Figure 6.3 shows the frequency impedance curve for the polyaniline thin films. In the MHz regime, the impedance decreases to 30 ohms, and this is equivalent to a conductivity value of 10^{-2} S/m, and at that frequency the sample behaves as a perfect semiconductor. This is in agreement with the with the ac conductivity results on plasma polymerised PANI films.

The variation of Z' with frequency in the case of both ac and rf plasma polymerised PANI films are almost identical. In the case of rf-PANI, R_0, the minimum impedance value corresponding to a particular frequency is less than that of the ac-PANI film. However, the rate of decease of impedance in the low frequency regime is almost the same in the case of both rf and ac films.

6.4 Dielectric studies on plasma polymerised phenyl hydrazine (PPH)

Both ac and rf plasma polymerised phenyl hydrazine films were subjected to dielectric measurements and the impedance studies. The variation of dielectric permittivity with frequency is depicted in figure 6.4

It is noteworthy that ac plasma polymerised phenyl hydrazine exhibited a high-k (high value of permittivity) in the lower frequency regime, while rf plasma polymerised PH exhibited a near constant k along the entire frequency region beginning from 100Hz.

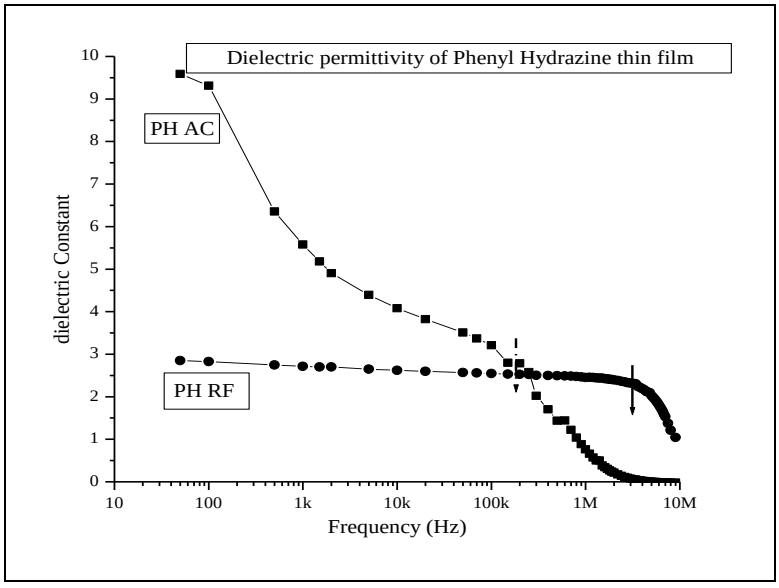

Figure 6.4: The dielectric constant vs. frequency of plasma polymerised phenyl hydrazine thin films. rf(prepared at a plasma current of 65mA, 150 nm thick) and ac(156nm, plasma current 65mA)

If one compares the behaviour of these films prepared under two dissimilar conditions, it can be seen that the variation of permittivity ε_r with frequency is almost in accordance with the theory of interfacial polarization. Ac plasma polymerised PH exhibited a dielectric permittivity value of 3.8 while, rf plasma polymerised PH showed a value of 2.8. The theory of interfacial polarization and the hypothesis of tunneling can be invoked here in explaining

the observed 'breakdown'. Here too in both cases, RF and ac plasma polymerised PH, they follow a frequency dependent polarization mechanism

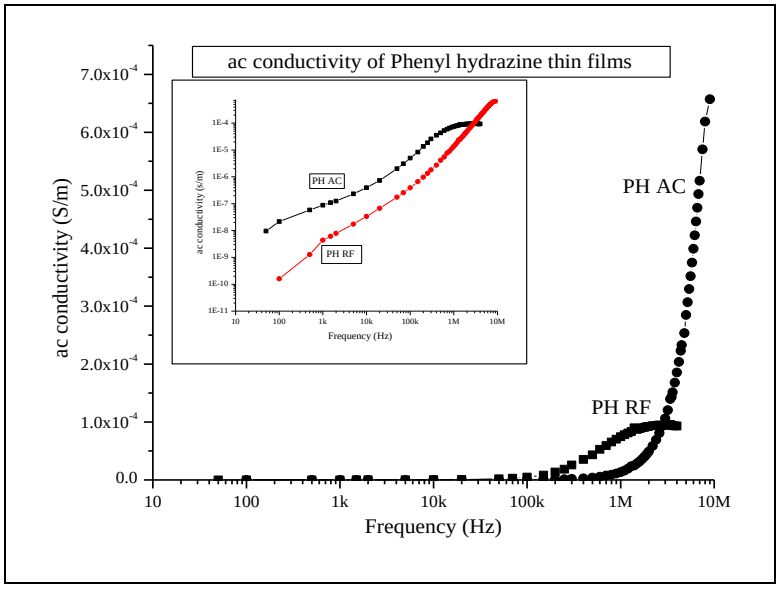

Figure 6.5: ac conductivity vs Frequency Plot of rf (prepared at a plasma current of 65 mA, 150 nm thick) and ac(156nm, plasma current 65 mA), plasma polymerised phenyl hydrazine thin films. b. Inset shows the frequency dependence of ac conductivity of RF and ac plasma polymerised phenyl hydrazine. The log- log plot (ac conductivity vs. frequency) is a straight line slope =0.87 in rf plasma polymer and a straight line slope of 0.92 in ac plasma polymer

In rf plasma polymerised PPH samples, at a higher frequencies the space charge developed in the samples crosses a threshold value, resulting in an enhanced mobility. This result is in conformity with the results obtained in *chapter 4* and *chapter 5*. It is noteworthy that the variation of J with V is different in RF and ac plasma polymerised samples are even though the predominant conduction mechanism in the case of rf and ac films are the same. Also it is found that the order of conductivity of rf and ac plasma polymers is different. The ac plasma polymerised thin films show a higher value of conductivity in the case of PH thin films.

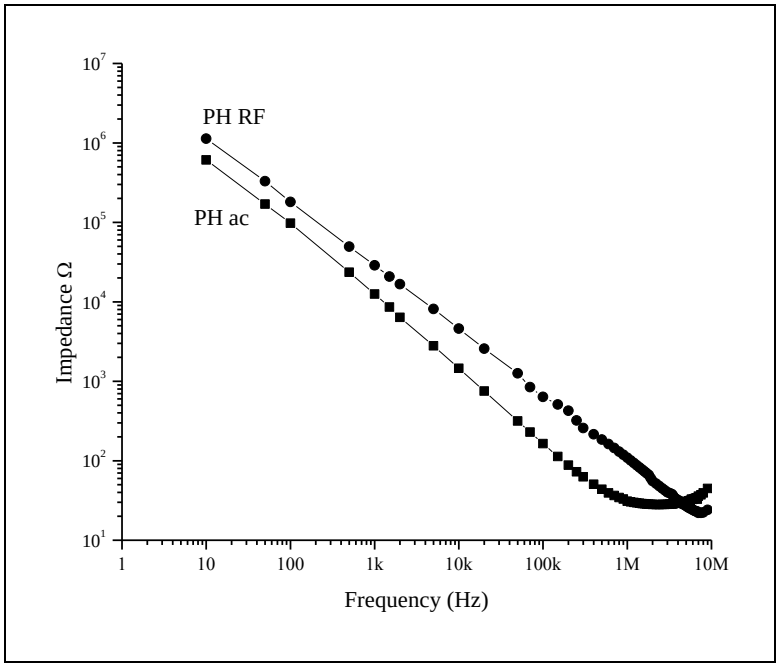

Figure 6.6: Impedance vs frequency of rf and ac plasma polymerised phenyl hydrazine

6.5 Dielectric permittivity studies on tea tree oil thin films

Both rf and ac plasma polymerised thin films of TTO were investigated for studying the variation of the dielectric constant and ac conductivity with frequency . These films too exhibit a similar behavior akin to the characteristic behaviour displayed by the plasma polymerised thinfilms of PANI and PH. From the J-V studies on tea tree oil thin films, it is found that these films are good semi conductors and shows space charge limited conduction at the room temperature. It is found that the frequency region with which the tea tree oil thin films shows a "break down" in the dielectric value is about 10 KHz, which is very much less that of the frequency observed in terms of the ac thin films.

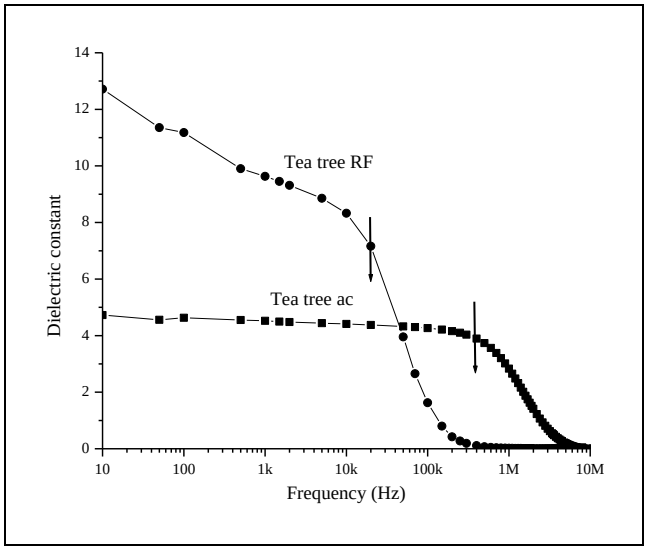

Figure 6.7: Dielectric permittivity vs. Frequency Plot of ac plasma polymerised tea tree oil thin film of thickness 220nm, Prepared at a plasma current of 60 mA.

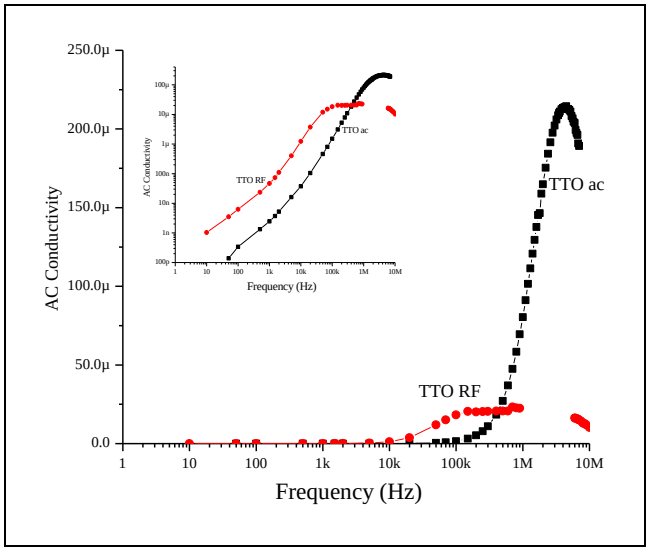

Figure 6.8: ac conductivity vs frequency plot of plasma polymerised tea tree oil thin film of thickness 156nm, Prepared at a plasma current of 60 mA, b. Inset shows the frequency dependence of ac conductivity of plasma polymerised phenyl Hydrazine. The log- log plot (ac conductivity vs frequency) is a straight line with a slope =1.328 for ac films and 1.12 for RF films.

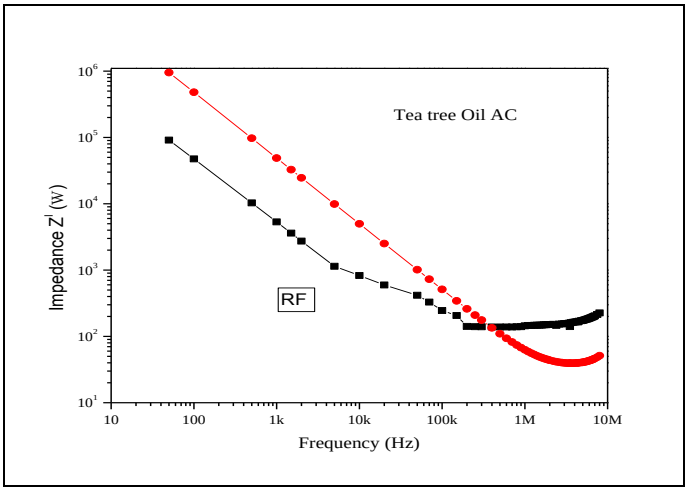

Figure 6.9: Impedance vs frequency of tea tree oil

Here in this case for RF TTO thin films the ω_c is 10 kHz and for ac TTO ω_c is 100 k Hz.

Conclusion

Dielectric and ac conductivity studies in RF and ac Plasma polymerised thin films of, Polyaniline, Phenyl Hydrazine, and tea tree oil were carried out and the results are explained. All the films show a breakage of dielectric value at higher frequencies for an applied biasing voltage of IV between the electrodes. A hopping conduction at higher frequencies as observed by *Lepienskiis* observed in all films. An inter electrode tunneling of carriers at high frequencies is observed in all films. The electric field induced polarisation and the hopping of carriers at high frequencies were observed in all the plasma polymers investigated.

References

[1] C.Joseph Mathai, S.Saravanan, M.R.Anantharaman, S.Venkitachalam, S.Jayalekshmi *J.Phys.D.Appl.Phys.* **35**,(2002),240

[2] C.Joseph Mathai, *Ph.D Thesis*, Cochin University of Science and Technology, 2002,

[3] M.T. Bohr,*Solid State Technol.* **9**, (1996),105

[4] G.maier, *Prog.Polym.Sci*,26(2001),3

[5] Ruxandra M. Costescu, Andrew J. Bullen, George Matamis, Keith E. O'Hara, and David G. Cahill, *Phys.Rev.***B**, **65**,(2002), 094205

[6] Bengi Hanyalogu, Atilla Aydinli,Michael Oye and Eray S.Aydi, Appl.Phys.Lett. 74,(1999),606

[7] S.Saravanan, C.Joseph Mathai, S.Venkitachalam, M.R.Anantharaman, *New J.Phys*, **6**,(2004),64

[8] Vera V.Daniel, Dielectric Relaxation, Academic Press, (1967), New York

[9] Gosami. A and Gosami A.P, *Thin Solid Films,* **16**, (1973),175

[10] Kai Wu, L. A. Dissado, Tatsuki Okamoto, *Appl.Phys.Lett* , **85**, (2004), 4454

[11] Nora E.Hill, *Dielectric Properties and Molecular Behaviour,* Van Nostrand Reinhold,(1969), New York

[12] C.M.Lepienski, R.M.Faria, G.F Leal Ferreia, *Appl.Phys.Lett.* **70,**(1997), 1906

[13] D.S.Galavao, D.A.Dos Santos, b.Laks, C.P.de Melo, M.J, Caldas, *Phys.Rev.Lett,* **63**,(1989), 786

[14] Koichi Shimakawa, J. Non. Cryst. Solids, **43**,(1981),141.

[15] A.N.Papathanassiou,*J.Phys.D:Appl.Phys*, **35**,(2002),L88

[16] Mott N.F and. Davis E.A, 1971, *Electronic Process in Non Crystalline Materials*,(Clarenndon Press, Oxford)

[17] S .R.Elliott, *Phil.Mag.***36**,(1977),1291

[18] R.D.Gould , A.K.Hassan,*Thin Solid Films*,**223**,(1993),334

[19] Silverstein M.S and Visoly Fisher I, *, Polymer*,**43**,(2002),11

[20] J.M.Ginder, A.F.Ritcher,A.G.Mac Diarmid, and A.J.Epstein, *Solid State Commun.***63**,(1987),91

[21] D.Jeon,J.Kim,M.C,Gallagher, and R.F.Willis,*Science,***256**,(1992),1662

[22] Tadashi Katsume,Masahiro Hiramoto,Masaaki Yokoyama,Appl.Phys.Lett.**64**,(1993),2546

[23] Tzung-Fang Guo, Gufeng He,Seungmoon Pyo,Yang Yang, *Appl.Phys.Lett.*,**80**,(2002),4042.

[24] M.A.L.Nobre and S Lanfredi, *J.Phys.Condens.Matter.* **12**,(2000),7833

[25] C.A.Mills, D.M Taylor, A.Riul.Jr, A.P Lee. *J.Appl.Phys,* **91**,(2002),5182

[26] D.M .Taylor, and C.A Mills. *J.Appl.Phys,* **90**,(2001), 306

[27] H.C.F.Martens, O.Hilt, H.B.Brom, P.W.M.Blom, J.N.Huiberts, *Phys.Rev.Lett,* **87**,(2001),86601

Chapter 7

Spectroscopic ellipsometric characterization of plasma polymerised aniline thin films

Polymer thin films display anisotropy under the influence of an electric field. Generally they are said to be displaying ordinary optical properties when the electric field is perpendicular to the c-axis and exhibit extra ordinary optical properties when the electric field is parallel to the c-axis. The anisotropy is a strong function of the crystallographic and textural orientations. If the polymer chains are alligned/oriented along the same direction, the anisotropy of the polymeric material would be similar to that of a single crystal. If the chains have the same probability of occurrence for all textures and orientation, the optical properties of the material would be isotropic. The effective dielectric function of a polymeric material can be evaluated as a tensorial average assuming that the medium is composed of uniaxial crystals, oriented in random directions. The spectroscopic ellipsometry (SE)is an excellent and handy tool for the characterization of thin films. The surface roughness, thickness, optical constants and the pseudo dielectric parameters, can be evaluated from the ellipsometric measurements. These experiments provide a wealth of information about the material under investigation.

The optical constants and dielectric functions of rf plasma polymerized polyaniline thin films in their pristine and iodine doped films were estimated by spectroscopic ellipsometry for different angles of incidence 55^0, 60^0 and 65^0, in the energy regime 0.75 eV to 4.6 eV. The optical constants n, k, e_1, e_2 and energy band gaps for different angles of incidence were evaluated. Polyaniline (PANI) was doped with iodine (*insitu*) and the effect of iodine doping on the optical properties these films was also carried out using spectroscopic ellipsometric studies. Both pristine and iodine doped PANI exhibited low-k

properties in the low frequency regime (100 Hz-2 MHz)[1,2]. So both pure and doped polyaniline films were subjected to the ellipsometric studies with a new objective of verifying their low-k behaviour at optical frequencies. By a simple calculation and employing the optical constant values at these frequencies, the optical conductivity of these pristine and iodine doped films were determined. It was found that there exists an insulator to metal transition at optical frequencies

This chapter describes the evaluation of the optical constants *viz.* n, k and the pseudo dielectric constants of both the pristine and iodine doped plasma polymerised polyaniline thin films in the energy regime 0.725 eV to 4.6 eV. This is carried out by employing *a J.A.Woollan Variable Angle spectroscopic ellipsometer (VASE)* with multiple angles of incidence 55, 60 and 65 degrees[3,4]. Finally Bruggman effective medium[3] model was applied to fit the data and it was found that the pseudo dielectric function of the randomly oriented polycrystalline material resembles that of a single crystalline material. Surface roughness and optical smoothness of these films were also found out and were compared with the results obtained from the AFM and from the *Dektac 6M* Stylus profiler.

7.1 Ellipsometry measurements

In the ellipsometry measurement, the polarizer wsa tracked with the measured ellipsometric angle 'Ψ' Measurements at negative and positive polarization angles were averaged and an automatic retarder allowed the accurate determination of the difference in phase Δ over the whole range of $0\text{-}360^0$ and of partial depolarization. All the measurements were performed at room temperature. From the ellipsometric angles Ψ and Δ, the ratio of the diagonal reflection Jonnes matrices elements $\frac{r_{pp}}{r_{ss}} = \tan\Psi \exp(i\Delta)$ can be calculated. Here r_{pp} and r_{ss} are the complex Fresnel reflection coefficients parallel and perpendicular to the plane of incidence. Extraction of useful information from the ellipsometric data begins with the construction of an optical model for the polymer thin film on glass substrate. The experimental setup is described in detail in *chapter 3*.

7.2 Optical modeling for ellipsometry measurements

Extraction of useful information from the ellipsometric data and its interpretation begins with the construction of an appropriate optical model for the polymer film on the glass substrate. The model taken into account must consist of surface roughness layer, polymer film and glass substrate. The surface roughness layer in the optical model for the polymer film was analysed with an Effective Medium Approximation (EMA). The thickness of the polymer film was obtained by fitting the data in the highly transparent region of the spectrum using Cauchy dispersion relation. The results for n and k in the transparent region obtained from the Cauchy dispersion relation by performing a point-by-point fit starting from the transparent region to extract approximate values of the optical functions. A brief theory about these aspects is already provided in *chapter 3*.

7.3 Measurements of film thickness and surface roughness

The thickness of pristine plasma polymerised polyaniline was estimated and found to be 745.9 ± 0.6nm. The surface roughness was evaluated and was 1.8 nm with a mean square error (MSE) of 6.79 Å. It is known that the Bruggeman Effective Medium approximation (BEMA)[6], provides the overall time evolution of the spectroscopic ellipsometry (SE) and is an accepted method for the analysis of the SE data for bulk as well as the thin film having microscopic rough surfaces and interfaces, and with out further characterization, the surface roughness and film thickness obtained are assumed to be believable. This value of surface roughness obtained in the case of plasma polymerised polyaniline match very well with that of the rms value of surface roughness measured by Guifang Li *et al* for PMMA films and estimated from the atomic force microscopy (AFM) and stylus probe[7]. Here the very low surface roughness value exhibited by these films is important and assume significance from an application point of view. The low surface roughness of plasma polymerised polyaniline (PPANI) could be attributed to the following. The PPANI surface consists of small hills and valleys. The sticking coefficient of valley is slightly

greater than that of the hills and there occurs significant lateral diffusions and surface migration of the adsorbed species on the surface. This confirms that the technique of plasma polymerization can be employed to produce extremely smooth films with very small surface roughness when compared to films prepared by other conventional techniques[8].

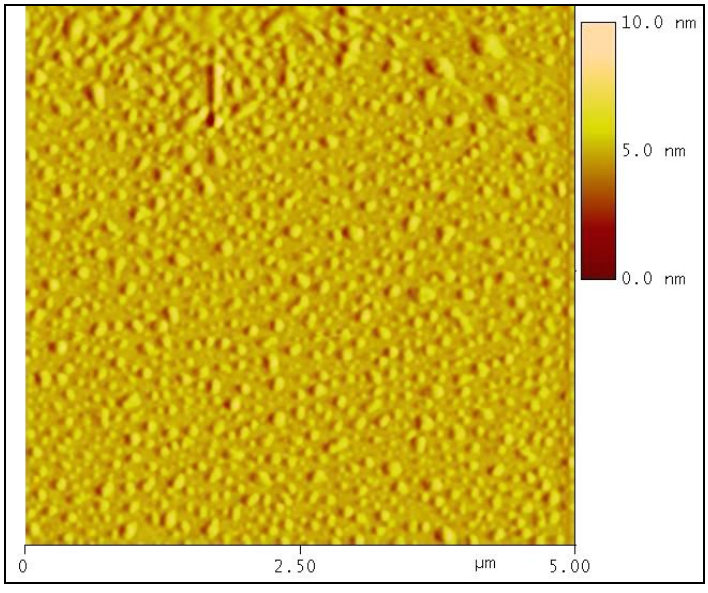

Figure 7.1.a: AFM photographs of RF plasma polymerised aniline thin films-Pristine

The surface roughness and the thickness of the plasma polymerised thin films obtained from the ellipsometric technique match very well with the values obtained from the measurements carried out by the stylus probe and AFM. Figure 7.1 shows the AFM picture of the pristine and iodine doped RF plasma polymerised thin film. Stylus probe analysis also showed the surface roughness of RF plasma polymerised polyaniline thin films 20 Å. For the iodine doped film, the film thickness is 2354.2 Å and the surface roughness is 17 Å.

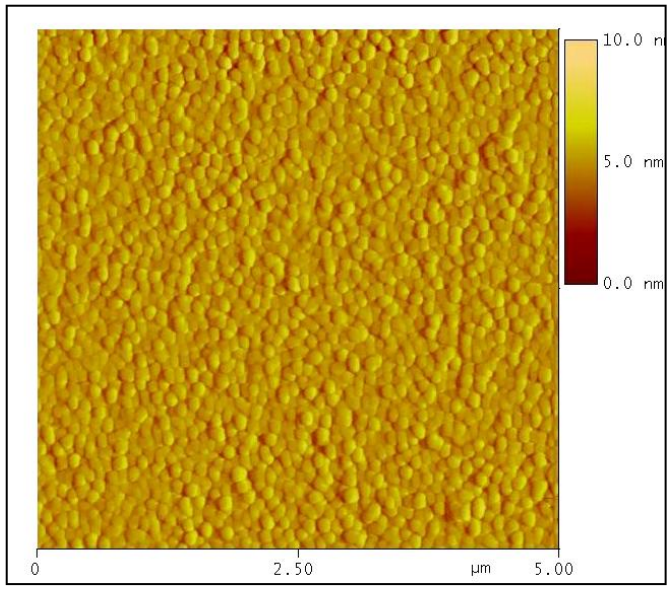

Figure 7.1.b: AFM photographs of RF plasma polymerised aniline thin films in the iodine doped form

The ellipsometric angle 'Ψ' vs photon energy graph for the pristine and iodine doped films are depicted in figure 7.2 and figure 7.3 respectively.

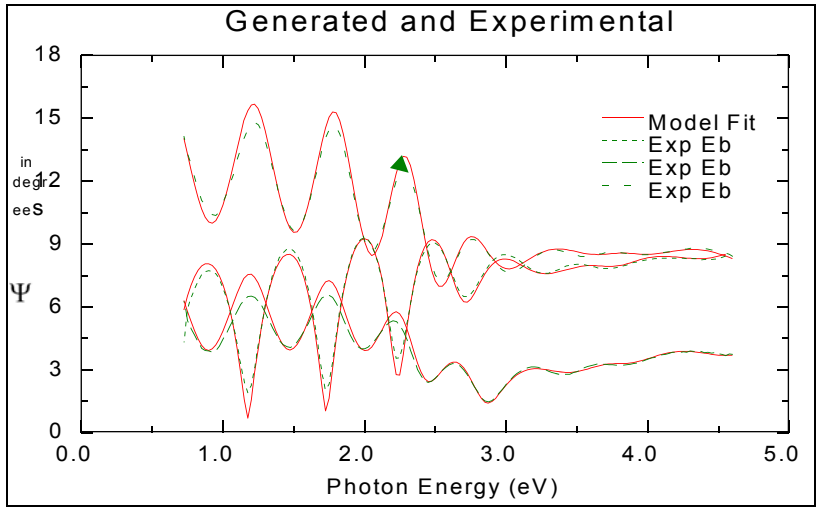

Figure 7.2: SE Experimental spectra of ellipsometric angles Ψ for the plasma polymerized films of poly aniline (PANI) as acquired at various angles of incidence. The model fit is also shown.

It can be seen that the variation of Ψ with energy is oscillatory in nature. There is marked difference in the behaviour for the pure and doped samples. This data provides information at different depths of the samples. At lower photon energies, the penetration depth can be longer than the film thickness and this leads to interference fringes. This can be clearly seen from figure 7.2.and figure 7.3. The experimental data were successfully fitted and this fit almost coincides with that of the experimentally observed data. At higher photon energies, the penetration depth decreases and the film become opaque.

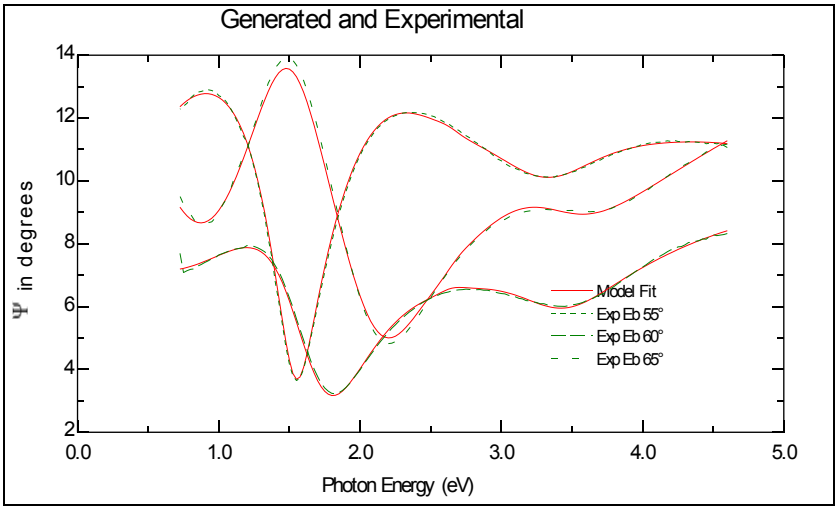

Figure 7.3: SE Experimental spectra of ellipsometric angles Ψ for the plasma polymerized films of poly aniline iodine doped (PANI) as acquired at various angles of incidence. The model fit is also shown.

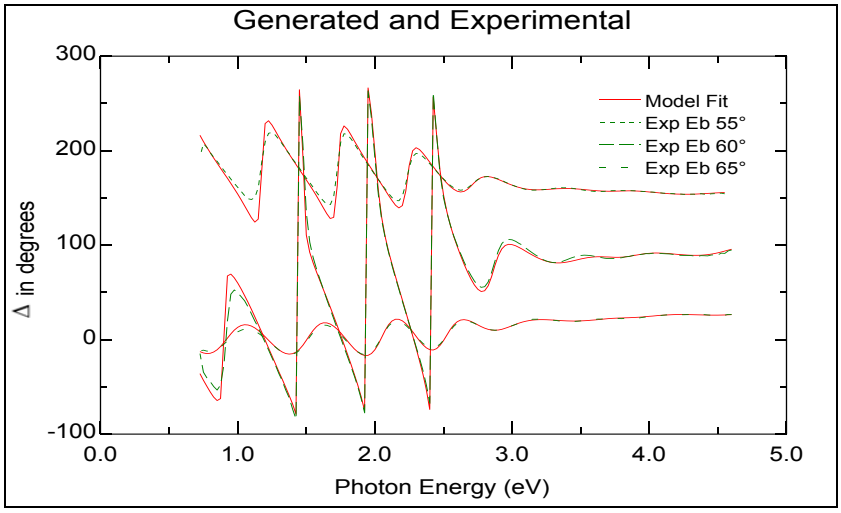

Figure 7.4: SE Experimental spectra of ellipsometric angles and Δ for the plasma polymerized films of poly aniline (PANI) as acquired at various angles of incidence. The model fit is also shown.

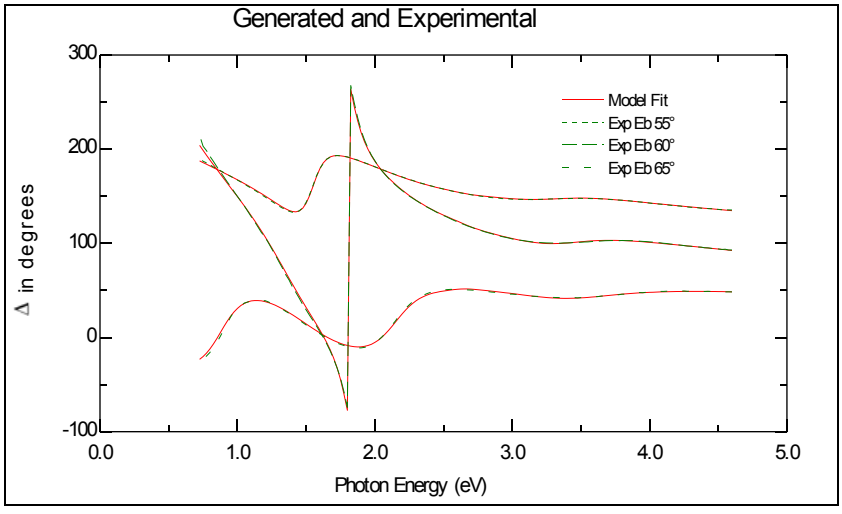

Figure 7.5: SE Experimental spectra of ellipsometric angles and Δ for the plasma polymerized films of poly aniline doped (PANI) at various angles of incidence. The model fit is also shown.

7.4 Pseudo dielectric functions and critical point transitions

The pseudo dielectric constants viz. ε_1 and ε_2 for the pristine and iodine doped plasma polymerised thin film samples are evaluated from the SE measurements. They are plotted separately and are shown in figure 7.6, 7.7, 7.8 and 7.9. From a study conducted in our lab[2], it was found that these films exhibited low-k behaviour at lower frequencies (100 Hz to 2 MHz). It was our endeavor, in this study, to verify the same findings at higher frequencies especially in the optical regime. It has been found that at optical frequencies also, the same behaviour is observed, both in the case of pristine and iodine doped plasma polymerised polyaniline.

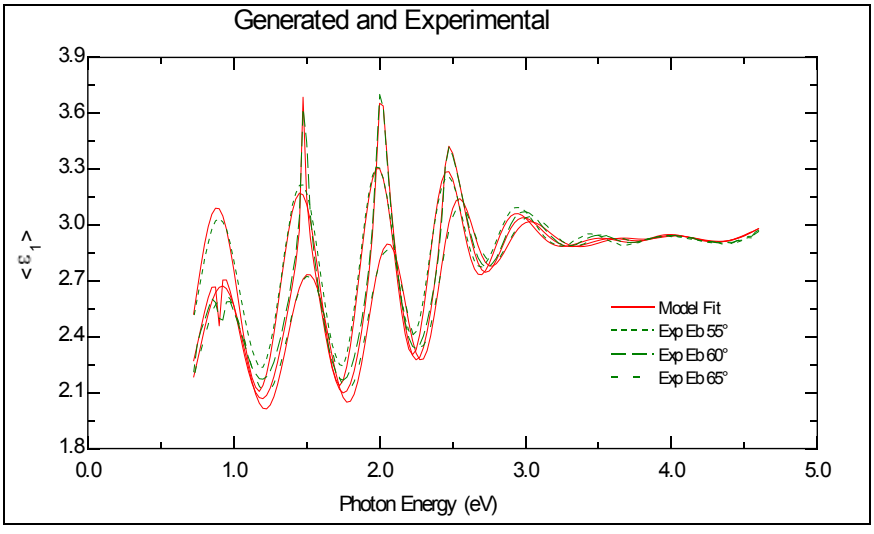

Figure 7.6: Pseudo dielectric constant (real) of plasma polymerised polyaniline sample in its pristine form. For different values of the angle of incidence. The model fit is also shown

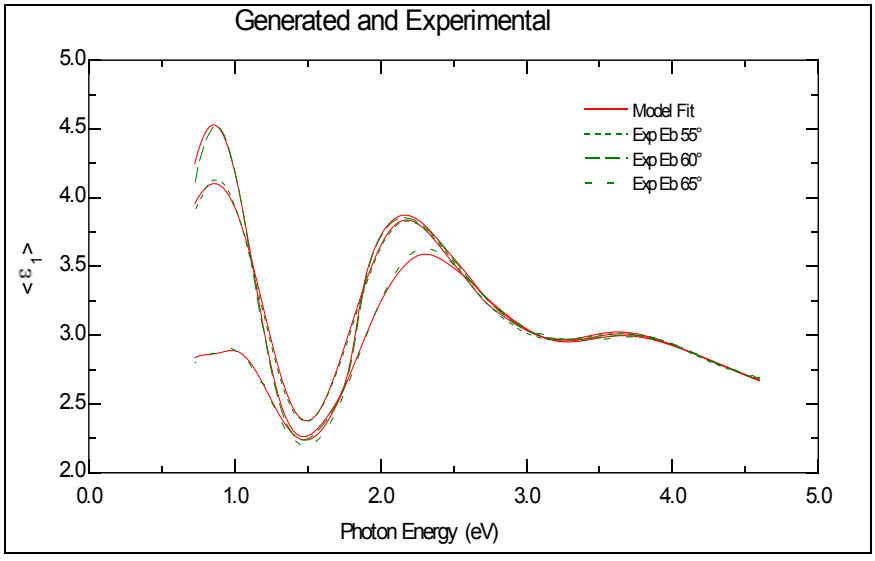

Figure 7.7: Pseudo dielectric constant (real) of plasma polymerised polyaniline sample in its iodine doped form. For different values of the angle of incidence. The model fit is also shown.

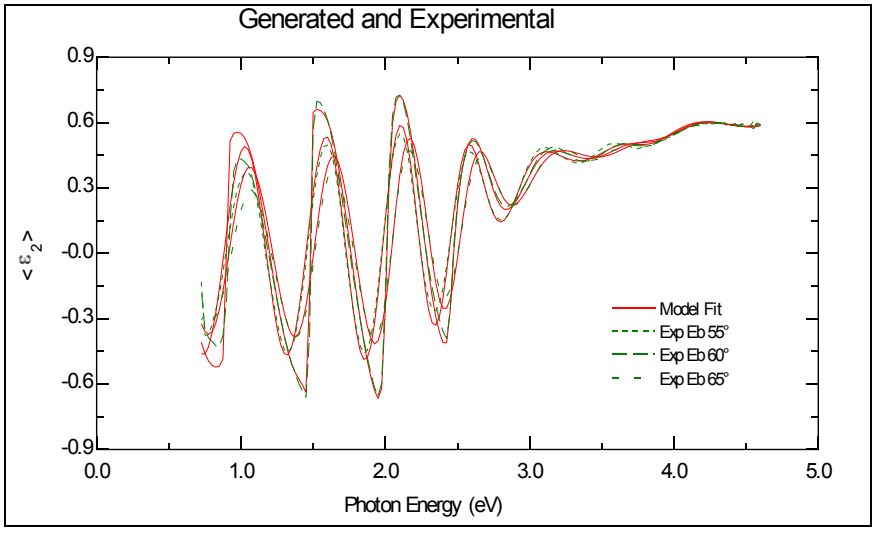

Figure 7.8: Pseudo dielectric constant (imaginary) of plasma polymerised polyaniline sample in its pristine form for different values of the angle of incidence. The model fit is also shown.

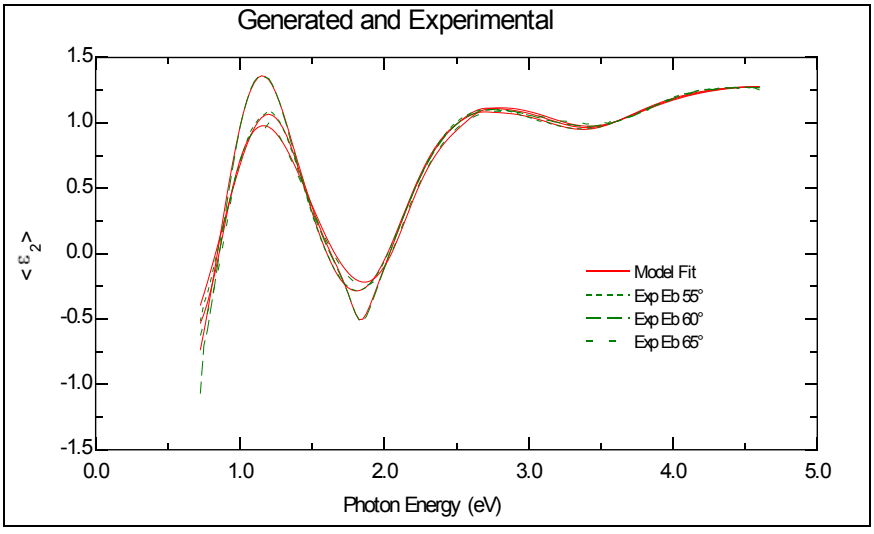

Figure 7.9: Pseudo dielectric constant (imaginary) of plasma polymerised polyaniline sample in its iodine doped form for different values of the angle of incidence. The model fit is also shown.

The pseudo dielectric functions of the films were calculated using the Bruggman Effective Model. The static dielectric constant is a limit of $E \rightarrow 0$ of the complex dielectric constant given by $\varepsilon = \varepsilon_1 - i\varepsilon_2$ the real ε_1 and imaginary ε_2 of the dielectric function are related by *Kramers-Kronig* relation and is as follows.

$$\varepsilon_1(E) = 1 + \frac{2}{\pi} P \int_0^{\infty} \frac{E'\varepsilon_2(E')}{E'^2 - E^2} dE' \qquad 7.1$$

Here P denotes the principal value of the integral. From this equation, it is clear that the dielectric function $\varepsilon_1(0)$ of the dielectric material originates from the absorption over the entire spectral range, which includes electronic, ionic and dipolar absorptions corresponding to the ultraviolet, infrared and microwave regions[10,11]. The electronic contribution of the dielectric constant originates from the inter band electronic transitions and gives rise to a refractive index dispersion in the visible region. The ionic contribution corresponds to the molecular vibration. Here in this case, the ionic contributions are disregarded since it is important only in polar liquids and gases but negligible for solids. The

SE measurement was recorded in the entire spectral range which covers ultraviolet, visible and near infrared regime. The measurements were taken for three angles of incidence *viz*. $55, 60^0$ and 65^0. The measured data was fitted to the model dielectric function and the values of ε_1 and ε_2 are plotted against the photon energies. The behaviour is found to be oscillatory in nature. The dependence of the real and imaginary parts of the dielectric constant with photon energy reveals an anisotropic behavior for the plasma polymerized films and this anisotropy is reflected in its refractive index and absorption coefficient[12,13]. The averaged value of pseudo dielectric functions (real) of the films is given in figure 7.10 and 7.11 respectively.

Figure 7.10 depicts the variation of the real part of the dielectric constant with photon energy (in log scale) for pristine and iodine doped RF-PPANI films.

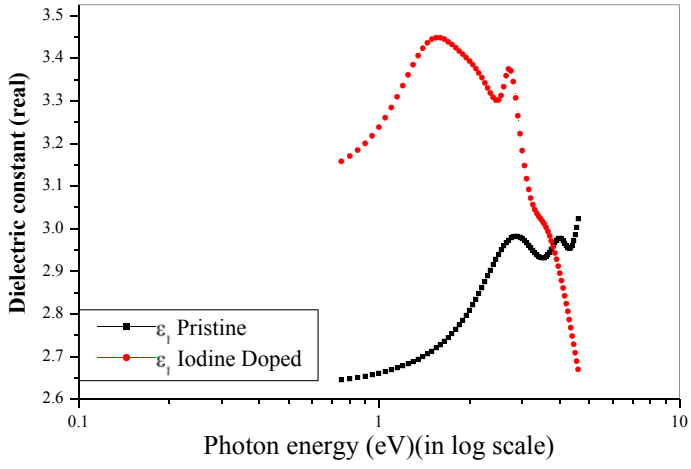

Figure 7.10: The averaged value of pseudo dielectric functions (real) of the rf PANI films

At lower photon energies the dielectric constant of the pure plasma polymerised polyaniline thin film is smaller when compared to that of the doped film up to a photon energy value of 3.8 eV. In the low energy regime up to 1.4

eV, the dielectric constant of the doped and pure films increases almost exponentially with the photon energy and from that energy onwards the dielectric constant value of the doped thin film decreases with increase in frequency. The dielectric constant of the pristine thin film increases and attains a maximum value at 2.8 eV and then decreases. At photon energy corresponding to 3.8 eV the value of the dielectric constant of pristine films becomes higher than that of the dielectric permittivity of the iodine doped samples. Beyond a photon energy corresponding to 3.8 eV the permittivity value of the iodine doped samples decreases sharply. This is because at IR frequencies the dominant contributing factor to keeping the low dielectric values is ionic polarization. In the case of doped samples, doping induces charged defects and contributes to the polarization caused by the ionic polarization[14]. This might increase the dielectric constant of doped samples in this energy regime. In the case of iodine doped films the relaxation of polarization occurs at energy of 1.4 eV. In the visible region the electronic polarization is dominant over the ionic polarization and as a result, the dielectric constant of the pristine samples increases while that of the doped samples decreases.

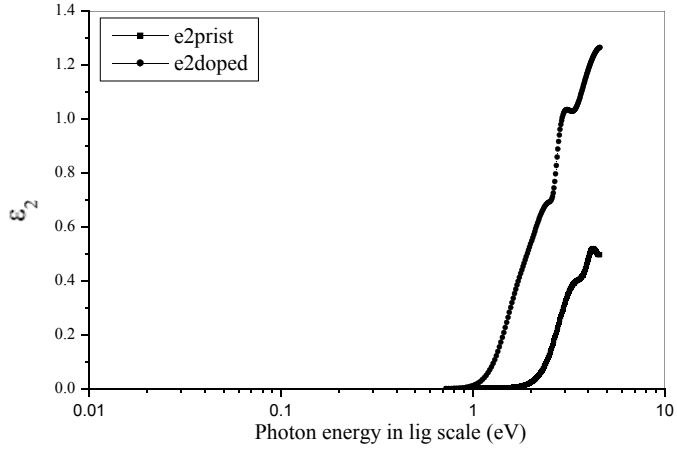

Figure 7.11: The averaged value of the imaginary part of dielectric constants for pristine and iodine doped films.

At higher values of photon energy the electronic polarization of the pristine films persists. The dielectric constant of the doped film decreases since in the doped films, since the ionized defect states contribute towards the conductivity of the samples at higher energy regime and the dielectric constant of the doped samples decreases. The average value of the imaginary part of dielectric constant is evaluated and depicted in figure 7.11

7.5 Evaluation of optical constants

The dielectric constant can also be considered as the manifestation of different interband transitions resulting from the applied electric field. The imaginary parts of the dielectric response is related to the combined density of states(DOS) μ , given in equation 7.2. The function δ represents the spatially joined DOS between valance v and conduction c band states differing by energy $E = \hbar\omega$ of the incident light. The imaginary part of the dielectric constant can be obtained from the equation [15]

$$\varepsilon_2 = \frac{4\varepsilon^2\hbar^2}{\pi\mu^2 E^2}\int dk \left|P_{cv}\right|^2 \delta\left(Ec - Ev - E\right) \qquad 7.2$$

Here $[Pcv]$ is the momentum matrix elements between the valance and conduction band states and the integration is performed over the first Brillouin zone(BZ). Critical points (CPs) in the second derivative of the spectrum correspond to the energy at which the joint DOS shows strong variations. The variations of DOS are a function of energy. It may be noted here that the critical point energies correspond to the fundamental E_1 and the second transition E_2 corresponds to the $\pi \rightarrow \pi^*$ transition in both pristine and iodine doped films[16].

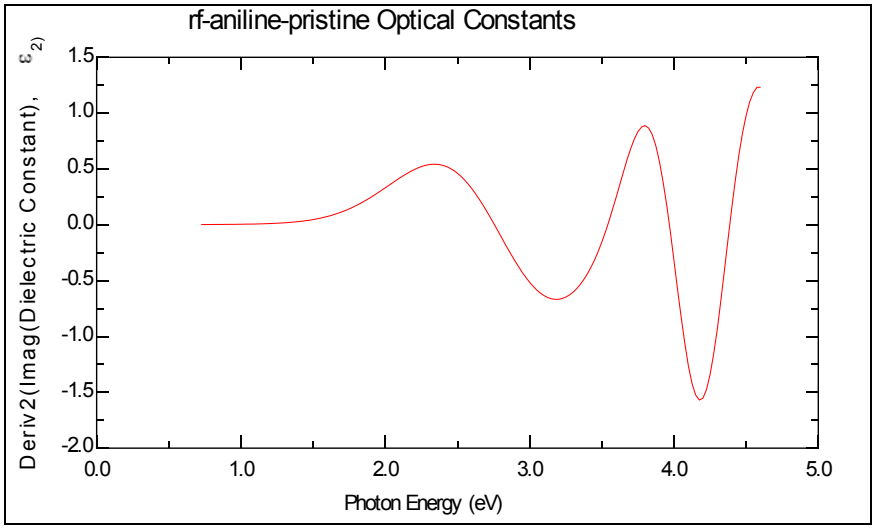

Figure 7.12: Second derivative of Epsilon2 of pristine PANI thin film. Minimum corresponds to the critical point energies. The figure shows two optical transitions-the fundamental optical bandgap at 3.185eV and second transition at 4.178eV

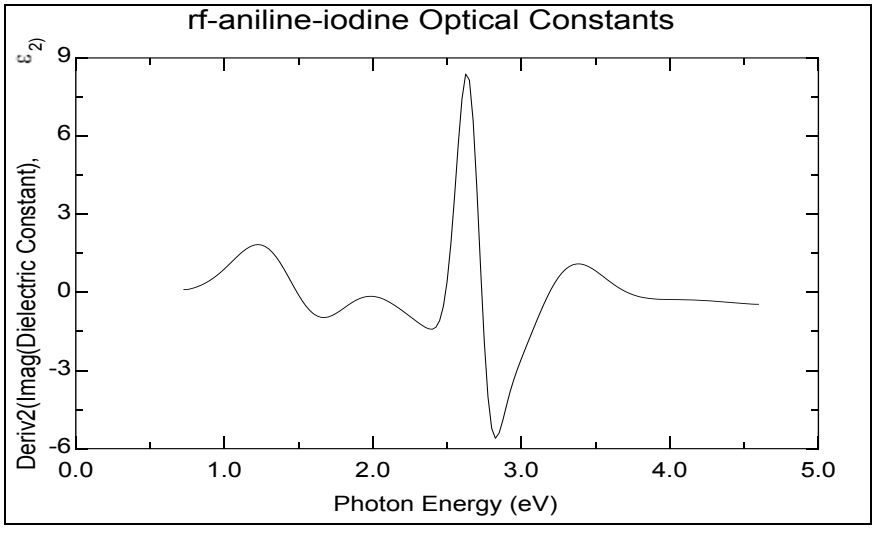

Figure 7.13 Second derivative of Epsilon2 of iodine doped sample. Minimum corresponds to the critical point energies. The figure shows three optical transitions; the fundamental optical bandgap at 1.66eV, second transition at 2.396eV and the third at 2.825eV.

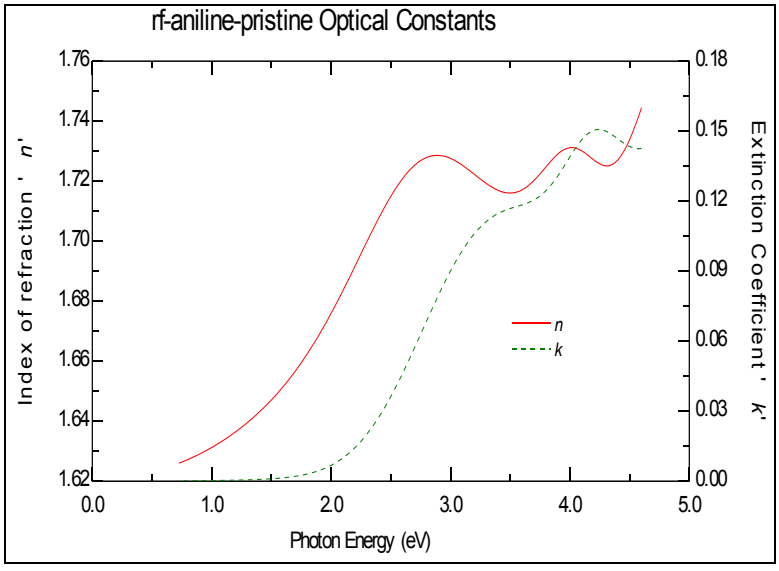

Figure 7.14: Optical constants, n and k of pristine plasma polymerised aniline film obtained from the best fit

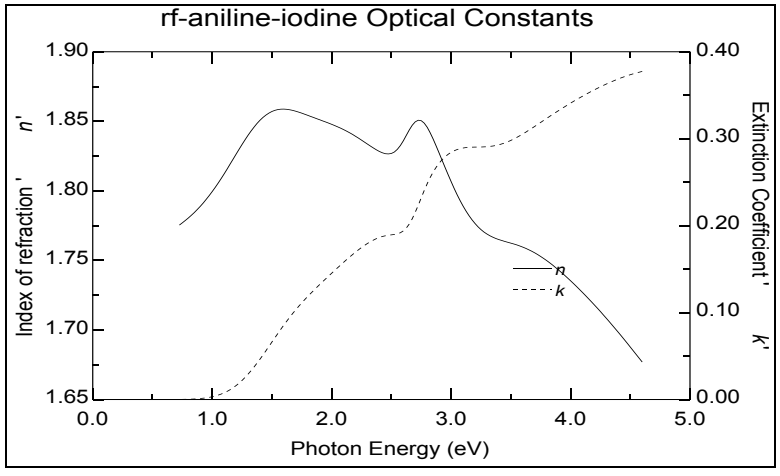

Figure 7.15: Optical constants, n and k of iodine doped plasma polymerised aniline film obtained from the best fit

7.6 Optical constants and optical anisotropy studies on plasma polymerised aniline thin films

The spectral dependence of the complex refractive index $n = n_1 + in_2$ and the investigations on the dependence of the fundamental $\pi \rightarrow \pi^*$ optical transition on a polymer backbone of thin conjugated polymer thin films are of

fundamental interest. This is also important from an application point of view. The internal quantum efficiency of a polymeric LED is related to the factor $1/2n^2$ where n is the real part of the refractive index of the polymeric film. The optical anisotropy strongly affects the quantum efficiency. This is because the refractive index n of the polymer is employed to evaluate the angular range of escaping light and the quantum efficiency depends on the incident angle of the light beam to the surface normal[16,17]. The ellipsometric angles Ψ and Δ at different angles of incidence reflects the anisotropic behavior of the film[18,19]. The phase relation of n and k with each other shown in figure 7.12 and 7.13 are an indication of optical anisotropy which leads to a possible non linear optical behavior of the films.

It must be mentioned here that the deposition parameters during plasma polymerisation greatly influences the dielectric behaviour of the polymer thin films. RF power, current density, vapour pressure, and monomer flow rate has a profound influence on the dielectric and optical properties of these films.

7.7 Optical conductivity measurements of plasma polymerised aniline thin films

The optical conductivity of the films is estimated by employing the *Drude model* which describes the contribution to the classical dielectric function. The dependence of ε with ω can be written as[20]

$$\varepsilon(\omega) = \varepsilon_1(\omega) + i\left(\frac{4\pi}{\omega}\right)\sigma(\omega) \qquad 7.3$$

This model has been successful in describing the electronic properties of simple metals. However when the disorder is introduced with the magnitude of disorder potential it is comparable to the band width and multiple scattering causes the electronic state near the Fermi energy (E_F) to become localized. In such a system, disorder induced localization causes transition from metal to insulator. As a result the charge dynamics of a disordered system become fundamentally different from that of metals[21].

The electronic states of conducting polymers are strongly degenerate on the amount of disorder. Although heavily doped conducting polymers have a metallic density of states at the Fermi Energy E_F, their transport properties are dominated by the disorder which originates from a combination of partial crystallinity (molecular scale disorder) and inhomogeneous doping[22,23].

The complex optical conductivity $\sigma = \sigma_1 + i\sigma_2$ is related to the real and imaginary parts of the dielectric constant as $\sigma_1 = \frac{\varepsilon_2 2\omega}{4\pi}$ and $\sigma_2 = -\frac{\varepsilon_1 - 1\omega}{4\pi}$ with angular velocity $\omega = 2\pi\nu$ and $\nu = c/\lambda$ in cm^{-1}

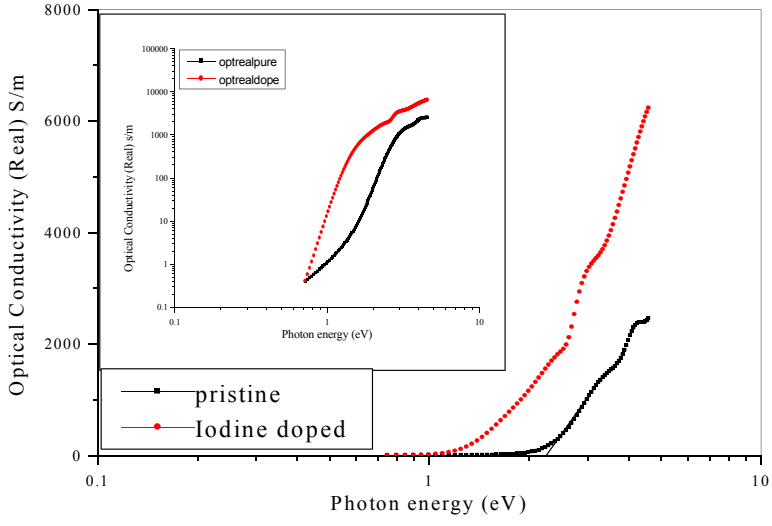

Figure 7.16: The real part of the optical conductivity of the thin films. The inset shows the log (real part of the optical conductivcity) vs. Photon energy in log scale.

The optical conductivity of the thin films is extremely small up to photon energy of 2.3 eV for pristine and 1.29 eV in the case of doped films respectively and then the optical conductivity increases. It is to be noted here that, a transition

occurs from insulator to metal in both pristine and doped samples in the optical frequency regime.

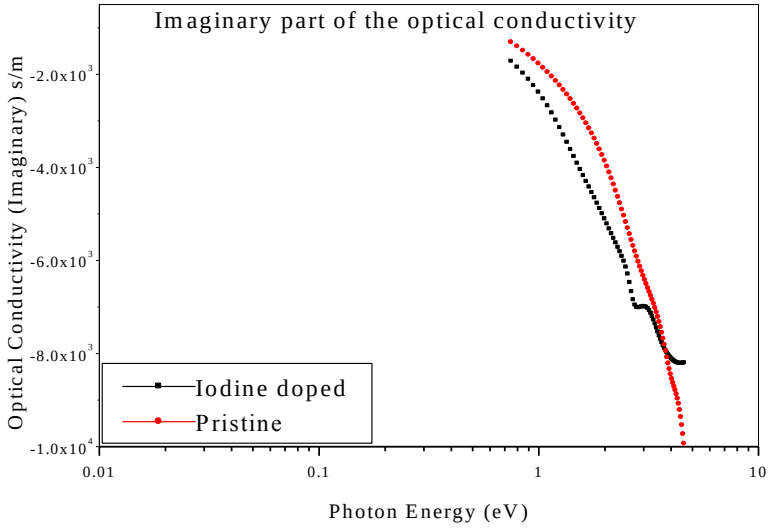

Figure 7.15 Imaginary parts of the optical conductivity

The enhancement of optical conductivity in doped and pristine samples correspond to the energy gaps of the pristine and iodine doped samples are calculated using Karammers- Kroning model.

Conclusion

By employing spectroscopic ellipsometric studies, the optical and the dielectric parameters of plasma polymerised thin films of polyaniline in its pristine and iodine doped forms are evaluated. It is found that the low dielectric constant (low-k) values exhibited by the thinfilms at lower frequencies are found to be existing in optical frequencies too. From optical conductivity calculations it is found that the optical conductivity attains metallic nature at high frequencies. These studies all points to the fact that plasma polymerised thin films are structurally anisotropic.

References

[1] C.Joseph Mathai, S.Saravanan, M.R.Anantharaman, S.Venkitachalam, S.Jayalekshmi *J.Phys.D.Appl.Phys.* **35**,(2002),240

[2] S.Saravanan, C.Joseph Mathai, S.Venkatachalam, M.R.Anantharaman, *New J of Phys.* **6**,(2004),64

[3] L.Levesque, *Phys.Educ*, **35**, (2000), 359

[4] P.D Paulson, B E Mc Candless, R W Birkmire, *J.Appl.Phys*, **95**. (2004), 3010

[5] D E Aspnes, *Thin Solid Films*, **89**, (1982), 249

[6] A.Fontcuberta I Morral and P.Roca J Cabarrocas and C.Clare, *Phys.Rev.***B** **69**,(2004),125307

[7] Guifang Li, Jeffrey A. Tobin, and Denice D.Denton, *Appl.Phys.Lett*, **64**, (1994),560

[8] G W Collins, S A Letts, E M Fearon, R L McEachern, and T P Bernet, *Phys.Rev.Lett.*,**73**, (1994),708

[10] C.Kittel, *Introduction to Solid State Physics.* 7th Ed. Chapter 11

[11] K.Postava, T.Yamaguchi, M.Horie, *Appl.Phys.Lett*, **79**,(2001),2231

[12] Maria Losurdo, Giovanni Bruno Eugine A.Irene, *J.Appl.Phys*, **94**,(2003),4923

[13] E.K.Miller, C.Y.Yang, and A.J.Heeger,*Phys.Rev.***B**, 62,(2000),6889

[14] Kwanghee Lee, A.J.Heeger, Y.Cao, *Phys.Rev.***B**, 48,(1993),14884

[15] S.Adachi, *Optical Properties of Crystalline and Amorphous Semiconductors*, 1st Ed., (Kluwer, Boston, (1999) Vol.**1**, Chapter 3

[16] Maria Losurdo, Giovanni Bruno, Eugene A.Irene, *J.Appl.Phys*, **94**,(2003),4923

[17] N.C.Greenham, R.H.Friend, D.D.C.Bradley, *Adv.Mater,* (1994),491

[18] M.Tammer,R.W.T Higgins, A.P.Monkman, *J.Appl.Phys*, **91**,(2002),4010

[19] D.Mc Branch, I.H.Campbell, D.L.Smith and J.P.Ferraris, *Appl.Phys.Lett*,**66**(1995),1175

[20] Kwanghee Lee, Reghu Menon, C.O.Yoon, and A.J.Heeger, *Phys.Rev.***B**, **52**,(1995),4779

[21] N.F.Mott, and E.Davis, *Electronic Process in Noncrystalline Materials*, (Clarendon, Oxford), 1979

[22] R.P.Mc Call, E.M. Scherr, A.G.Mac Diarmid, A.J.Epstein, *Phys.Rev.***B**, **50**,(1994),5094

[23] Kwanghee Lee,A.J.Heeger, *Phys.Rev.***B**, **68**,(2003),035201m

Chapter 8

Investigations on the nonlinear optical properties of plasma polymerised thin films by z-scan technique

Nonlinear optical materials based on polymers are commercially important because of their potential optical limiting properties[1]. Optical limiters are extensively used as protective layers in sensors and also for eye protection devices like gogle when exposed to intense lasers[2]. Polyaniline is a guest-host matrix has been found to be exhibiting nonlinear optical properties. Buckminister Fullerene[3,4] (C_{60}) has also been found to be displaying good optical limiting properties and they have been extensively studied. Materials exhibiting nonlinear optical properties also exhibit optical limiting and hence they are of concrete interest[5]. From a fundamental point of view, materials exhibiting nonlinear optical properties can be categorized into many, depending on the particular mechanism with which they execute this process[6]. For example saturable absorption (SA), two photon absorption (TPA) and excited state absorption (ESA) are the most relevant types of nonlinear absorptive processes. Transitions involve one photon and two photons have different selection rules. TPA involves the simultaneous absorption of two photons to excite a material. SA involves the saturation of a given transition, by populating the excited state of the material so that the material, which initially absorbed at that wavelength, becomes more transparent. ESA involves a sequential process in which a photon is initially absorbed and the molecule remains in an excited state of the material so that a second photon that arrives during that time is also absorbed to put the molecule into an even higher excited state[1,7,8]. Open aperture z-scan is an essential tool to evaluate these properties. They not only give a handle to ascertain the usefulness of a material as an optical limiter or as a nonlinear optical (NLO) material, but also focus on the mechanism of the process of

nonlinear absorption[9,10]. The theory of the z-scan technique is provided in *chapter 2* and the experimental details are detailed in *chapter 3*.

During the elucidation of the conduction mechanism of the plasma polymerised thinfilms, it has been noticed that the presence of trap levels with in the energy bands of these polymers are a reality. It must be noted that the plasma polymers investigated here forms a part of the thesis exhibited space charge limited conduction (SCLC). This observation leads credence to the belief that plasma polymer thinfilms also might exhibit nonlinear optical properties. Moreover doping with iodine substantially modifies the polymer structure. Thus the effect of iodine on the NLO properties of these polymers can also be investigated. Moreover literature reports on the NLO properties of plasma polymers are scanty. These factors motivated to carryout extensive study of NLO properties of plasma polymerised thinfilms using the open aperture z-scan technique. This chapter presents the results of such a study carried out on plasma polymerised aniline and tree oil in their pristine and iodine doped forms. The effect of iodine doping on the nonlinear properties on these films are also dealt with, with respect to a particular mechanism of the transmittance/ absorbance of the LASER beam.

8.1 Open aperture z-scan measurements on ac plasma polymerised aniline thin films

The open aperture z-scan plot of rf plasma polymerised polyaniline is shown in figure 8.1. In the open aperture z-scan plot for plasma polymerised polyaniline, the value of transmittance decay from the maximum absorbance when the film turns away from the focus. The nonlinear absorption of the polymer can be explained by the use of Bruggemaan effective model[11,12] , in which one can consider the plasma polymerised thin film as an inter dispersed model. This model was applied (*chapter 7*) to analyse the optical anisotropy exhibited by polyaniline thin films using spectroscopic ellipsometry.

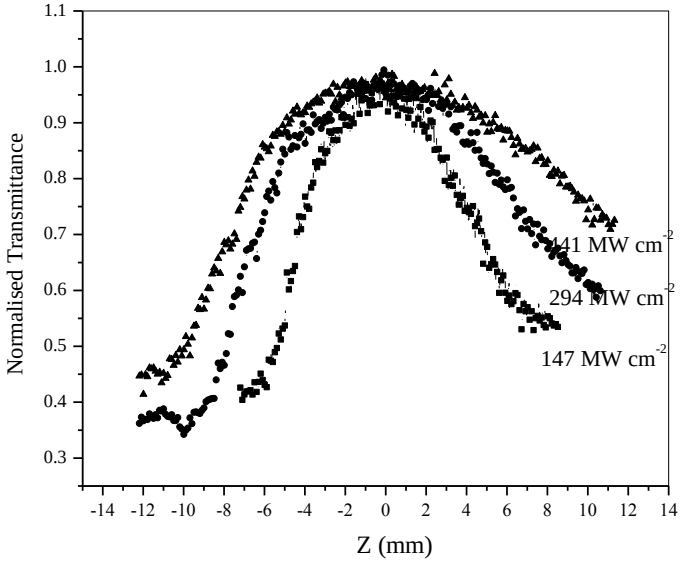

Figure 8.1: Open aperture z-scan plot of rf plasma polymerised aniline in its pristine form

It can be noticed that, as the input energy of the pumping beam increases, the transmittance value exhibits saturation far from the focus, in both sides[13]. The width of the z–scan curve increases with the increase in intensity. It is also interesting to note that in the case of plasma polymerised polyaniline films in its pristine and iodine doped forms, the post focus (+ve z values) transmittance curve is not symmetric with the pre-focus transmittance, or the transmittance value does not drop to the initial value, when the sample is brought from the focus. This effect is more prominent when the beam intensity is increased. A probable reason for this phenomenon could be the trap controlled slow relaxation[14,15] of the intermediate levels which are excited by the irradiation of the laser beam. The dependence of the photorefractive (PR) response of the polymers is explained in the following section.

8.2 Trap-controlled PR response in polymers and nonlinear optical properties

The determination of the nature of traps and their number are unknown for a polymeric material. The trap levels of different polymer structures can be determined from the Urbach tail analysis of the optical absorption spectra in *chapter 4*. Due to the hopping mechanism for the charge transport in amorphous glasses or polymers and basically every charge transporting moiety may act as a shallow trap. These traps strongly influence the optical response of a polymer refractive material. This is the reason for the difference in the z-scan curve of the iodine doped sample when compared to that of the pristine samples and the fluence dependence of the nonlinear transmittance. The saturation intensity is enhanced in the iodine doped sample in the case of polyaniline[16,17]. The maximum value for the space charge field for a given material depends on the trap density and the dielectric constant. The plasma polymer in its pure and doped forms consist of trap states and these states will strongly affect the nonlinear optical properties of the polymers.

8.3 The nonlinear optical properties in the presence of iodine

Figure 8.2 depicts the optical absorption vs. photon energy of pristine and iodine doped polyaniline thin films. The occupation of the intermediate energy levels and the enhanced absorbance is shown in the spectrum. Due to the stable incorporation of the iodine into the polymer matrix the optical polarizability of the material enhanced and this could be the reason for the change in the nonlinear optical properties of the polymer in its doped form.

It is known that the nonlinear optical properties of the polymers differ substantially due to the doping of electron accepting or withdrawing species. It is also seen that the defect levels are created with in the LUMO and HOMO levels because of doping, which generate polarons and bipolarons[18]. By the doping of iodine, the trap levels and the structural disorder of the films increase due to the

incorporation of the charged species. Since polyaniline is found to be a p-type material the iodine doping creates a reduction of binding energy of the charged species and the corresponding levels can be treated as equivalents to the creation of intermediate levels in the iodine doped plasma polymers. Another effect of doping is the enhancement of hole density in the polymer chain.

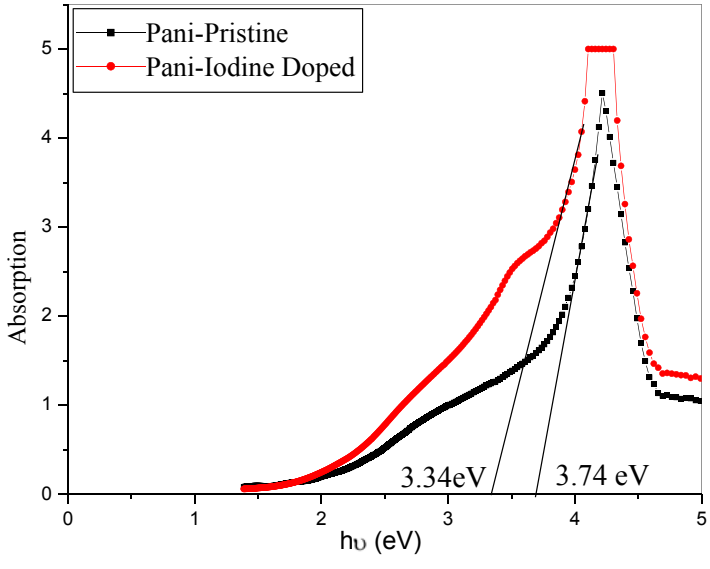

Figure 8.2: UV-VIS absorption spectra of plasma polymerised polyaniline in its pristine and iodine doped. vs. Photon energy ($h\nu$)

It must be noted here that, plasma polymerised aniline films exhibited a saturable absorption [19]which is typical to an optical switching at this wavelength.

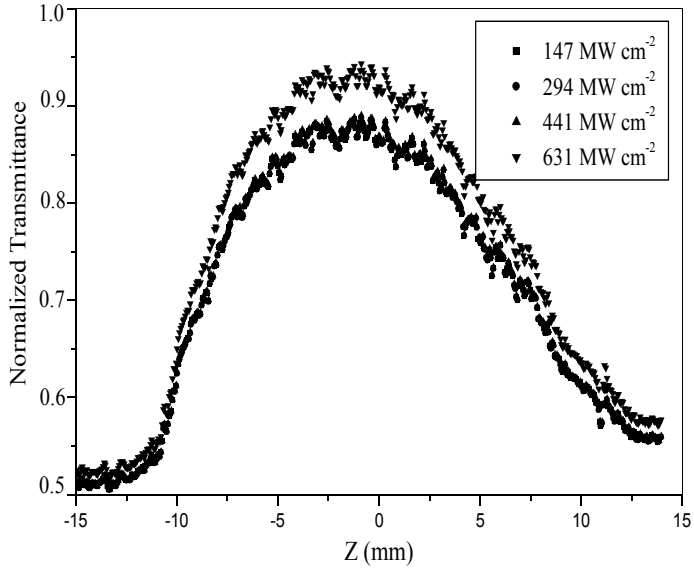

Figure 8.3: Open aperture z-scan plot of rf plasma polymerised aniline in its Iodine doped form

Another plausible explanation for the modification of the z-scan curve is as that, a polymer with non degenerate ground states, with intergap energy levels, positive or negative bipolarons can be produced by doping. For p-type bipolarons, there is no electron on either of the two intergap levels, and the transitions between those two levels do not occur, and the linear absorption spectrum does not have a peak at a frequency corresponding to 2ω, where ω is the frequency of the beam used to excite the material. But under intense pumping of light, the electron occupation can be altered. In that case the photo excited electrons from the valance band will occupy the inter gap levels. In addition to this change, the electronic occupations readjust the structural distortion of the polymer to minimize the total energy[18]. The electronic occupation of the bipolaron like topological defects are sensitive to the pumping intensity. In the p-type bipolaron, photo induced change in the energies and the electronic populations of the discrete inter gap levels causes a remarkable third order optical nonlinearity. This mechanism is a resonant mechanism utilizing the

structural repositioning under pumping and is contrary to the off resonant phenomena due to purely electronic correlation.

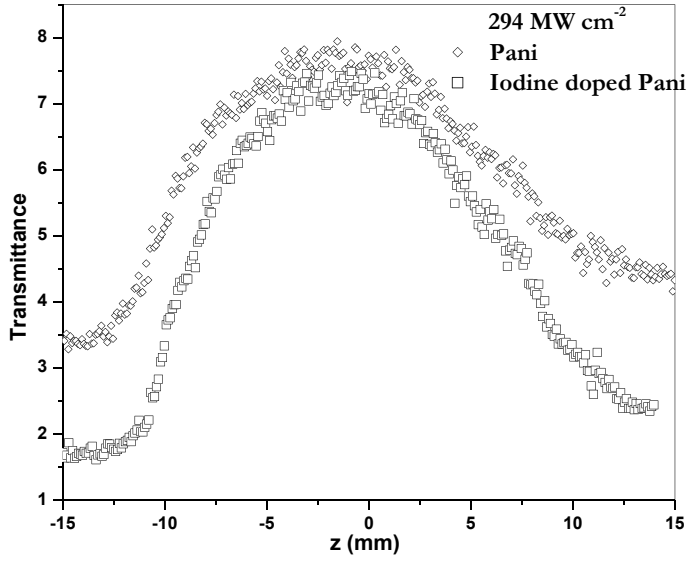

Figure 8.4: Open aperture z-scan plot of rf plasma polymerised aniline in its Iodine doped form. Here the transmittance value is not normalized for a better comparison of the transmittance amplitudes.

Figure 8.4 gives a comparison of the z-scan curves of the plasma polymerised PANI films in its pristine and doped form for a pumping intensity of 294 MW cm^{-2}**.**

8.4 Calculation of saturation intensity and model fit

In the presence of saturable absorption, the intensity dependent nonlinear absorption coefficient is given by the equation[20]

$$\alpha(I) = \frac{\alpha_0}{1 + I/I_s} \qquad 8.4$$

Where α_0 is the linear absorption coefficient, I is the excitation intensity and I_s is the saturation intensity. Here the probability of TPA/ESA along with SA is discarded. We can consider a case when the excitation intensity is less than that of the saturation intensity I_s, then $-\alpha / I_s$ can be considered as equivalent to the TPA coefficient or fit parameter β_{eff}. To a good approximation in the case of SA $-\alpha / I_s$ gives the nonlinear absorption coefficient. From the open aperture z scan data β_{eff} can be calculated and from this, the imaginary part of the third order optical susceptibility $\mathrm{Im}\left[\chi^{(3)}\right]$ can be calculated by the equation

$$\mathrm{Im}[\chi^{(3)}] = \frac{\lambda \varepsilon_0 n^2 c \beta}{4\pi} \qquad 8.5$$

In this study the theoretical fit for SA reported by *Samac*[21] et al,

$$\alpha(I) = \frac{\alpha_0}{(1 + I/I_s)^{0.5}} \qquad 8.6$$

$$\alpha(I) = \frac{\alpha_0}{1 + (I/I_s)^{0.5}} \qquad 8.7$$

These equations were applied for two different systems, one for a two level system with a homogeneous broadening and another for a picket-fence polymer, represented by the equations 8.6 and 8.7 respectively. However these fits do not match with that of the experimental observations. A model proposed and used by Kandasamy[20] *et al* was utilized to fit the experimentally observed data.

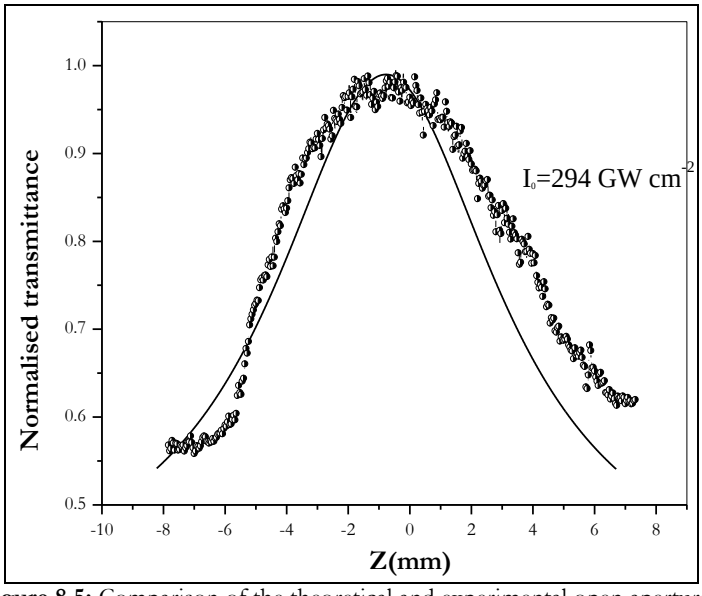

Figure 8.5: Comparison of the theoretical and experimental open aperture z-scan plots PPANI plots.

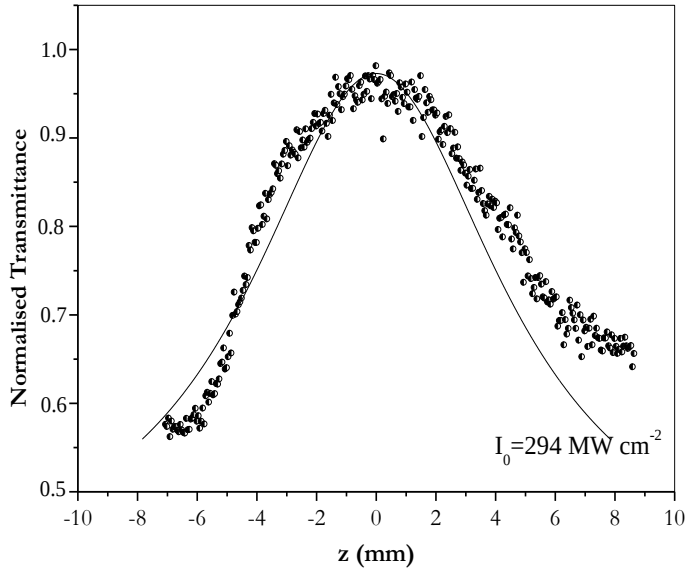

Figure 8.6: Comparison of the theoretical and experimental open aperture z-scan plots PPANI plots in the iodine doped form.

Figures 8.5, and 8.6 show the theoretical and experimental curve of the PPANI thin films in its pristine and iodine doped forms respectively for a laser beam out put of 294 MW cm^{-2}.

Sample/ Linear absorbance α_0	Io (MW cm^{-2})	β (cm GW^{-1})	$Im(\chi^{(3)})$ x 10^{-13}(cm^2V^{-2})
PPANI Pristine α_0 =0.3829 cm^{-1}	294	85.9	3.211
	441	68.1	2.538
	637	33.0	1.230
PPANI Iodine doped. α_0 =0.5464 cm^{-1}	294	57.1	1.875
	441	42.2	1.386
	637	30.1	0.9907

Table 8.1: Nonlinear optical coefficient and third order susceptibility of polyaniline

The curves corresponding to other power output are not given, but the estimated values of the imaginary part of the nonlinear susceptibility are given in table 8.1. The theoretical curves in both cases deviate considerably that from the experimental curves due to the slow relaxation of the excited levels of the plasma polymer, occupied by the irradiation

8.5 Open aperture z-scan studies on tea tree oil thin films

The open aperture z-scan of tea tree oil thin film of thickness 326 nm was investigated at 532nm, nanosecond pulses. The effective nonlinear absorption coefficient was measured for the thin film sample with open aperture z-scan measurement. The z-scan results along with the model fit are shown in figure 8.8. It is apparent from the figure, the process of two photon absorption (TPA) in tea tree oil can be discarded and the possibility of ESA is more

probable here[22]. It can be noted that ESA is different from that of TPA. TPA does not involve any real intermediate levels and two photons are absorbed simultaneously, but ESA consists of two successive one photon transitions involving real intermediate energy levels. The excited state of the sample plays a significant role in determining the nonlinear and the photo refractive properties. Detailed studies on the excited state dynamics and non linear properties of different organic and in organic materials like phtalocyanines (Pc) in different forms have been carried out by many researchers. Such a study in the case of tea tree oil has not been found in the literature since this is virgin material and the present study is the first such attempt. From the open z-scan measurements carried on tea tree oil thin films prepared by rf plasma polymerization, it is found that these material has a non linear response. The thin films of tea tree oil are nearly transparent with very low surface roughness in its thin film form and its optical band gap is found at 3.75 eV in its pristine form. When the thin film is prepared in the iodine atmosphere the band gap is shifted to 3.2 eV and an additional transition at 2.2 eV is observed. The details of the optical absorption studies are given in *chapter 4*.

The basic difference between two photon and excited state transition is that the former involve intermediate, extremely short lived virtual energy states, where as the later involve intermediate real states whose lifetimes can be determined by the electronic structure of the molecules in a material. Two photon absorption (TPA) depend on the intensity of the incident light, where as the in the excited state absorption (ESA) process are depend dent on the fluence of the incident light[23]. The two processes can be resolved by obtaining measurements of the samples for different incident pulse widths. For optical power limiters the fluent dependent absorption has profound importance because the nonlinear transmission characteristics of the sample are intensity dependent that would make the amount of power limiting dependent on the incident laser pulse width, which is undesirable.

.

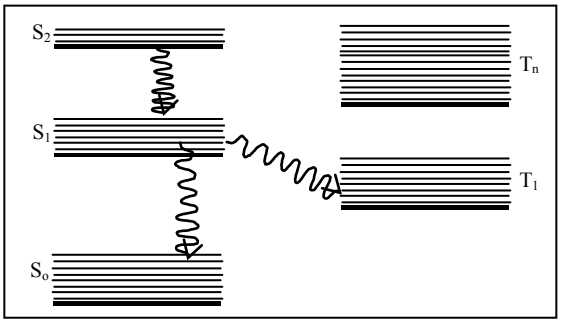

Figure 8.7: the five level model, for explaining the ESA behavior of tea tree oil.

For an ESA material, the ground state absorption cross section is smaller than the excited state absorption cross section. Thus a suitable material for optical power limiting must have as large as possible a ratio of excited state absorption state cross section to ground state absorption cross section. A tentative five layer model for the nonlinear optical transitions of tea tree oil is given in figure 8.7.

Here S_n and T_n represent singlet and triplet states (n=0,1,2) respectively. Due to the existence of large, bounded molecules in the polymer thin films, each electronic levels will consists of a collection of vibrational levels with in each electronic level. At thermo dynamic equilibrium nearly all atoms occupy the lowest vibrational energy level $(\nu = 0)$ of S_0. On irradiation with the laser pulse, atoms in the lowest vibrational energy level of S_0. On the irradiation with the laser pulse, atoms in the lowest vibrational energy level of S_0, initially get excited to some upper vibrational energy levels of S1 through a one photon transition. Subsequently, the excited atoms relax to the lowest vibrational energy level of S_1 through a one photon transition. Subsequently the excited atoms relax to the lowest vibrational energy level of $S_1(\nu = 0)$ through a non radiative decay with in a few picoseconds. From $S_1(\nu = 0)$ state, molecules again get excited to vibrational levels of S_2. However under nano second time scales, $S_2 \leftarrow S_1$ singlet transition does not deplete the population in S_1 as atoms excited to S_2

decay to $S_1(\nu = 0)$, with in picoseconds. It may be noted that the transitions $S_1(\nu = 0) \leftarrow S_0(\nu = 0)$ and $S_2(\nu = 0) \leftarrow S_1(\nu = 0)$, are forbidden because of the even parity of the energy levels involved. Involvement of vibrational levels with appropriate parity is essential to preserve the parity conservation in these transitions. From $S_1(\nu = 0)$ atoms can decay to T_1 $(\nu = 0)$ through intersystem crossing.

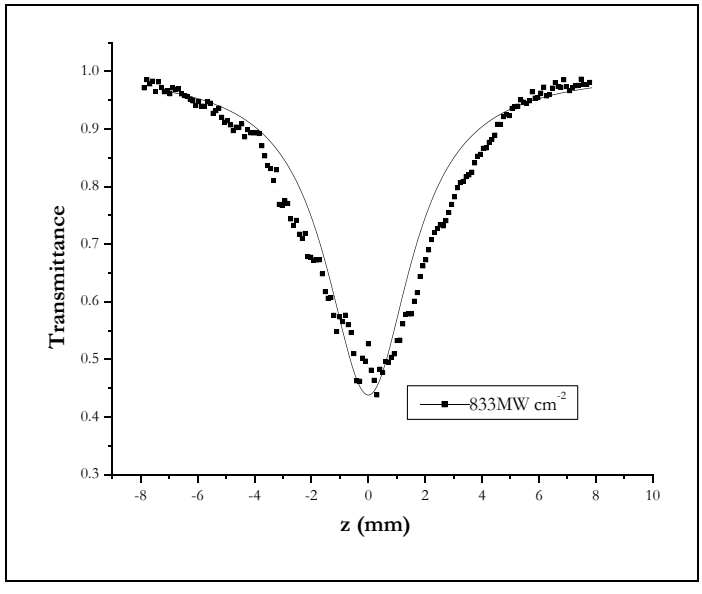

Figure 8.8: Open aperture Z-scan plot of rf TTO in its pristine form. The model fit is also shown (representative plot)

8.6 Calculation of the effective nonlinear absorption coefficient.

For materials showing RSA, the absorption coefficient α, according to the Beers Law is $\frac{dI}{dz'} = -\alpha I$, increases with the irradiance I (energy per unit area) z' gives the propagation depth inside the material. In t6his case the sample experiences the strongest intensity and energy at the focus and it absorbs most of the energy and allows least transmittance.

The effective nonlinear absorption coefficient β_{eff} can be calculated from the theory developed by Sheik Bahae[24] et al. The open aperture Z-scan plots of Tea tree oil thinfilms is given in figure 8.6. These plots are typical of samples exhibiting ESA. Here it can be found that the transmittance is minimum at the focus and increases steadily on both sides of the focus. β_{eff} can be calculated by fitting the experimental open aperture z-scan plot in the equation[9]

$$T(z) = \frac{C}{q_0\sqrt{\pi}} \int_{-\infty}^{\infty} \ln(1 + q_0 e^{-t^2}) dt \qquad 8.8$$

where

$$q_0(t) = \beta I_0(t) L_{eff} \qquad 8.9$$

here C is the normalizing constant L_{eff} is the effective length and I_0 is the irradiance at the focus. The measured value of β_{eff} for tea tree oil thinfilms is given in table 8.2 with its value of irradiance at the focus.

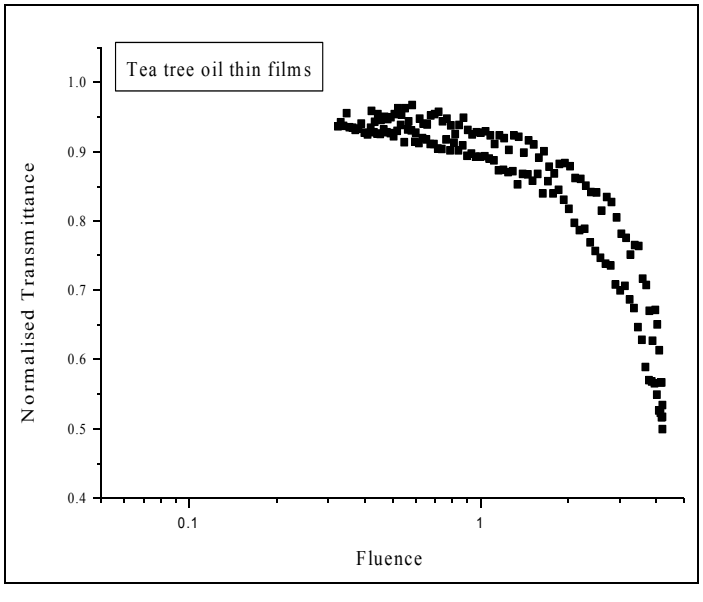

Figure 8.12: Transmittance vs Fluence of Tea tree oil thin films.

The fit parameter β_{eff} is calculated for different intensity values of the sample. It is a measure of the strength of nonlinear absorption and optical power limiting[25]. It is an effective quantity and depends on the intensity of excitation. Here in this case the nonlinear transmission is a function of input fluence. The nonlinear transmission for plasma polymerised tea tree oil thin films as a function of fluence is plotted and shown in figure 8.12 . The plot is generated from the Z-scan measurements. From the value of fluence at focus, fluence value at other sample positions are calculated by assuming the standard equations for the Gaussian beam waist. The fluence level at which the nonlinear transmission begins to deviate from its linear behaviour is also shown.

The beam waist width of the laser beam at the focus is calculated by the formula,

$$\omega_0 = \frac{F\lambda}{D} \qquad 8.10$$

Where F is the focal length of the lens, λ is the wavelength (532 nm) D is the beam width. For the Gaussian beam profile of the Nd:Yag-Laser the beam width is 8.5 nm. ω_0 is calculated as $13\mu m$. By this the diffraction length z_0 in the sample is by $z_0 = k\omega_0^2 / 2$, is calculated as 1 mm in this experiment. $q_0(t) = \beta I_0(t) L_{eff}$ for different irradiance for tea tree oil thinfilms are calculated and given in table 8.2

Irradiance (MW cm^{-2})	β (cm GW^{-1})
637	211
833	33.64
980	21.54
1127	12.7

Table 8.2: β linear absorption coefficient of tea tree oil thin films for different value of irradiance

8.7 Nonlinear absorption in tea tree oil in its doped form

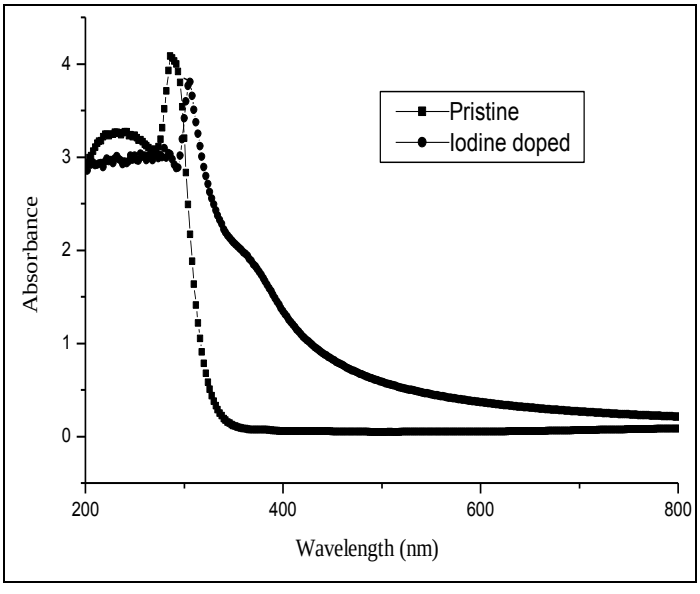

Figure 8.13: Absorbance vs. wavelength of plasma polymerised tea tree oil thin films.

The optical absorption of the iodine doped films indicates that intermediate energy levels are occupied in the tea tree oil thin films and in the pristine forms they are empty, but these levels can be populated.

Also it is unknown that, since the tea tee oil, in its monomer form consists of many components, which of the components is responsible for the nonlinear optical properties of the thin films. However an attempt is made here to explain the open z-scan results obtained in the tea tree oil thin films on the basis of the existing models. The existing models which can be correlated to the non linear absorption observed in the case of tea tree oil thin film can be explained using a five level model as shown in figure 8.7.

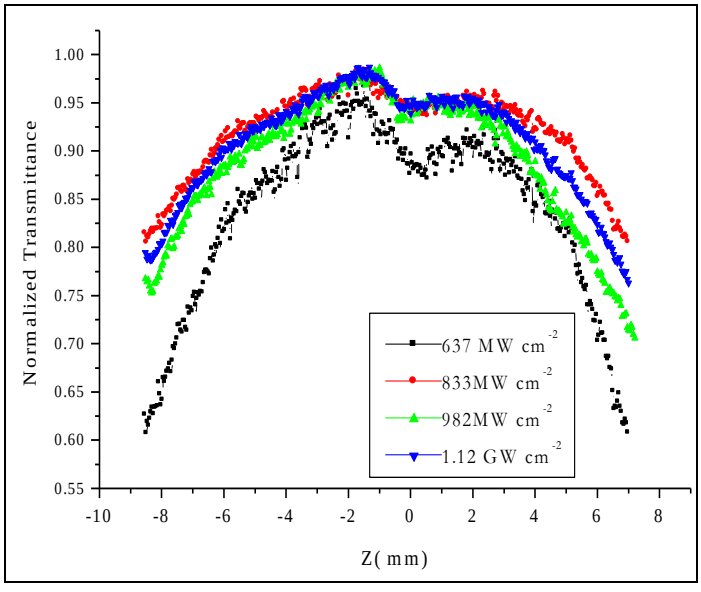

Figure 8.14: Open aperture z-scan plot of rf plasma polymerised tea tree oil thin film in its iodine doped form. Theoretical fit is also shown.

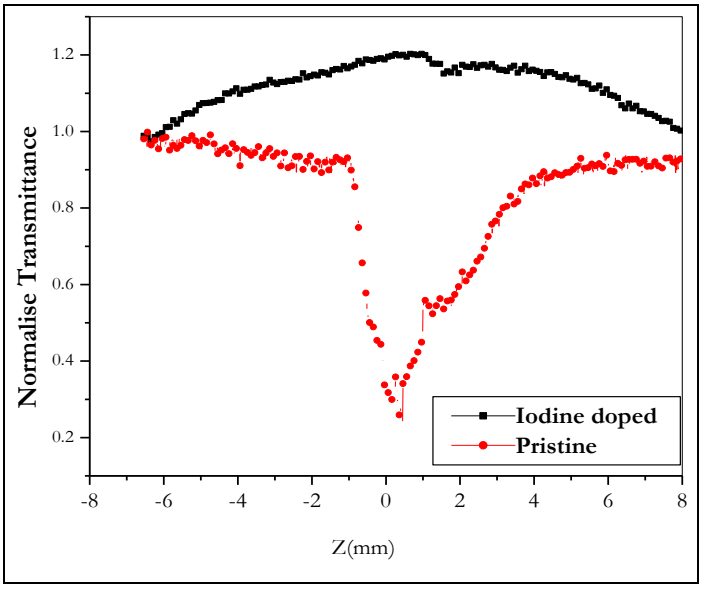

Figure 8.15: The combined plot for the normalized transmittance for pure and iodine doped thin film samples under identical fluence

For the iodine doped samples instead of the RSA, saturable absorption is observed. At sufficiently high input fluence it has been observed by Swatton[26] *et. al* that RSA has been converted into SA due to the saturation of the excited state absorption. The saturation behaviour of the ESA relates to the life time of excited singlet states, and the observation of RSA transforming SA can be used to determine the life time of excited singlet state[8]. From the absorption spectra it can be seen that the optical absorption in the form of intermediate levels is observed for the iodine doped samples. The effect of doping of iodine for a polymer thin film is already discussed under section 8.3. Here in the case the intermediate energy levels are filled. By the filling of these levels it can be observed that the defect levels associated with the polymers will be occupied and the dependence on the trap filled saturation field on will be enhanced. The combined plot for the normalized transmittance for pure and iodine doped thin film sample under identical fluence is given in figure 8.10.

Conclusion

Nonlinear optical studies of plasma polymerised thinfilms of polyaniline and tea tree oil in their pristine and iodine doped forms were carried out by employing the open aperture z-scan technique. The optical and electrical studies carried out on plasma polymerised thinfilms of polyaniline and tea tree oil confirms a trap-controlled PR response and this indicates that these thin films are potential nonlinear optical materials. The z-scan studies revealed that polyaniline exhibited a saturable absorption where as tea tree oil exhibited a reverse saturable absorption which qualities them as potential candidates for optical limiting and optical switching respectively. Incorporation of iodine in the polymer network of these films modifies the nonlinear optical properties of these thinfilms considerably.

References

[1] Donald L.Wise, Gary E. Wnek, Derbra J.Trantolo, Thomas M.Cooper, Joseph D. Gresser, *Photonic Polymer Systems*, Marcel Dekker, New York, 1998

[2] Boon Yi Soon, Joseph W, Haus, Michael Scalora, Concita Sibilia, *Optics Express,* **11**,(2003),2007

[3] W.Ji, Hendry Izaac Elim, and Jun He, F. Fitrilawati, C.Basker, S.Valiyaveettil, W.Knoll, *J.Phys.Chem*, **B**, **1-07**,(2003),11043

[4] M.Cha,N.S.Sarriciftci,A.J.Heeger, J.C. Hummelen, *Appl.Phys.Lett*,**67**,(1995),3850

[5] Mukesh P.Joshi, J.Swiatkiewicz, Faming Xu, Paras N. Prasad, B.A. Reinhardt, Ram Kannan, *Optics Letters* , **23**,(1998),1742

[6] K.P.Unnikrishnan, *Ph.D thesis*, Cochin University of Science and Technology , 2003

[7] Yuhua Haung, Yizhong Yuan, Jingxin Ding, Zhenrong Sun, and Heping Zeng, *Appl.Phys.Lett*, **80**,(2002),4855

[8] S.N.R Swatton ,K.R. Welford, S.J.Till, J.R.Sambells, *Appl.Phys.Lett,* **66**,(1995), 1865

[9] Mansoor Sheik-Bahae,Ali A.Said, Tai-Huei Wei, David J.Hagan, E.W.Van Stryland, *IEEE J. Quantum Electr.* **26**,(1990),760

[10] Tai-Huei Wei, Tzer-Hsiang Huang, Huang-Der Lin, and Sheng-Hsien Lin, *Appl.Phys.Lett.***67**,(1995),2266

[11] A.Fontcuberta I Morral and P.Roca J Cabarrocas and C.Clare, *Phys.Rev.***B** **69**,(2004),125307

[12] P.D Paulson, B E Mc Candless, R W Birkmire, *J.Appl.Phys*, **95**. (2004), 3010

[13] Takashige Omatsu, Naoyuki Hayashi,Hirofumi Watanabe, Akira Hasegawa,and Mitsuhiro Tateda, *Optics Letters*, **23**,(1998),1432

[14] C.H.Lee, G.Yu, A.J.Heeger, *Phys Rev.**B***, **47**,(1993),15543

[15] K.S.Narayan, N.Kunar, *Appl.Phys.Lett*, **79**,(2001),1891

[16] M.J.Rice and Yu.Gartsteinm *Phys.Rev*.**B**, **53**,(1995),10765.

[17] B.Xu, Jaewu Choi, A.N.Caruso,and P.N.Dowben,*Appl.Phys.Lett.* **80**,(2002),4342

[18] Chih-Ming Lai, Hsin-Fei Meng, *Phys Rev.**B*** , **54**,(1996),16365

[19] K.P.Unnikrishnan, J.Thomas, V.P.N.Nampoori, C.P.G.Vallabhan, *Appl.Phys.***B** **75**,(2002),871

[20] K.Kandasami,S.J.shetty.P.N.Puntambedkar,T.S.Srivastava,*Appl.Phys.*B,**64**,(1997),479

[21] M.Samoc, A.Samoc, B.L.Davies, H Hasai,H Reisch and U. Scherf. *Optics Letters*, **23**,(1998),1295

[22] K.P.Unnikrishanan, J.Thomas,V.P.N.Nampoory, C.P.G.Vallabhan, *Opt.Commun.* **204,**(2002),385

[23] K.P.Unnikrishanan, Jayan Thomas,Binoy Paul,A Kurian,P Gopinath,V.P.N.Nampoory, C.P.G.Vallabhan, *J.Non.Opt.Phys.Mater*, 10,(2001),113

[24] Mansoor Sheik-Bahae, Ali A.Said,D.J.Hagan, M.J.Soileau, Eric W.Van Stryland, *Opt. Eng*.**30**,(1991),1228

[25] M.S.Bahae, A.A.Said and E W Van Stryland, *Opt.Lett*. **14**,(1989),955

Chapter 9

Studies on rf plasma assisted surface modification of magnetic nanoparticles

Polymer passivated and surface modified magnetic nanoparticles are of great technological interest, as the polymer coating provides a matrix for binding of the particles and also prevents grain growth and agglomeration[1]. These coatings also provide passivation and prevent further oxidation. The polymer coating on the nanoparticles provide effective encapsulation of individual nanoparticles. The polymer coating on the nanoparticle itself can provide additional functionality. The multifunctionality of the polymer coated magnetic nanoparticle has tremendous application potential and leads to improved materials[2]. The applications of surface modified magnetic nanoparticles include magneto resistive damping [3], Biological high gradient magnetic separation for cell sorting[4], DNA isolation, magnetic resonance imaging contrast agents[5] and low loss tunable microwave devices. Ferrites like Fe_3O_4 and $\gamma - Fe_2O_3$ functionalised with polymers, can be employed in the biomedical field especially for magnetic hyperthermia and drug delivery.

Plasma polymerised coating of polymer thinfilm on inorganic oxides provides a surface passivation thus preventing further oxidation[6]. The surface modification also gives provision for fuctionalization. Surface modification is also known to modify the electrical and magnetic properties of these oxide materials. This chapter deals with the surface modification of iron oxide nanoparticles by employing an improvised rf plasma polymerisation setup. The effect of polymer coating on the dielectric properties is also studied. A suitable model will be applied to fit the experimentally observed dielectric permittivity values.

Magnetic nanoparticles of iron oxide and nickel ferrite in the ultrafine regime were prepared by sol-gel techniques and co-precipitation technique respectively. They were then structurally characterised by XRD and TEM techniques. An ultrathin coating of polyaniline is provided on the surface of

these ultrafine particles by rf plasma polymerisation technique. At the nanolevel the surface properties have a significant control over the physical as well as the chemical properties of these materials since in that regime the surface to volume ratio is quite large.

Uniform deposition of polymer thin films on nanoparticles in the plasma polymerisation process is difficult due to aggregation and large surface area per unit mass of the particle[7]. During the deposition process it is necessary to expose the surface of nanoparticles to plasma, and the unexposed portion of the nanoparticles surface is hardly modified. To overcome this difficulty fluidized bed reactors are used for the surface passivation of non magnetic nanoparticles. In the present investigation, since the particles are magnetic, instead of a fluidized bed reactor, an external magnetic stirrer is sufficient to expose the surface of the nanoparticles uniformly to the plasma region. The details of the experimental setup are given in chapter 3. The magnetic nanoparticles are vigorously stirred at the bottom of the plasma chamber and the surface of the nanoparticles can be continuously renewed and exposed to the plasma for their film deposition during the deposition process.

The present study deals with the surface passivation of magnetic nanoparticles of $\gamma - Fe_2O_3$ and $NiFe_2O_4$, with polyanilne. The effect of surface passivation on the structural and dielectric properties of the magnetic nanoparticles is described in this chapter.

9.1 Preparation of maghemeite and $NiFe_2O_4$ samples

γ-Fe_2O_3 nanoparticles are prepared by sol-gel method as described in chapter 3. The particle size of the nanocomposites is further reduced by high-energy ball milling. An ultrathin coating of polyaniline is provided on these particles by rf plasma polymerization. Nickel ferrites belonging to the series $NixOFe_2O_3$, with x varying from 0.1 to 0.5 were also prepared and coated with polyaniline. All the samples prepared above are insulating and show magnetic behaviour.

9.2 Characterisation of the nanoparticles by X-Ray diffraction and TEM

Maghemite and $NiFe_2O_4$ nanoparticles synthesised by sol-gel technique were further, reduced in size by high energy ball milling (HEBM). They were then characterized by TEM and X-ray diffraction. The particle size of the magnetic nanoparticles in the pure and surface modified form was estimated from the X-Ray diffraction studies and the selected samples were then subjected to TEM studies. The X-Ray diffraction pattern of the nanoparticles prepared by sol-gel method is given in figure 9.1. The average particle size was determined by using Debye-Scherrer formula[8].

$$D = \frac{0.9\lambda}{\beta \cos\theta} \qquad 9.1$$

Here λ is the wavelength of Cu K_α radiation (λ = 1.5418 Å), β is the angular width which is equal to the full width half maximum and in radian. The X-rd analysis indicates that, the particles lie in the nanoregime and they are single phase in nature.

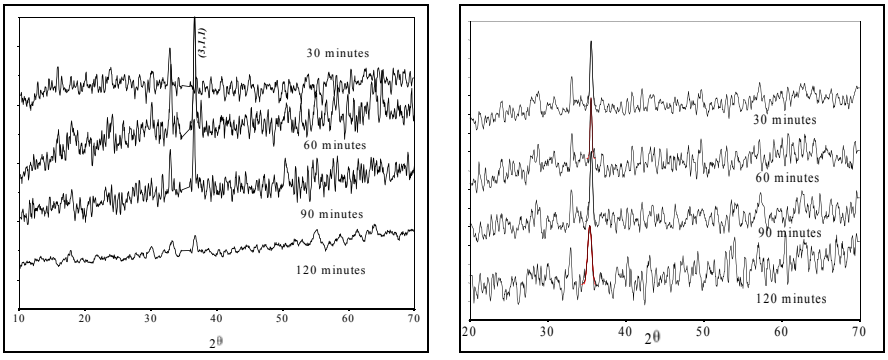

(a) (b)

Figure 9.1: X-Ray diffraction pattern of $\gamma - Fe_2O_3$ in the (a)pure and (b)surface modified form.

Particle size estimated for the samples as a function of the milling time is shown in table 9.1 and is schematically given in figure 9.2.

HEBM time (minute)	Particle size (nm)	
	$\gamma - Fe_2O_3$ (Pure)	$\gamma - Fe_2O_3$ surface passivated.
30	23.3	36.4
60	19.2	27.3
90	17.3	24.2
120	14.5	16.8

Table 9.1 Particle size distribution of the $\gamma - Fe_2O_3$ nanoparticles estimated from XRD

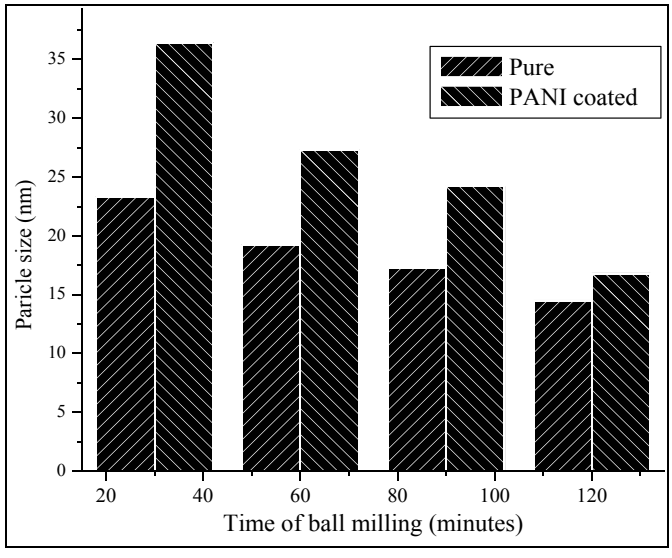

Figure 9.2: Particle size distribution of the $\gamma - Fe_2O_3$ nanoparticles estimated from XRD

The $\gamma - Fe_2O_3$ particles were then subjected to transmission electron microscopy (TEM) studies and the particle size distribution was estimated. They are shown in figure 9.3 and in figure 9.4. The Gaussian fit shows that most of the particles in the pure form is lie with in the particle size regime of 20 -30 nm. For the surface modified particles it is found that the particles are distributed with in the size range of 30-50 nm.

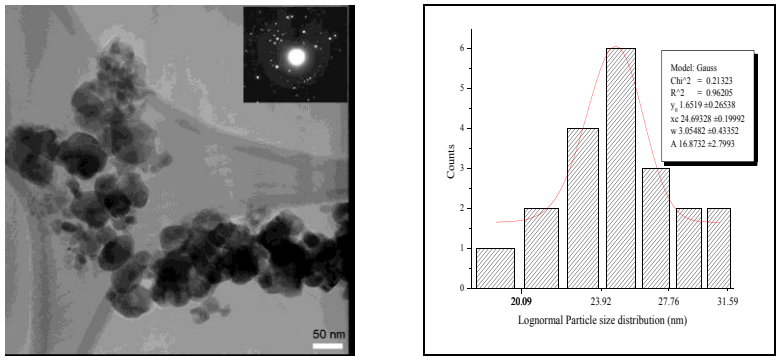

(a) (b)

Figure 9.3: (a)TEM Image of $\gamma - Fe_2O_3$ ball milled for 30 minutes before plasma treatment. (b)Gaussian fit for the particle size distribution of the nanoparticles.

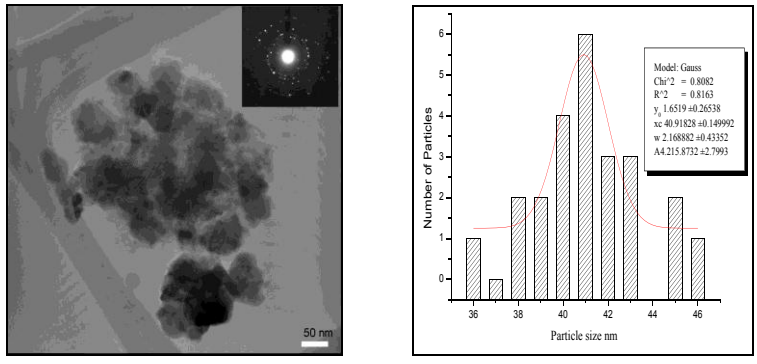

(a) (b)

Figure 9.4: (a)TEM Image of $\gamma - Fe_2O_3$ ball milled for 30 minutes after plasma treatment. (b)Gaussian fit for the particle size distribution of the nanoparticles.

It is also found that the particles are almost spherical in shape with irregular boundaries. This irregularity may be attributed to the effect of ball milling[9,10]. In the case of polymer coated samples the particle size distribution is more or less uniform when compared to the uncoated particles.

9.2.1 TEM studies of the nickel ferrite samples

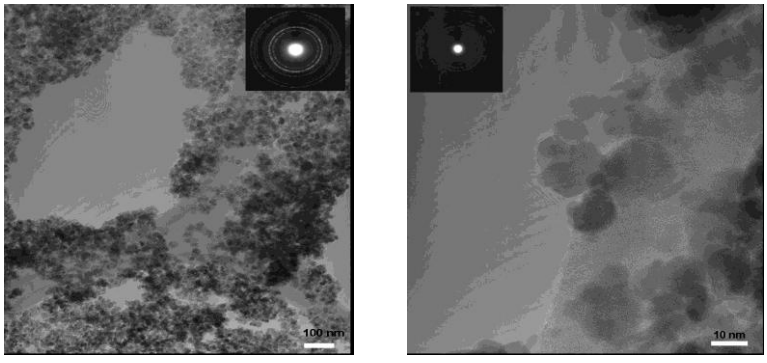

(a) (b)

Figure 9.5 (a)TEM Image of a. $Ni_{0.1}Fe_2O_4$ pure (Provided by Rajesh S[11]. *et al)* (b)Polyaniline coated $Ni_{0.1}Fe_2O_4$ nanoparticle.

TEM image of $Ni_{0.1}Fe_2O_4$ nanoparticles prepared by co precipitation method is shown in figure 9.5. It is to be noted that the average size distribution of the particles is more or less uniform and it lies between 5 nm ~ 10 nm. In the polyaniline coated samples the size distribution is found lying between 8 nm ~ 20 nm. Here in this case the coating thickness is 2 nm and 5 nm. It is found that the thickness of the coating layer under identical conditions depends on the core size too. The nickel ferrite particles with smaller particle size are only coated with an ultra thin coating of thickness of about 2 nm.

The thickness of the polymer thin film deposited on the surface of a micro or nanosized particle is controlled by the time of deposition. In the present study, for all the set of particles taken for the surface modification process, the deposition is carried out for 10 minutes under identical conditions. Experiments were performed with four different particle sizes in the case of $\gamma - Fe_2O_3$ samples. It is found that in all cases the thickness of the thinfilms deposited on the nanoparticle differ considerably and the distribution is shown in figure 9.2. It can be seen from the TEM micrographs that the deposition uniformity around the particle varies. The deposition rate[6], $\frac{dD_p}{dt}$, where D_p is the thickness of the film deposited on the particle, has a marked dependence of the on the original size of the particle. Here in both type of the particles this

phenomenon aggress well with the above results. It is also seen that it is possible to prepare a thinfilm layer of merely a few angstrom. The inorganic components in the composite have been found to be lying in the ultra fine regime.

9.3 Dielectric permittivity studies on surface modified magnetic nanoparticles

The experimental details of the dielectric measurements of the magnetic nanoparticles in the as prepared and in the surface modified form are given in chapter 3. The capacitance, dielectric constant and the ac conductivity values of the ferric oxide samples were evaluated. The theoretical formulation of the dielectric properties is based on the assumption that the system of particles in a given sample is spherical, crystalline and the particle size distribution is uniform to a fair degree of approximation. For dielectric studies these samples were made into pellets of appropriate thickness.

The variation of the thickness of the plasma polymer layer with the original diameter of the particles is described in the previous section. The thickness of the coating layer depends on the time of deposition, current density and the monomer flow rate. However, previous knowledge on plasma polymerization and intuition were applied for getting a uniform coating of the polymer film on the surface of the inorganic particles.

9.3.1 The effect of the ultra thin polymer layer on the dielectric permittivity of the nano composites.

The dielectric permittivity of the magnetic nanoparticles and Maxwell-Wagner fit[12] for the dielectric constants of magnetic nanoparticles in the pure and Surface modified form is given in figure 9.6 and 9.7 respectively. The dielectric permittivity of the samples decreases as the frequency increases.

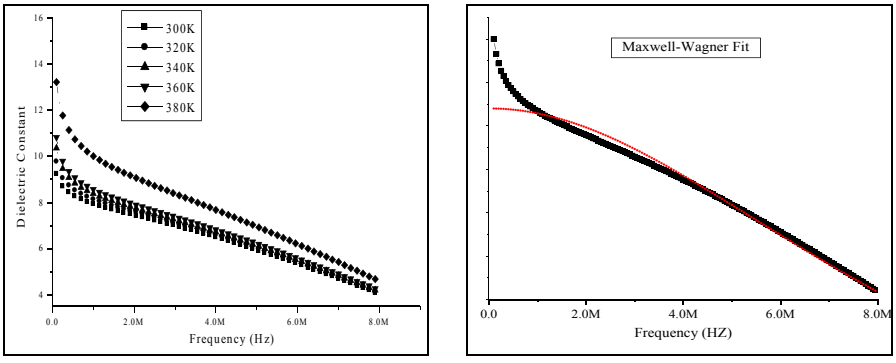

(a) (b)

Figure 9.6 (a) Dielectric constant of $\gamma - Fe_2O_3$ nanoparticles (uncoated) ball milled for 1hr (b)Maxwell-Wagner fit. The Y-axis of figure b is the normalised value of dielectric permittivity.

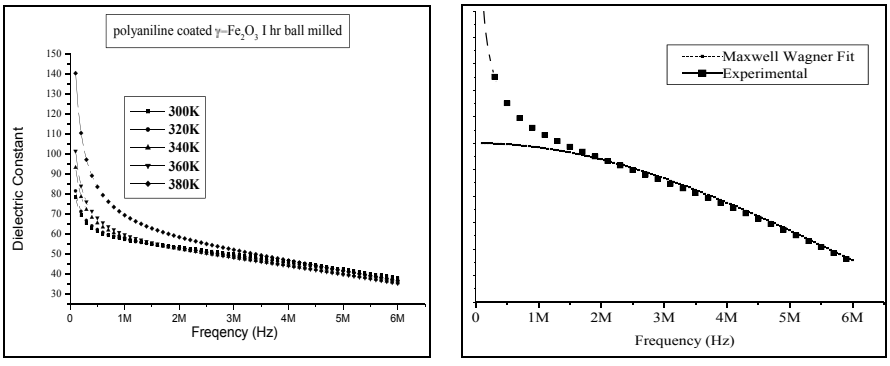

(a) (b)

Figure 9.7 (a) Dielectric constant of surface passivated $\gamma - Fe_2O_3$ nanoparticles ball milled for 1hr (b) Maxwell-Wagner fit. The Y-axis of (b) is the normalised value of dielectric permittivity.

The Maxwell-Wagner fit is performed using the equation[13]

$$\varepsilon' = \varepsilon_\infty + \frac{\varepsilon_1' N}{1 + \omega^2 \tau^2} \qquad 9.2$$

Here in both cases, pure and surface modified particles, from the fit the relaxation time τ are calculated. These are given in table.9.2

Temperature	$\gamma - Fe_2O_3$ pure	$\gamma - Fe_2O_3$ surface modified
	τ - 10^{-8}s	τ - 10^{-8}s
300 K	1.542	1.1358
320 K	1.703	1.183
340 K	1.7888	1.304
360 K	1.871	1.483
380 K	1.9255	1.643

Table 9.2: The value of dielectric relaxation time τ of $\gamma - Fe_2O_3$ as a function of temperature from the Maxwell-Wagner fit.

The relaxation time of the polyaniline coated particles exhibited a reduced value, when compared to that of, as prepared nanoparticles.

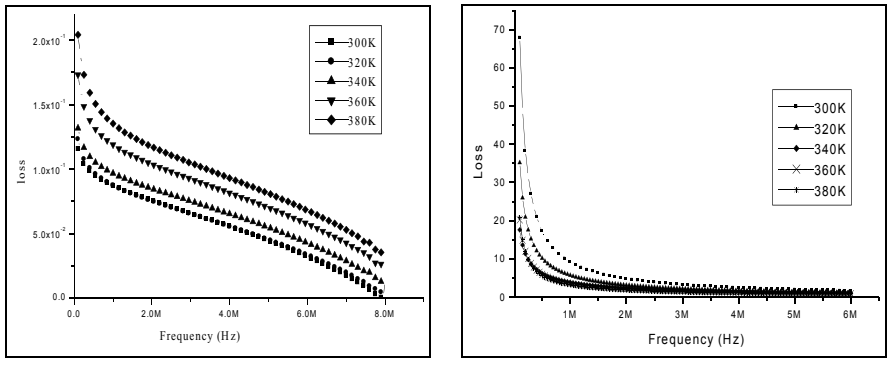

(a) (b)

Figure 9.8: (a)Dielectric loss of $\gamma - Fe_2O_3$ nanoparticles ball milled for 1hr. (a) Pure and (b) Doped

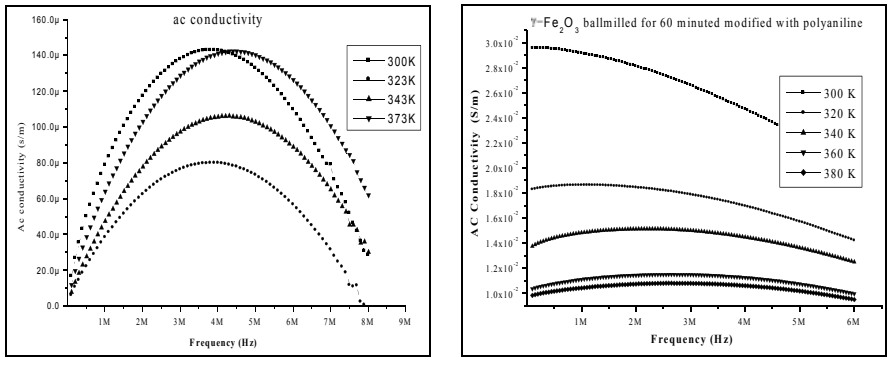

Figure 9.9: Enhancement of ac conductivity of $\gamma - Fe_2O_3$ nanoparticles ball milled for 1hr. (a) Pure and (b) Doped

From dielectric permittivity measurements it is important to note that there is substantial enhancement of the dielectric permittivity values. This increase assumes significance and the method of plasma polymerisation can be employed to tailor the permittivity for different needs.

An increase in the ac conductivity value has also been noticed. If the permittivity values of the composites are correlated with an existing model or by proposing a new model, the surface of inorganic oxides can be modified accordingly to suit various applications. For this, the permittivityof the individual components were evaluated. Plasma polymerised polyaniline has a dielectric constant of 2-4 at room temperature. These values were substituted in a mixture equation of the form

$$\log\varepsilon' = y_1\log\varepsilon_1 + y_2\log\varepsilon_2 \qquad 9.3$$

However the fitted values and the observed values did not agree and alternate models were invoked.

The variation of dielectric permittivity with frequency for the composite samples as well as pure oxides are typical of a system obeying Maxwell-Wagner type interfacial polarisation. The variation of dielectric permittivity with film coating is determined at various frequencies and are tabulated and shown in table 9.3

Temperature	Ball milled for 30 minutes		Ball milled for 60 minutes		Ball milled for 90 minutes		Ball milled for 120 minutes	
	Pure	Pani coated	Pure	Pani coated	Pure	Pani coated	Pure	Pani coated
300K	7.01	102.97	7.92	57.0	9.61	44.34	12.24	42.1
320K	7.53	104.11	8.13	57.37	10.89	53.66	13.32	44.01
340K	7.60	106.25	8.38	58.61	11.72	61.71	14.40	45.30
360K	8.42	110.25	8.56	59.86	12.71	96.39	15.73	47.32
380K	9.43	118.10	10.01	69.57	14.65	105.59	17.92	50.26

Table 9.3: The variation of dielectric permittivity of $\gamma - Fe_2O_3$ for different particle size at different temperature at 1 MHz

In the case of $\gamma - Fe_2O_3$, it can be observed that the value of dielectric permittivity decreases with increase in frequency. The ac conductivity of the samples increases with increase in frequency and after reaching a maximum value it is relaxed to a lower value

9.3.3 Particle size dependence of dielectric properties of surface modified $\gamma - Fe_2O_3$

Dielectric studies were conducted on the surface modified $\gamma - Fe_2O_3$ samples for different milling time. All the samples exhibited similar dielectric behaviour and as a representative sample, polyaniline coated $\gamma - Fe_2O_3$, ball milled for 1hr is given here. The dielectric permittivity values at 1MHz for all the samples at different temperature is given in table 9.3

9.3.4 Effect of polyaniline coating on the dielectric properties of iron oxide nanoparticles-Model fitting

Let us consider the nanocomposite as a matrix consisting of a dielectric medium with permittivity ε_1 having a uniform electric field with intensity E_0, receives inclusions of another dielectric material with permittivity ε_2. The presence of inclusions will distort the electric field produced by ε_1. The distortion will be noticeable if the difference between ε_1 and ε_2 is large. A schematic of the matrix consisting of a bilayer is shown in figure 9.10.

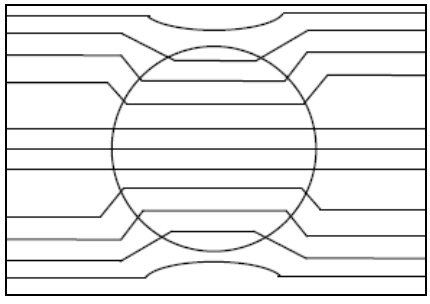

Figure 9.10: Dielectric inclusion into a material of different dielectric permittivity values

It can be shown that

$$E_A = E_0 \frac{3\varepsilon_2}{2\varepsilon_1 + \varepsilon_2} \qquad 9.4$$

Where E_A is the field inside the spherical region and E is the applied field. In this way, an isolated sphere made of a material with high permittivity can increase the field intensity in a dielectric. The plausible reasons for the increment in the dielectric constant are as follows[12].

The polymer coated ferrite particles forms an inhomogeneous medium, with the core and the outer shell having different dielectric permittivity. The effective field is different for the coated particles and this field causes an interfacial polarization between the grain boundaries and the polymer layer in contact with the particle surface according to the Koop's Phenomenon. This polarization causes an increase in the dielectric susceptibility of the system and hence the dielectric permittivity.

The capacitance of coated iron oxide particles was determined by the principle of parallel plate capacitor method. The effective capacitance C_{eff} is given by equation 9.5.

$$C_{eff} = \frac{4\pi\varepsilon_0}{\frac{1}{r}\left(\frac{1}{\varepsilon_1}-\frac{1}{\varepsilon_2}\right)+\left(\frac{1}{\varepsilon_1 a}-\frac{1}{\varepsilon_2 b}\right)} \qquad 9.5$$

In this case the surface coated nanoparticle is assumed as a spherical nanocapacitor consisting of two layers of different dielectric constant and thickness values. Here a is the radius of the core and b is the radius of the coating. The capacitance of the γ-Fe_2O_3 nanocomposite in the pellet form in its pure form is given by,

$$C_0 = \frac{\varepsilon_0 \varepsilon_r}{Ad} \qquad 9.6$$

It is the value of a spherical capacitor formed by two dissimilar dielectric materials. The charge stored in such a system in terms of the effective electric field is given by

$$q = CE'.2(a+b) \qquad 9.7$$

The capacitance of the pelletized samples can then be written as

$$Ce_{ff} = \frac{Nq}{V} \qquad 9.8$$

Here 'N' is the total number of particles present in the pellet, 'q' is the charge accumulated in a particle and 'V' is the applied potential difference. The calculations performed using the equations agree well with the obtained value of capacitance in the pure and polymer coated magnetic nanoparticles. The particle

size and the thickness of the coating are the main factors influencing the value of dielectric permittivity in addition to the permittivity values of the core and the coating. The frequency dependence and the effect of plasma coating on the dielectric and ac conductivity values can be calculated as follows.

Here the specimen is not homogeneous, but contains regions of different permittivity. The conductivity of the medium also contributes towards the dielectric value of the sample. By using a simplified model using Maxwell-Wagner effect, apparent permittivity can be calculated as

$$\varepsilon_T = \frac{\varepsilon_2(\varepsilon_1 - j4\pi\sigma/\omega\varepsilon)}{(\varepsilon_1 - j\pi\sigma/\omega\varepsilon)f_2 + \varepsilon_2 f_1} \qquad 9.9$$

Here ε_T, is the apparent dielectric constant, σ is the conductivity of the medium of dielectric constant ε_1 (coating layer), ε_2 is the dielectric constant of the core material. Here,

$$f_1 = d_1/(d_1 + d_2) \text{ and } f_2 = d_2/(d_1 + d_2), \qquad 9.10$$

where d_1 is the thickness of the coating and d_2 is the diameter of the core.

The limiting cases for this equation (real part) of the equation. When $\omega \to 0$, is

$$\varepsilon_T = \varepsilon_2 / f_2 . \qquad 9.11$$

The numerical value of ε_T, agrees well with the experimentally observed dielectric constant at low frequencies. The figure shows the calculated as well as measured values of the apparent dielectric constant of PANI coated $\gamma - Fe_2O_3$ samples. It can be observed from the plot that, the experimentally observed values corresponds to a coating thickness of 2 nm, which is less than that of the value obtained from the X-RD and TEM. The reason for this discrepancy may be the nonuniformity in size distribution of the core particles. Here in this calculation a uniform particle diameter and core thickness and such an ideal case is not possible.

At higher frequency regime the apparent value of the dielectric constant will possesses the value

When $\omega \to \infty$, $\varepsilon_T \to \varepsilon_\infty = \varepsilon_1\varepsilon_2/(\varepsilon_1 f_2 + \varepsilon_2 f_1)$ 9.12

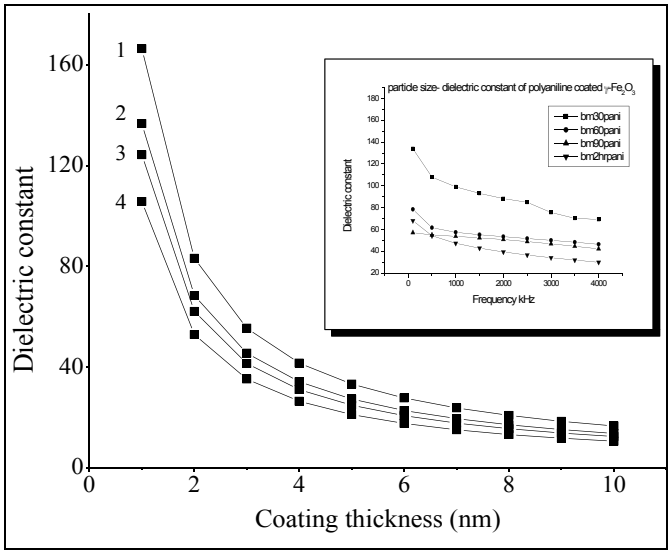

Figure 9.10: The calculated value of the dielectric constant of surface modified magnetic nanoparticles as a function of the surface layer thickness at 100 kHz. Variation of Dielectric parameters of γ-Fe_2O_3 for different milling time. In this calculation it is assumed that the particles are spherical and the coating is uniform. The assumed radius of the nanoparticles after the surface passivation. (1) milling time 30 minutes-18 nm, (2) 60 minutes-14 nm, (3) 90 minutes-12nm and (4) 120 minutes-8.5 nm. The experimentally observed value is given in inset.

This value is not applicable in this case because the upper frequency of the experiment carried out is 8MHz and far below the infinite limit of frequency.

The relaxation time of such a medium is given by

$$\tau = \frac{\varepsilon_1 f_1 + \varepsilon_2 f_2}{f_2 \sigma} \frac{\varepsilon}{4\pi} \qquad 9.13$$

It can be seen that as the conductivity of the coating layer increases the relaxation time decreases. In the present case the conductivity value of the polyaniline, is comparable to that of the core particles at room and a large variation of τ is not expected.

Conclusion

RF plasma polymerisation unit is modified for the surface passivation of magnetic nanoparticles. The deposition rate of the plasma polymerised thin films on the surface of the nanoparticles is found to be a function of the core radius under identical conditions. The dielectric constant of the nanoparticles enhanced considerably when a surface coating is provided. The modification of the dielectric properties of surface modified magnetic nanoparticles are modelled using Maxwell-Wagner theory.

Chapter 9

References

[1] H.Srikanth, R.Hajndl, C.Chirinos, J.Sanders, A.Sampath and T.S.Sudarsan, *Appl.Phys.Lett*, **79**(2001),3503

[2] E. Tronca,*, D. Fioranib, M. Nogu"esc, A.M. Testab, F. Lucarid, F. D'Oraziod,J.M. Gren"echee, W. Wernsdorferf, N. Galvezg, C. Chan!eaca, D. Maillyh, J.P. Joliveta, *Journal of Magnetism and Magnetic Materials* **262** (2003) 6

[3] J.P.Tetre, K.B.Hathaway, and A E Clark, *J.Appl.Phys.,*B79,(1996),6213

[4] R.Gerber and R Briss, *High Gradient Magnetic Separation,* Wiley, New York, 1983.

[5] R.Weissleder, G.Elizondo, J.Wittenberg, C A Rabito, H H Bengle, and L.Josephson, Radiology, **175**, (1990),489.

[6] Donglu Shi, S.X.Wang, Wim J, Van Ooji, L.M.Wang, Jiangang Zhao and Zhou Yu, *Appl.Phys.Lett*, **78**, (2001), 1243

[7] Deposition kinetics on particles in a dusty plasma reactor, Jin Cao and Themis Matsoukas, *J. Appl.Phys.* **92**, 2916, 2002

[8] C Suryanarayana and M Grant Norton, *X-Ray Diffraction,* (1998), Plenum Press, New York

[9] C.C. Koch 2003 *Rev. Adv. Mater. Sci.* **5** 91-99

[10] X B Yu, T Dou, Z Wu, B J Xia and J Shen 2006 *Nanotechnology* **17,** 268-271

[11] V.S. Abraham, S. Swapna Nair, S. Rajesh***, U.S Sajeev*** and M.R Anantharaman, *Bull. Mater. Science,* **27** (2), 2004, pp165.

[12] Vera V.Daniel, *Dielectric Relaxation*, Academic Press, (1967), New york

[13] Nora E.Hill, *Dielectric properties and molecular behaviour*, Van Nostrand Reinhold,(1969), New York

Chapter 10

Conclusion

Polymers and polymeric materials are constantly playing a vital role in making new devices and thus paving the way for removing the obsolete. They play a lead role in making life more humane. The 20th century witnessed an exploding activity in this area. This has resulted in the birth of new disciplines like molecular electronics, synthetic metals, organic semiconductors, and plastic electronics. The advent of high-end workstations and supercomputers augmented the design of various molecules for specific applications. During the last 10 years or so, tremendous progress has been made in making new optoelectronic devices based on polymers like new display elements fluorescent materials, LEDs etc. Both bulk and thinfilms based on these polymers were synthesised/fabricated. Normally as far as the applications are concerned devices are thinfilm based and hence the preparation of polymer thinfilms assumes certain significance. Plasma polymerisation is a known technique for producing ultrathin films which are homogeneous, smooth and pinhole free. Both rf and ac plasma polymerisation techniques can be employed to prepare thinfilms. Polymers are increasingly finding new applications in the form of passivating medium for fuctionalization and as biocompatible materials for drug delivery and drug targeting. In plasma polymerisation, since the precursors are the monomers themselves, new polymers can be synthesised by using precursors like natural oils. This might lead to new electronic materials based on natural products or endup as value added products for biomedical applications. This thesis is thus an attempt towards this objective. The salient findings, conclusions drawn out of these studies and the scope for further investigations are listed in this concluding chapter.

It has been found that, by optimizing the process parameters namely, plasma current, monomer flow rate and monomer vapour pressure, good quality

thinfilms could be fabricated using the technique of both rf and ac plasma polymerisation. Any study on polymer thinfilms is complete without structure-property correlation. Thus extensive spectroscopic investigations are carried out on polymer thinfilms. It has been found that in plasma polymerised aniline thinfilms the benzene ring is intact during plasma polymerisation. The optical band gap is modified by doping of iodine. An *insitu* method and an improvised set up for iodine doping has been fabricated indigenously. Elaborate studies were carried out on pristine and iodine doped samples. It was found that the *insitu* method of iodine doping could be modified and any dopant vapour could be admitted. Another feature of this setup is that the admittance of the dopant vapour can be monitored and the dopant concentration can be pre determined.

Engineers worldwide are struggling hard to cope up with the Moore's law, to increase the component density in a chip. This has resulted in search for low-k materials. Though conventional low-k materials are based on silicon, search for non conventional low-k materials based on polymers are also on. It must be noted here that low-k materials are good inter layer dielectrics and thus enable to reduce the RC time constant which in turn help to decrease the crosstalk. This thesis is also an endavour to delve in to the fundamental aspects of the formation of plasma polymers based on aniline, phenyl hydrazine and tea tree oil. Emphasis was also laid in preparing plasma polymerised thinfilms based on tea tree oil

Plasma polymer of phenyl hydrazine was never before investigated and it was found that thinfilms of plasma polymerised phenyl hydrazine is a potential candidate for applications such as low-k films. Spectroscopic investigations carried out on plasma polymerised natural oils like tea tree oil indicated that the plasma polymerised thinfilms based on tea tree oil contain optically active groups (species) like chromophers and can then be useful for device applications. The complexity of the structure and the presence of large groups like terpinen-4-ol, p-cymene, 4-iso- propyl toluene and para methyl cymene etc is a major impediment in clearly stating that a particular group is responsible for the properties exhibited by these films. Great amount of investigations is

necessary to decipher the role of different groups with respect to a particular property. This needs further studies using FTIR and NMR. The presence of optically active groups like chromophores in plasma polymerised tea tree oil thin films increases the application potential as an active layer for the fabrication of the electroluminescent devices like polymer light emitting devices (PLEDs) etc.

Earlier investigations on plasma polymerised polyaniline and iodine doped polyaniline indicated that plasma polymerised polyanile can be a potential low k material. However these studies were carried out in the low frequency regime. Inorder to revalidate these findings, spectroscopic ellipsometric experiments were performed. Pristine and iodine doped polyaniline thinfilms exhibited low k characteristics even at optical frequencies. This augurs well as well as applications are concerned. These experiments also establish the fact that rf plasma polymerisation is an effective tool for producing optically smooth films. It must be noted here that the findings on roughness by ellipsometric technique is in full conformity with that of the results obtained using AFM and SEM. The optical conductivity of these films was evaluated from spectroscopic ellipsometric data and has been found that the iodine doping increases the conductivity substantially. This is an important finding and in tune with the results obtained from the optical absorption studies.

Elaborate studies were carried out on the conducting properties of plasma polymerised thinfilms of aniline, phenyl hydrazine and tea tree oil inorder to elucidate the possible conduction mechanism of these polymer thin films. It is found that the dominant conduction mechanism found in rf plasma polymerised aniline, phenyl hydrazine and tea tree oil is space charge limited conduction (SCLC), where as the ac plasma polymerised form of aniline exhibited Schottkey type conduction mechanism. Conductivity of all the plasma polymers subjected to the J-V measurements were found in the semiconducting regime.

Dielectric and ac conductivity studies on rf and ac plasma polymerised thin films of polyaniline, phenyl hydrazine and tea tree oil were carried out and the results are explained. All the films exhibit a 'breakdown' at higher

frequencies for an applied biasing voltage of 1 V between the electrodes. Up to this "breakdown frequency" the thinfilms show low-k properties. A hopping conduction at higher frequencies is observed in all films. The phonon frequencies corresponding to different frequencies for these films were evaluated. Inter electrode tunneling of carriers at high frequencies is observed in all films. The electric field induced polarisation and hopping of carriers at high frequencies were observed in all the plasma polymers subjected to the dielectric measurements.

Nonlinear optical studies of plasma polymerised thinfilms were carried out by employing the open aperture Z-scan technique. The optical and electrical studies carried out on plasma polymerised thinfilms of polyaniline and tea tree oil confirms a trap-controlled PR response. This indicates that these thinfilms are potential nonlinear optical materials. The z-scan studies revealed that polyaniline exhibited a saturable absorption and the tea tree oil exhibited a reverse saturable absorption which qualities them as potential materials for optical limiting and optical switching respectively. Incorporation of iodine in the polymer network of these films modifies the nonlinear optical properties of these thinfilms considerably.

An indigenous method for surface passivation using rf plasma polymerisation of inorganic materials was developed. Initial experiments carried out on magnetic oxides indicate the passivation of oxide particles with an ultra thin polymer layer can easily be carried out by plasma polymerisation. A model based on Maxwell-Wagner theory of interfacial polarisation was applied to explain the observed enhancement of dielectric permittivity. This model can be applied for a bilayer or a trilayer coating and can be employed to tune the dielectric properties of oxide materials by surface modification.

There is huge scope for further work on plasma polymerised thinfilms, based on phenyl hydrazine and tea tree oil. Phenyl hydrazine based thinfilms are being investigated using plasma polymerisation technique for the first time. A complete evaluation of the structure of these polymer thinfilms with the help of FTIR spectroscopy in combinational with the NMR technique will shed light on

the structure of plasma polymerised phenyl hydrazine thinfilms. There is ample scope exists to investigate the electrical and photoconductive properties of these films. It has been found that the plasma polymerised tea tree oil films are semi conducting and transparent. They are bio compatible too. So scope exists to to coat inorganic magnetic particles with tea tree oil films and functionalise them for drug delivery applications. These is also scope for carrying out a detailed investigation on the optical properties of plasma polymerised tea tree oil thinfilms for applications LEDs and active materials.

Journal Papers

1. The optical and electrical properties of properties of RF and ac plasma polymerized aniline thin films ***U.S.Sajeev***, C.Joseph Mathai, S.Saravanan, Rajeev.R.Ashokan, S.Venkatachalam, M.R.Anantharaman *Bull. of Mater. Sci. 29, (2006), p159*
2. Evidence for intergranular tunnelling in Polyaniline passivated α -Fe nano particles. Vijutha Sunny, T N Narayanan, ***U S Sajeev,*** P A Joy, D Sakthi Kumar, Yasuhiko Yoshida and M R Anantharaman (Nano technology)
3. Magnetic field induced assembling of nanoparticles in ferrofluidic liquid thin films based on $Ni_xFe_{1-x}Fe_2O_4$, V.S. Abraham, S. Swapna Nair, S. Rajesh***, U.S Sajeev*** and M.R Anantharaman, *Bull. Mater. Science,* **27** (2), 2004, pp165.
4. Optically transparent and electrically semi conducting thin films based on tea tree oil by RF plasma polymerization: Mohan V. Jacob, ***U. S. Sajeev***, and Rajeev. R. Ashokan, M.R.Anantharaman (Communicated)
5. Insitu doping of phenyl hydrazine thin films with iodine for the Modification of optical and electrical properties: ***U. S. Sajeev*** and M.R.Anatharaman (Communicated)
6. Studies on

Conference Papers

7. The optical and electrical properties of poly aniline thin films deposited under rf and ac plasma polymerization ***U.S.Sajeev,*** C.Joseph Mathai, S.Saravanan, S.Venkatachalam, M R Anantharaman DAE-BRNS symposium on application of Plasma, Laser and Electron beam in Material processing to be held at Babha Atomic Research Centre, Mumbai during September 23-26, 2002
8. .Modification of magnetic and electrical properties of $Ni_xFe_{1-x}Fe_2O_4$ by polymer surface coating, M.R. Anantharaman, P.A. Joy, S. Swapna Nair, ***U.S Sajeev*** and V. Sooraj. International conference in inorganic materials, Andwerp, Belgium, Accepted.
9. Surface Modification of Magnetic Nanoparticles by RF Plasma Polymerisation, V. Sooraj, ***U.S Sajeev***, S. Swapna Nair, M.R.Anantharaman.

National Symposium on Instrumentation 28, Vallabhai Panth University, Panth Nagar, Utharanchal, Nov. 1-3, 2003.

10. Surface Modification of Ultrafine Iron Particles by Plasma Polymerized Aniline. Vijutha Sunny, ***U. S. Sajeev***, S. Swapna Nair, P.A.Joy, M.R.Anantharaman, DAE-BRNS Symposium, BARC, 2004 September,
11. Saturable absorption in plasma polymerized aniline thin films probed by z-scan technique: ***U.S. Sajeev***, Vinu.V. Namboodiri, Anwar Salah, V.P.N Nampoori, P.Radhakrishnan., M.R.Anantharaman. Presented in Photonics 2004 (International Seminar), Cochin , Kerala, India, 2004 December.
12. Band gap Tuning in RF Plasma Polymerised Tea Tree oil Thinfilms by Swift Heavy Ion Irradiation: Rajeev. R. Ashokan, M.R.Anantharaman, D.K.Avasthi, ***Sajeev U.S***, Mohan Jacob, Ambuj Tripathi. Presented in International Seminar on Optoelectronic Materials and Thin Films for Advanced Technology (OMTAT-2005), Cochin, Kerala, India, 2005 October.
13. Evidence for the Occurrence of Inter Granular Tunnelling in Passivated Ultrafine Fe Particles with Polyaniline: Vijutha Sunny, T.N. Narayanan, ***U.S.Sajeev***, M.R.Anantharaman, Presented in International Seminar on Optoelectronic Materials and Thin Films for Advanced Technology (OMTAT-2005), Cochin, Kerala, India, 2005 October.
14. Urbach Tail Analysis of Pristine and iodine doped Polypyrrole Thinfilms Prepared by AC plasma Polymerisation, Joseph John, ***U.S.Sajeev***, M.R.Anantharaman, S.Jayalekshmi. Presented in International Seminar on Optoelectronic Materials and Thin Films for Advanced Technology (OMTAT-2005), Cochin, Kerala, India, 2005 October.
15. Persistent Photoconductivity in AC Plasma Polymerised Phenyl Hydrazine thin films, ***U.S.Sajeev***, M.A.Sanoj, Hysen Thomas, M.R.Anantharaman: Presented in International Seminar on Optoelectronic Materials and Thin Films for Advanced Technology (OMTAT-2005), Cochin, Kerala, India, 2005 October.

List of Abbreviations

1	Alternating Current	ac
2	Camphor Sulphonic Acid	CSA
3	Effective Medium Approximation	EMA
4	Electroluminescent	EL
5	Excited State Absorption	ESA
6	Fourier Transform Infrared	FTIR
7	Gaussian Broadened Polynomial Superposition	GBPS
8	Highest of the Occupied Molecular Orbit	HOMO
9	Indium Tin Oxide	ITO
10	Integrated Circuit	IC
11	Kramers-Kronig	KK
12	light emitting diodes	LED
13	Linear Variable Differential Transformer	LVDT
14	Lowest of the Unoccupied Molecular Orbit	LUMO
15	Mean Square Error	MSE
16	Metal-Polymer-Metal	M-I-M
17	Nonlinear Optical	NLO
18	Nuclear Magnetic Resonance	NMR
19	Phenyl Hydrazine	PH
20	Photo Refractive	PR
21	Plasma Polymerised Phenyl Hydrazine	PPH
22	Plasma Polymerised Polyaniline	PPANI
23	Plasma Polymerised Tea Tree Oil	PPTTO
24	Polyaniline	PANI
25	Radio Frequency	rf
26	Saturable Absorption	SA
27	Source Measurement Unit	SMU
28	space charge limited current	SCLC
29	Spectroscopic Ellipsometry	SE
30	Super paramagnetic ion oxide nanoparticles (SPION)	SPION
31	Trap Charge Limited Current	TCLC
32	Trap Filled Limit	TFL
33	Two photon absorption	TPA
35	Ultra Violet- Visible-Near Infrared	UV-Vis-NIR
36	Variable Angle Spectroscopic Ellipsometry	VASE

List of figures

Chapter 7

Spectroscopic Ellipsometric characterisation of plasma polymerised aniline films